

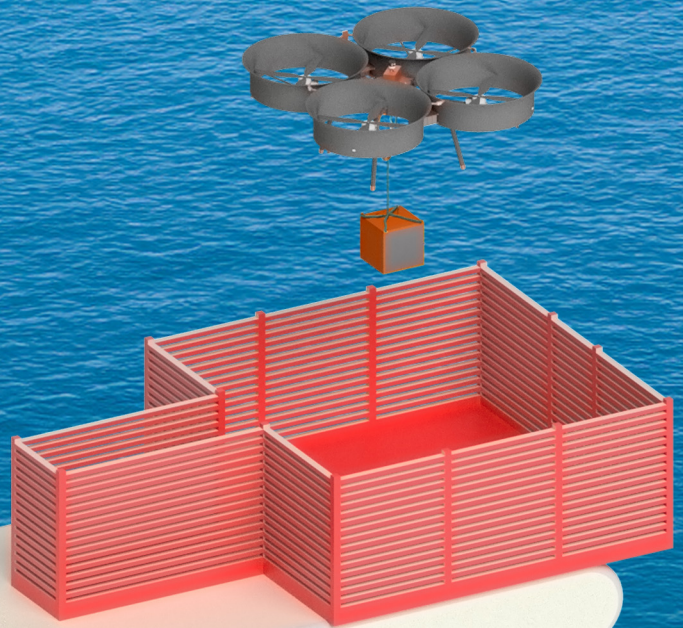
PeliCrane

Unmanned VTOL Platform for Offshore Operations

AE3200: Design Synthesis

Group 4

Delft University of Technology



PeliCrane

Unmanned VTOL Platform for Offshore Operations

by

Group 4

Barnabás Szeibert	5474450
Elliot Van Bunderen Robberechts	5090075
Folkert de Klerk	5072549
Julia van Sminia	4858328
Joonas Rengers	4998618
Lorenzo Gaeta	5507332
Nikodem Dudek	5525365
Paula Bustamante Alonso-lasheras	5279445
Ries van Heur	5535832
Vladimir Markov	5221277

Instructor:	Dr. D. Ragni
Coaches:	B. Puroja and B. Mohammadikalakoo and E. Ntouroso
Teaching Assistant:	H.M. Powis
Project Duration:	04, 2024 - 07, 2024
Faculty:	Faculty of Aerospace Engineering, Delft

Executive Overview

The executive overview acts as an independent overview of the entire project and design of the autonomous offshore cargo UAV (Unmanned Aerial Vehicle) dubbed PeliCrane. This UAV system focuses on delivering a 25kg payload to offshore wind turbines, however it has a flexible mission profile that can be extended to offshore logistical operations between platforms and ships, as well as on-shore operations. This project aims to provide an innovative, competitive, sustainable, and accessible design capable of fulfilling this mission, all while serving as an educational environment in which a group of 10 students can develop academically.

Project Objective

The project objective is given with the following 2 statements

Mission Need Statement

Deliver a 25kg payload by air to a wind turbine generator located in an offshore environment with a reduction in cost compared to current methods.

Project Objective Statement

Design of a VTOL UAV capable of transporting 25kg of payload and moving it within an offshore platform by 10 students in 10 week's time.

Market Analysis

In order to bring the opportunities of the drone into scope, both the competitor market as well as the customer market is analysed and combined in a concluding SWOT (Strengths, Weaknesses, Opportunities, and Threats) Analysis. This analysis will provide a pragmatic approach to bring the strengths and weaknesses of the PeliCrane into perspective in the context of the concurrent potential opportunities and threats in the market.

The global drone market is a very rapidly growing sector, with an estimated global value of 19.89 billion USD in 2022 [1]. The worldwide cargo drone market, where the PeliCrane falls under, is expected to grow exponentially from 828 million USD in 2023 to 17.88 billion USD in 2030 [3]. The largest producer of commercial drones is the Chinese company DJI, with a market share of 76% [4]. Furthermore, products like the HLM Industrial Octocopter and Aurelia X6 MAX offer similar cargo transport possibilities. The drone that is most comparable to the project objective is the DJI Flycart 30, serving as a starting reference for the PeliCrane design. Based on the average normalised cost of the similar drones, the competitive price of the PeliCrane is estimated to be 45k USD.

An identified most promising customer market is the offshore wind energy sector. However, this can extend to maritime logistic companies, offshore platforms and rigs, renewable energy companies, defence applications, and delivery to remote communities with limited access. Essentially, the potential use entails transportation of cargo to and from any type of offshore platform.

Within the offshore wind energy section, PeliCrane aims to provide delivery of tools, lubricants, components, and other parts necessary for wind turbine preventive and corrective maintenance. Current operations involving helicopters, ships, and cranes require a large amount of personnel to be involved in each link of the logistics chain. This introduces high cost and organisational complexity. Furthermore, the legal limit of 25kg allowed to be carried by a single wind turbine maintenance technician makes these methods highly inefficient. An autonomous, independent and accessible cargo drone system like the PeliCrane would provide a cheap, fast and efficient solution to these problems.

Top level requirements

The top-level requirements derived from the project objective, are as follows Table 1

Table 1: Top Level Requirements

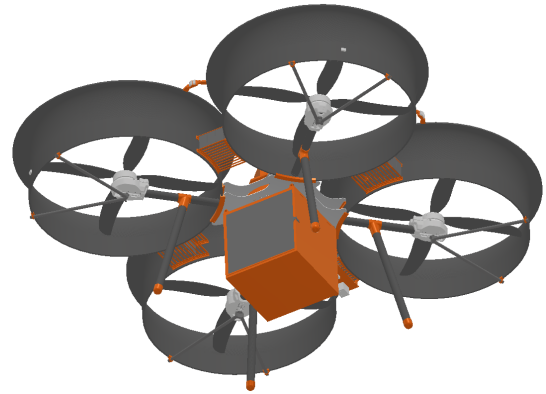
Top level requirements
The UAV shall be able to hover for at least 30 minutes
The UAV shall have a range of at least 5 km
The UAV shall operate autonomously
The UAV shall avoid obstacles autonomously
The UAV shall be safe to operate
The UAV shall consist of at least 50% off-the-shelf components
The UAV shall be able to operate with winds of 6 bft, in an offshore environment

System Overview

The system overview is presented below.



(a) Top Isometric View



(b) Bottom Isometric View

Figure 1: Pelicrane Isometric View

Top Level Specifications

The top level specifications of PeliCrane are presented in Table 2.

Table 2: Top Level Specifications

Characteristic	Value
Maximum hover endurance	34 min
Maximum cargo delivery range	27 km
Maximum cargo delivery range 6bft winds	6.6 km
Maximum thrust per engine	56 kgf
Maximum Take Off Weight	98 kg
Total battery capacity	6660 Wh
Height	1155 mm
Width	2718 mm
Configuration	4-bladed propeller, conventional electric quadcopter
Total production cost	48.59k euro

Structures and Materials

The structure is essential to support the weight of PeliCrane, carry loads introduced during operation and protect all electrical components from the environment. After an engineering trade-off process, a conventional ducted quadcopter design was chosen to be most suitable. The structure is made of Aluminium alloys, polycarbonates and carbon fibre composites, divided into the central box housing electronics, rods supporting the motors and propellers, landing gear, and the ducts. The structure incorporates as many off the shelf components as possible, with a focus on sustainability, availability and manufacturability. Where possible, 3d printing is utilised to manufacture required parts.

For the payload system, a 50x50x50 cm payload box is designed, to accommodate a 25kg payload. The payload is attached to a winching system, consisting of a spool with a 10m rope and off the shelf motor. This winch can subsequently lower the payload from a height of 8m.

Lastly a parachute system has been included, to reduce the falling speed of the PeliCrane in case of failure, and to ensure the UAV does not get significantly damaged upon impact with the ground.

The structure was first designed by hand calculation while using smart assumptions. Afterwards a CAD model was created, and the structurally verified using FEM. This enables rapid and efficient optimisation of the structure.

Propulsion System

The propulsion system consists of the motors, ESC's (electronic speed controllers), and propellers. The propellers provide thrust and are driven directly by the motors. The motors are driven/controlled by the ESC's and get powered by the batteries. The rotors are surrounded by ducts, increasing safety but also propeller efficiency due to the shape incorporating aerodynamic effects, boosting propeller performance.

Electronic Components & Power

The heart of PeliCrane's electronic system is the flight controller (FC). The Cube Orange FC running on Ardupilot firmware, is chosen for its robust compatibility and efficiency in managing the PeliCrane's subsystems. To address the limitations in sensor capacity and data processing, the flight controller is complemented by a Raspberry Pi, enhancing the system's overall performance.

For navigation, PeliCrane relies on the Global Positioning System using an onboard component. The navigation system both includes redundant sensors to ensure reliability, and additional sensors like a more accurate barometer for atmospheric conditions and a pitot tube for measuring air speed.

The communication system of PeliCrane is supported by a high-definition Video Transmission System and a telemetry link. The camera system ensures real-time video transmission to the operator, with a range of up to 30 km, while the telemetry link can span over distances up to 40 km. These systems ensure PeliCrane can operate effectively within its mission profile. Additionally a Remote ID system is integrated to meet regulatory requirements, broadcasting the drones location and identification details.

Collision avoidance is a critical aspect of PeliCrane's operation, particularly in high risk offshore platform environments. Advanced sensors, including radar, lidar, and infrared cameras are used to detect and navigate around obstacles.

The power system of PeliCrane has a low-voltage and high-voltage group. The low-voltage system includes a battery, power distribution board, and various low-current components. A 6S Battery with a capacity of 10Ah and 22.2V voltage, is selected to ensure sufficient power for the low-voltage system. The high-voltage system powers the motors and requires careful battery sizing to meet the UAV's hover and range requirements. 12 6S 25Ah batteries are arranged in series and parallel to provide the necessary voltage and capacity, resulting in a total capacity of 6.66 kWh.

Control and Stability

Control & stability is a crucial subsystem, ensuring PeliCrane is able to navigate and perform operations autonomously. Using the above mentioned sensors as inputs, the following conclusions are drawn after an extensive analysis of the design.

Stability

Initial stability analysis shows that the system is inherently statically and dynamically unstable. To address this, precise RPM control of the propellers is essential. This stability is achieved through a flight controller capable of managing these RPMs effectively.

Static Simulation

Static simulation assesses the forces when there are no net accelerations. The simulation evaluated the effects of center of gravity (CG) shifts on stability. Results indicate that even small CG shifts require significant constant adjustments in thrust per engine, emphasising the need for precise balance to maintain performance.

Dynamic Simulation

Dynamic simulations, conducted using Python and SimuLink, further evaluated the system's behaviour under various conditions. The simulations revealed insights into the control system's performance and stability margins. Key results include:

- Take-Off Scenario: The drone model ascended to cruise altitude in 60 seconds at 60% throttle, consuming 0.125 kWh, and achieved the same in 16 seconds with a 5% increase.
- One engine inoperable: During an emergency the model is able to fly to 160m altitude, adjusting throttle on operational rotors creates a rapid z-axis rotation until 27 rad/second, assuming no angular drag and instantaneous engine response.

Operations & Logistics

Operations and logistics, involve the common operational and logistical aspects when performing cargo operations with the UAV. Examples of possible mission profiles involve ship to wind turbine cargo delivery or ship to ship cargo delivery. These mission profiles are specified in Figure 2.

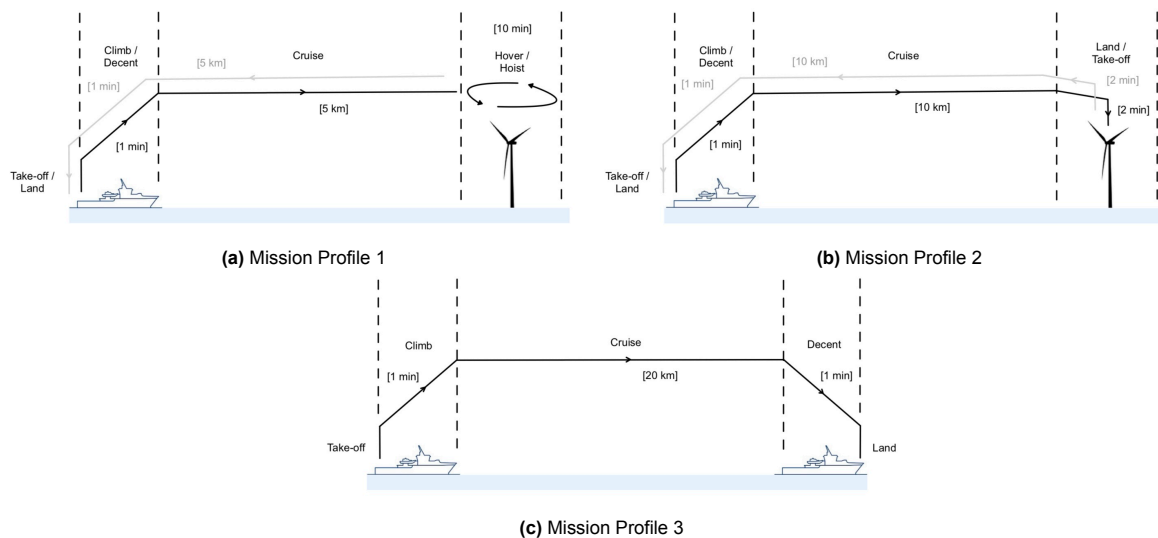


Figure 2: Mission Profile Examples

The UAV is able to hoist a payload, while hovering from a height of 8m or lower, ensuring sufficient spacing between the hoisting platform and UAV. On top of this, the dimensions of the UAV are sufficiently small such that it is able to land on top of a wind turbine hoisting platform, an area of 4x4m, or most other offshore landing/hoisting platforms. This flexibility ensures PeliCrane can be tailored to a specific mission need. Lastly it is important to note that PeliCrane has been designed with the offshore environment in mind, being able to operate in winds up to 6bft, rain, and low visibility conditions. However, the mission can be extended further, within the given flight endurance and range specifications.

In order to ensure safe, reliable, and efficient operation with as little downtime as possible, regular preventative maintenance is performed on PeliCrane. This is to extend the lifetime of components and subsequently the entire system. This regular maintenance consists of primarily visual inspections, benchmark tests and cleaning. Importantly, PeliCrane has been designed in such a way that crucial components needing frequent maintenance are accessible.

The design of PeliCrane has incorporated a fail-safe design philosophy. Where possible redundancy has been applied to components and subsystems to ensure that in the unlikely event of component failure the system remains safe. Furthermore the incorporation of a parachute system lowers the impact energy of the UAV significantly in case of rotor failure. Additionally all possible risks and their impact PeliCrane can encounter in its life time are classified and mitigated in an extensive technical risk assessment. Lastly the inclusion of an advanced collision avoidance system and ducted propeller improves upon the safety of infrastructure and ground personnel, as well as protecting PeliCrane.

The high degree of off-the-shelf components used means corrective maintenance is straightforward and cost efficient. Malfunctioning or damaged components can simply be replaced. Damaged structural elements can be manufactured using cheap methods such as laser-cutting and 3d printing. This ensures minimal downtime when maintenance has to be performed.

Financial Overview

The financial overview is designed to project potential profits over the coming years. This projection includes various expenses, such as development costs—these include labour, licensing fees, and facility rentals—and production costs, which cover the manufacturing and assembly of all subsystem components. By analysing these expenditures, the return on investment can be estimated, illustrating the projected profitability of this drone. It was concluded that total development cost is 153,000 EUR and the production costs per drone is 36,000 EUR. The market price was estimated to be 45,000 EUR. The profit depends on production rates, as more production gives more profit, the break even point was calculated to be 17 units sold. This being done the operational costs that potential customer's could encounter were also explored.

Sustainable development

Using the UN sustainable development goals as a guideline [2], sustainability has been of large importance throughout the entire design process. Sustainability strategies have been developed and enforced, such as the use of renewable materials, energy sources, crash resistance, and safety. On top of this, the design team itself adhered to sustainability strategies in order to make the actual design process as environmentally friendly as possible.

Future development

Due to the very limited time and facilities available, the design presented is only the first step in designing a functional product. Firstly, more refined models have to be developed and used to ensure a proper design. This includes methods such as more advanced Finite Element Methods, Computational Fluid Dynamics, and other advanced engineering design methods. On top of this a more robust control & stability software must be developed. With a more refined design developed, funding can be secured in order to start prototyping and testing, in order to verify the correct functioning of all components and systems, and refining the design where necessary. Once the first system prototype is constructed, rigorous testing can take place and the system can be finalised. Lastly the product assembly line can be developed, and certification, marketing and finally full production can take place with PeliCrane becoming available on the commercial market.

Contents

Executive Overview	i		
Nomenclature	ix		
1 Introduction	1		
2 Market Analysis	2		
2.1 Competitor Market Analysis	2		
2.2 Customer Market Analysis	3		
2.2.1 Market Evaluation	3		
2.2.2 Market Niche	4		
2.3 SWOT Analysis	5		
2.3.1 Strengths	5		
2.3.2 Opportunities	5		
2.3.3 Weaknesses	6		
2.3.4 Threats	6		
3 Functional Analysis	7		
3.1 Functional Flow Block Diagram	7		
3.2 Functional Breakdown Structure	7		
4 Propulsion System	10		
4.1 Assumptions	10		
4.2 Theoretical propeller performance	11		
4.3 Verification and Validation	13		
4.4 Duct Design	13		
4.4.1 Inlet	14		
4.4.2 Diffuser	15		
4.4.3 Final Duct Design	16		
4.5 Propeller Selection	18		
4.5.1 Two Sets of Two-bladed Propellers	18		
4.5.2 Off-the-Shelf four-bladed Propeller	19		
4.6 Motor Selection	21		
4.7 Sensitivity Analysis	22		
4.8 Budgets	23		
5 Structures and Materials	24		
5.1 Configuration Selection	24		
5.2 Materials	25		
5.3 Components	26		
5.3.1 Rods	26		
5.3.2 Arm Brackets	28		
5.3.3 Ducts	30		
5.3.4 Landing Gear	31		
5.3.5 Vibrations	33		
5.3.6 Payload and Winch System	33		
5.3.7 Central Box	35		
5.3.8 Electronics Box	36		
5.3.9 Parachute Box	36		
5.4 FEM	37		
5.4.1 Safety Factor and Standard	37		
5.4.2 Load Cases and Combinations	37		
5.4.3 FEM Setup	39		
5.4.4 Unducted Drone Results	39		
5.4.5 Ducts FEM	43		
5.5 Sensitivity Analysis	44		
5.6 Structures Budget	46		
6 Electronics	47		
6.1 Low-voltage Electrical Components	47		
6.1.1 Flight Controller	47		
6.1.2 Navigation	47		
6.1.3 Automatic Dependent Surveillance–Broadcast	48		
6.1.4 Communication	48		
6.1.5 Collision avoidance	48		
6.1.6 Warning System	50		
6.1.7 Winch System	50		
6.2 High-voltage Electrical Components	50		
6.2.1 Hover Requirement	51		
6.2.2 Range Requirement	51		
6.2.3 High Voltage Battery Sizing	52		
6.2.4 High Voltage Battery Management System	53		
6.3 System Integration	53		
6.3.1 Electrical Block Diagram	53		
6.3.2 Components Connection	54		
6.3.3 Placement in the Structure	57		
6.3.4 Electronics Budgets	58		
6.3.5 Wiring	59		
6.4 Sensitivity Analysis	61		
6.5 Verification and Validation	61		
6.5.1 Hover Requirement	62		
6.5.2 Range Requirement	62		
6.5.3 High Voltage Battery Sizing	62		
7 Control and Stability	63		
7.1 Stability	63		
7.2 Flight Controller Firmware	63		
7.2.1 ArduPilot Configuration	63		
7.2.2 Controllers	64		
7.2.3 Tuning	65		
7.3 Companion Computer	66		
7.3.1 Protocol	66		
7.3.2 Pseudo Code	66		
7.4 Software Block Diagram	67		
7.5 Static Simulation	67		
7.5.1 CG Shift	68		
7.5.2 Static moments	69		
7.5.3 Control resolution	69		
7.6 Dynamic Simulation	70		
7.6.1 Model Description	70		
7.6.2 Interfaces	73		
7.6.3 Scenario description	73		
7.6.4 Scenario results	73		

7.7	Sensitivity Analysis	78	10.1.1	Reliability	101
7.8	Verification and Validation	79	10.1.2	Availability	101
7.9	Control summary	79	10.1.3	Maintainability	101
			10.1.4	Safety	103
8	Final Configuration	80	10.2	Mission Profiles	103
8.1	Budget Analysis	80	10.3	Technical Risk Assessment	105
8.2	CAD Model	81	11	Sustainability Strategy	115
8.3	Performance Analysis	84	11.1	Development Strategy	115
	8.3.1 Hover Performance	84	11.2	Environmental Impact	116
	8.3.2 Cruise Performance	84	12	Production Plan	118
	8.3.3 Performance Summary	87	12.1	Components	118
	8.3.4 Verification and Validation	88	12.2	Configuration Assembly	122
	8.3.5 Sensitivity Analysis	88	12.3	Production Flowchart	125
8.4	Compliance Matrix	89	13	Future Outlook	126
9	Financial Overview	97	13.1	Gantt chart	127
9.1	Development Cost	97	14	Conclusion	129
9.2	Production Cost	98	References	131	
9.3	Return of Investment	98	A	Consulted Resources	136
9.4	Customer Operational Cost	99			
10	Operations & Logistics	101			
10.1	RAMS	101			

Nomenclature

Abbreviations

Abbreviation	Definition
ADS-B	Automatic Dependent Surveillance–Broadcast
APDL	Ansys Parametric Design Language
AWG	American Wire Gauge
bft	Beaufort
BMS	Battery Management System
BOM	Bill of Materials
BVLOS	Beyond Visual Line Of Sight
CAD	Computer-Aided Design
CAN	Controller Area Network
CF	Carbon Fibre
CG	Center of Gravity
CFD	Computational Fluid Dynamics
CNC	Computer Numerical Control
DOT	Design Option Tree
DR	Ducted Rotor
EKF	Extended Kalman Filter
EPF	Extruded Polystyrene Foam
ESC	Electronic Speed Controller
FBD	Free Body Diagram
FBS	Functional Breakdown Structure
FEM	Finite Element Modelling
FFBD	Functional Flow Block Diagram
FOV	Field Of View
GCS	Ground Control Station
GNSS	Global Navigational Satellite System
GNC	Guidance Navigation & Control
GPS	Global Positioning System
HD	High Definition
I2C	Inter-Integrated Circuit
IMU	Inertial Measurement Unit
IR	Infrared
ISA	International Standard Atmosphere
LC	Load Case
LCO	Load Combination
LiDAR	Light Detection and Ranging
MTOW	Maximum Take-Off Weight
MW	Mega-Watt
OR	Open Rotor
OTSC	Off the Shelf Component
PCB	Printed Circuit Board
PDB	Power Distribution Board
PC	Polycarbonate
PID	Proportional–Integral–Derivative
PWM	Pulse Width Modulation
RADAR	Radio Detection And Ranging
RAM	Random Access Memory

Abbreviation	Definition
RAMS	Reliability, Availability, Maintainability, and Safety
RC	Radio Control
RPM	Revolutions Per Minute
RTK	Real Time Kinematic
SAIL	Specific Assurance Integrity Level
SLS	Selective Laser Sintering
SORA	Specific Operation Risk Assessment
SWOT	Strengths, Weaknesses, Opportunities, and Threats
UAV	Unmanned Aerial Vehicle
UART	universal asynchronous receiver / transmitter
UAS	Unmanned Aerial System
UC	Unity Check
USD	United States Dollars
UV	Ultraviolet
VTOL	Vertical Take-Off and Landing

Symbols

Latin Symbols

A	Area	[m ²]
AR	Aspect Ratio	[-]
B_p	Number of Blades	[-]
C_D	Development Cost	[EUR]
C_d	Drag Coefficient	[-]
C_m	Moment Coefficient	[-]
C_T	Thrust Coefficient	[-]
C_M	Torque Coefficient	[-]
C_{fd}	Zero Lift Drag Coefficient	[-]
C_P	Production Cost	[EUR]
D	Drag	[N]
D	Diameter	[m]
D_p	Propeller Diameter	[m]
E	Energy	[J]
E	Young's Modulus	[GPa]
F	Force	[N]
g	Gravitational Acceleration	[m/s ²]
H_p	Blade Pitch	[inch]
I	Moment of Inertia	[kg/m ²]
J	Polar Moment of Inertia	[kgm ²]
K	Gain	[-]
KV	RPM per Volt	[RPM/V]
kgf	Kilogram-Force	[kg]
L	Length	[m]
l	Moment Arm	[m]
M	Moment	[Nm]
m	Mass	[kg]
N	Production Volume	[-]
P	Power	[W]
P_R	Product Price	[EUR]
p	Roll Rate	[rad/s]
q	Pitch Rate	[rad/s]
R	Radius	[m]
ROI	Return of Investment	[%]
r	Yaw Rate	[rad/s]
SF	Scaling Factor	[-]
T	Thrust	[N]
T/W	Thrust over Weight	[-]
t	Time	[s]
V	Velocity	[m/s]
W	Weight	[N]
Z	Section Modulus	[m ³]

Greek Symbols

α	Angle of Attack	[°]
α_0	Zero-Lift Angle of Attack	[°]
ΔT	Thrust difference	[N]
ϵ	Downwash Correction Factor	[-]
ζ	Damping Coefficient	[-]
η	Efficiency	[-]
λ	Blade Lift Correction Factor	[-]
ϕ	Roll Angle	[rad]
ψ	Yaw Angle	[rad]
ρ	Density	[kg/m ³]
ρ_A	Area Density	[kg/m ²]
σ	Stress	[N/m ²]
σ_d	Duct Diffuser Ratio	[-]
τ	Shear Stress	[N/m ²]
θ	Pitch Angle	[rad]
ω	Angular Velocity	[rad/s]
\mathbb{T}	Rotation Matrix	[-]

1. Introduction

The offshore wind energy sector is rapidly expanding, leading to increased maintenance needs for offshore wind turbines, including the efficient delivery of tools and materials to turbines. The development of Vertical Take-Off and Landing (VTOL) technology for Unmanned Aerial Vehicles (UAV), marks a significant advancement in the field of offshore operations. Recent years have witnessed a shift towards using UAVs for wind turbine inspections [3], and there is growing interest in utilising UAVs for transporting maintenance supplies, thereby reducing costs. This technology promises to revolutionise the way offshore logistical tasks are performed, by providing a flexible and efficient means of transportation and delivery. The ability to operate in a more sustainable manner, combined with the capability to hover and perform precise movements, makes UAVs an ideal solution for various offshore applications.

The primary purpose of this project is to design, analyse, and develop an efficient and reliable UAV tailored for offshore operations. The focus is on creating a system that can withstand harsh environmental conditions while ensuring safety, reliability, and performance. The UAV, dubbed PeliCrane, is intended to assist offshore personnel by carrying a standard 25kg payload on platforms and delivering payloads over longer distances. It must operate efficiently in cruising mode for at least 5km and in hovering mode for at least 30 minutes.

First, Chapter 1 introduces the project. Chapter 2 presents a thorough market analysis to understand the demand and requirements for VTOL platforms. Chapter 3 covers the functional analysis, detailing the operational capabilities and requirements of the system. In Chapter 4, the propulsion system design and detailed aerodynamics are discussed, highlighting the theoretical and practical aspects of propeller performance and duct design. Chapter 5 examines the structural design and material choices. Then, Chapter 6 describes the electronics of the system, which covers critical components such as the flight controller, navigation systems, and communication infrastructure. Chapter 7 focuses on control systems essential for stable flight. Chapter 8 presents the final configuration along with budget and performance analyses. The subsequent Chapter 9 addresses the financial overview, including market growth, production and operational costs, and revenue projections. Chapter 10 outlines operations and logistics considerations, and Chapter 11 discusses sustainable development strategies and their adherence to UN's Sustainable Development Goals. Finally, the report concludes with a comprehensive production plan and overall conclusions in Chapter 12 and Chapter 14, respectively. Additionally in the Appendix, consulted references are listed and a project Gantt chart is formulated.

2. Market Analysis

To make sure the PeliCrane fits the market needs, it is valuable to perform a market analysis. This allows to gain insights into existing challenges and potential solutions. The analysis was divided into a competitors market analysis, as in Section 2.1, which considers existing drones and companies. Then a target market was described in terms of the market evaluation and market niche in Section 2.2. Both include an overview of the current situation, trends and predictions for future development. The analysis is concluded with a pragmatic approach of a SWOT analysis in Section 2.3.

2.1. Competitor Market Analysis

The identified global competitor market for this product is the drone market. The markets global value is estimated to be 19.89 billion USD in 2022 and is expected to grow at a compound annual growth rate of 13.9% from 2023 to 2030 [4]. This is due to an expanded range of applications in various industries, and technological advancements in areas such as electronics. The more specific market category is short- to medium-range delivery and logistics. This includes cargo drones for which the distinction can be made between: Hybrid wing (wing and propeller based lift), Fixed (wing based lift) or Rotary Wing (propeller based lift). This is visualised in Figure 2.1. When looking at the figure it instantly becomes clear that the rotary wing sector shall grow the quickest. The most important conclusion that can be drawn is that the market revenue for all three configuration types will grow significantly. This is confirmed by the forecast of the total value of the worldwide cargo drone market, which is assumed to grow exponentially from 828 million USD in 2023 to 17.88 billion USD in 2030 [5].

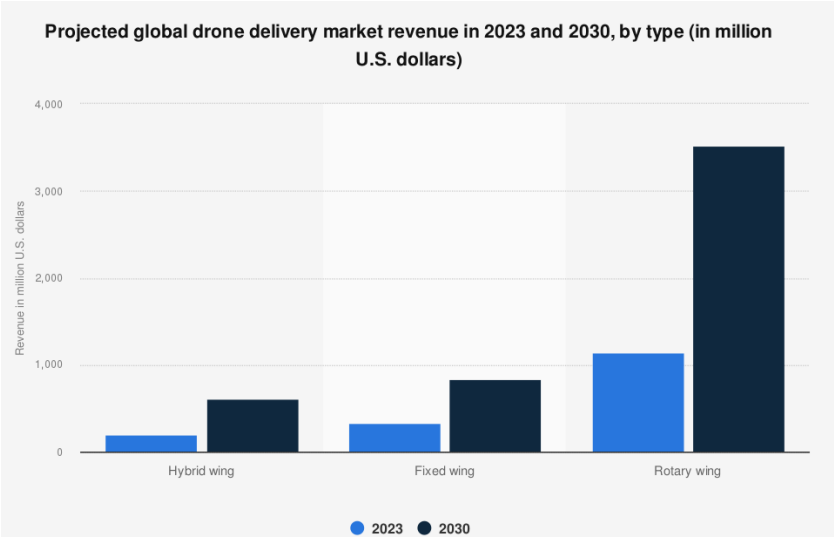


Figure 2.1: Prediction on Market Revenue by Drone Type[6]

Subsequently, the key competitors in the market are identified, with DJI being the most prominent. DJI, a Chinese company, dominates the global drone market with a 76% market share [1]. It offers a wide range of high-quality drones for professional and consumer use, featuring obstacle avoidance, 4K cameras, and GPS. DJI specializes in agriculture and delivery, leveraging its scale to offer competitive prices through mass production. However, its access to specific markets can be limited by political factors, such as the U.S. sanctions imposed in 2021 [7]. Other significant players, including Autel Robotics, Parrot, and Yuneec, each hold market shares below 6% and primarily offer camera drones [1].

In conclusion, considering the specialisations of DJI and similar companies, the delivery and cargo segments remain underexploited. Another opportunity lies in providing a drone suited for specific environments, such as offshore operations. Given the higher humidity, salinity rates, and potential wind gusts, a drone explicitly designed for these conditions would create a reliable tool for companies operating in such challenging environments [8]. This gives the PeliCrane a competitive advantage over the standard general cargo drones.

The analysis of the competitor market also requires to inspect the products from other companies to provide insights in an estimation for a competitive price as well as the current status of performance. Among them those that have the most compatible configurations and similar payload, range and endurance requirements were selected. Their characteristics are provided in Table 2.1.

Table 2.1: Characteristics of Compatible Drones

Drone Model	Payload [kg]	Endurance [min]	Range [km]	MTOW [kg]	Cost [USD]	Cost/MTOW [USD/kg]
Freefly Alta X	15	11	NA	35	25650	733
DJI FlyCart 30	30	18	16	95	21200	223
FB3 Heavy-Lift Multirotor Drone	100	NA	2.5	170	76900	452
HLM Industrial Octocopter	30	17	11.5	72	36500	507
Aurelia X6 MAX	6	69	5	16	8400	525
Hercules 20	15	15	NA	50	13900	278

Even though the reference drones can carry similar amount of cargo, they are of different scales as can be seen in Table 2.1. In order to estimate a cost of the new drone, the cost per mass was calculated in the last row. Its average is 453 USD/kg. The most similar available product on the market that has similar mission capabilities and scale is the DJI FlyCart 30. Therefore, the MTOW of the PeliCrane is estimated to be 100 kg and its competitive price is set to 45,000 USD, based on the average normalised cost of the similar drones.

2.2. Customer Market Analysis

The drone designed in this project is intended for cargo services within the offshore environment. In order to make sure the design is compatible for this use it is of utmost importance to bring the market needs into perspective and assess the competitive landscape. Potential industries for the offshore environment entail maritime logistic companies, offshore platforms and rigs, renewable energy companies, defence applications and delivery to remote communities with limited access. Essentially, the potential use entails transportation of cargo to and from any type of offshore platform.

2.2.1. Market Evaluation

An identified most promising market is the offshore wind energy market. Currently there is a rising demand for renewable energy sources and lowering carbon emissions. The global market for offshore wind energy was worth 33.52 billion USD in 2021 and is experiencing an increase in the following years as shown in Figure 2.2 [9]. The global energy production is estimated to reach 630 GW in 2050, growing from 40 GW in 2020 [10]. Important to note is that while the product is intended to target the offshore wind energy market, its cargo transportation capabilities can be utilised in many fields. If it succeeds in the designated market, its use can be extended to the above-mentioned contexts.

The global wind energy market can be segmented on the basis of region as can be seen in Figure 2.2. The respective regions are North America, Europe, Latin America, Middle East & Africa and Asia Pacific. Comparing the regions, Europe is leading and will be the easiest to access as the cargo drone will be mainly manufactured and fully assembled in Europe. However, Asia Pacific has the greatest growing potential and will therefore be worth exploring further [10]. The key companies acting within the global

wind energy market are [9]: *ABB, DEME, Doosan Heavy Industries and Construction, EEW Group, Envision, General Electric, Goldwind, Hitachi, Ming Yang Smart Energy Group Co., Nexans, Nordex SE, Rockwell Automation, Shanghai Electric, Siemens Gamesa, and Vestas*. These could be potential customers considered in the global scope for the UAV.

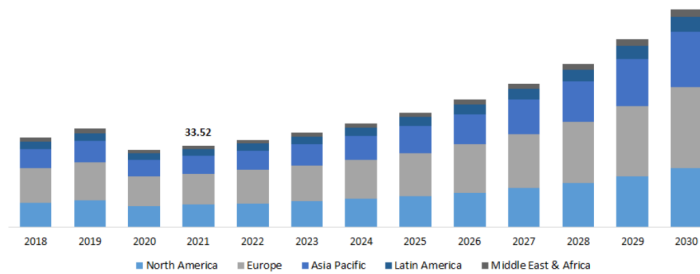


Figure 2.2: Offshore Wind Energy Market size in billion USD [9]

Within Europe, the offshore wind energy market in the Netherlands is one of the biggest and fastest growing on the continent. The Government of the Netherlands has set a goal for the energy supply to be climate neutral by 2050 [11]. Its offshore wind electricity supply currently equals to 4.7 GW and by the end of 2032 the Government wants to increase this to 21 GW [12][11]. One of the biggest companies acting in this field is Vattenfall. It owns Hollandse Kust Zuid, the biggest offshore wind farm in the Netherlands. The offshore wind farm consists of 139 Siemens Gamesa 11MW wind turbines with blades of 97 m long and a tip height of 225 m from sea level [13]. The vehicle could serve as a versatile support for this offshore wind farm maintenance and operations.

2.2.2. Market Niche

As the offshore wind energy market exhibits high potential for expansion, it requires new technologies and operational solutions. The identified area within that market is wind turbine maintenance. As with every operational machine, wind turbines are subject to failures and require repairs. Routine inspections have to be carried out to check the current health of the system and perform preventive maintenance. This preventive maintenance can exist of replacing parts, making adjustments, and/or adding lubricants. Therefore, it requires the provision of relevant tools, electronic components, and maintenance substances such as oils and grease. Current operations heavily rely on manual labour by technicians, whom are transported by boat or helicopter, together with the use of cranes. This reliance drastically increases costs and slows down operations. On top of this, according to regulations, one male worker is allowed to deal with a maximum 25 kg of payload, for female workers this is 16 kg [14]. Therefore, an optimal solution to help these technicians is a drone that can rapidly transport payload 25 kg to and from turbines and vessels. This disqualifies means of transport such as helicopters that are optimally used for higher payloads.

Globally, most of the offshore wind turbine installations are done in shallow water due to accessibility and foundation requirements. However, deep water locations are becoming more popular, which makes the use of a cargo drone even more vital [9]. Moreover, once floating wind turbines are being implemented, they can be placed at any depth as they are not fixed to the sea bed shelf. The use of an offshore cargo drone will be a flexible way of transporting cargo to these turbines. Additionally, transporting the payload between the vessels and platforms is also burdened by the multiple operators involved. Having multiple parties involved can cause potential delays because the scheduling will need to align. Apart from that, the operations such as the installation of a crane is connected to a high expense. The above outlined problems can be solved by the use of an UAV. Firstly, it will reduce the involvement of the human workforce with direct air paths between the storage and the target locations. Secondly, it does not need additional infrastructure for full operations. A level surface with aerial clearance suffices. Finally, such a vehicle is mostly a fixed one-time cost and maintenance is drastically lower than current solutions with high offshore employment costs. The information for the niche identification and the current solutions in the field was conveyed to the team via consultation with Dr. Daniele Ragni and Dr. Donatella Zappalá.

The customers will benefit by implementing the drone solution for offshore cargo transportation. As already described, not only will it enhance and assist in operations, but it will lower the cost. This is especially relevant in the Dutch offshore wind energy market where the employment costs are very high. The drone will make sure that cargo can be transported to the wind turbine with a higher speed compared to the existing solution of transporting it by boat which takes up at least 3 times as much time. In the case of corrective maintenance, the wind turbine is inoperable until the maintenance has been executed. In order to reduce the downtime, and thus the loss in revenues, it is of great importance that the cargo for maintenance is transported as quickly as possible. Therefore, the drone will decrease the valuable downtime of the wind turbine by at least a third. Apart from saving cost through time, the drone will save cost by reducing the amount of offshore workers that need to be present to transport cargo. Assuming that one drone can contribute the work equivalent of one wind turbine technician, the company can save about 40,000 EUR for the yearly salaries [15]. This is very conservative estimation resulting in the value similar to the market value of a drone.

2.3. SWOT Analysis

In order to conclude the market analysis, a pragmatic approach of a SWOT analysis will be used to bring the strengths and weaknesses of the cargo drone into perspective in the context of the current potential opportunities and threats in the market. In an ideal situation, the strengths of the new design shall be protected against all threats. The aim is furthermore to mitigate the weaknesses to counteract as many of the threats as possible and to set up measures to prevent the weaknesses from threatening the opportunities. Moreover, the strengths shall be exploited to maximise the opportunities. Considering these elements are significantly reliant on each other, performing a SWOT Analysis will not only clarify and give a visual clear overview, but it will also give great insight in the overall reliability of the project. Looking at Figure 2.3, the internal factors of the project itself, such as the UAV's strengths and weaknesses, are at the top side of the diagram. On the bottom of the diagram the external factors, the opportunities and threats, that the project might encounter are listed.

2.3.1. Strengths

One of the strengths of the PeliCrane is that its relatively small size (2.7x2.7 m) makes it possible to land on any flat surface of approximately the span of the UAV. Therefore, no helipad is needed and the UAV can be used on numerous different offshore platforms regardless of their applications. This will create flexibility in purpose and enlarge the amount of potential customers. Another strength is that it will be able to carry the maximum amount of payload that is allowed to be carried by one person. This will make sure that the person on the wind turbine will not have to carry more than allowed, and it will allow for multiple applications. The third strength is that the UAV will be designed for offshore environments specifically. In marine atmospheres, the salinity rate fluctuates significantly (<5 to >300 mg Cl^- $\text{m}^{-2}\text{d}^{-1}$) [16]. Considering the salinity rates in the atmosphere cause a corrosive environment, the design will be adapted to be able to withstand these rates to ensure the material properties do not get adversely affected through corrosion. Apart from the salinity, the humidity in the offshore environment also increases the corrosion rate significantly [17]. As the design of the UAV will be designed to withstand the discussed humidity, saline corrosive environment, it will go hand in hand with the opportunities that flow out of the growing offshore wind energy market.

2.3.2. Opportunities

Opportunities become clear when looking at the market niche, as discussed in Subsection 2.2.2. The offshore wind energy market is expanding rapidly, as is discussed in detail in Subsection 2.2.1. The alternative solutions for transporting offshore cargo in this market now consist of time consuming methods such as boats and helicopters, which increase the amount of downtime of a wind turbine and cause great losses of revenues. The drone will reduce the valuable downtime by a third, which creates a great opportunity to decrease the losses of revenues. Apart from time, it will save on man-hours as less workers are required when using the cargo drone, the estimation of reduction in cost has been discussed in Subsection 2.2.2. Another opportunity flows from the demand for a sustainable solution for transporting offshore cargo. A sustainable development strategy, explained in Chapter 11, has been set up such that the drone will be designed in the most sustainable way possible and the environmental impact is minimised. It is certain that the drone will have a significantly reduced environmental impact com-

pared to the highly polluting vessels and helicopters, which are currently used for transporting cargo for offshore wind turbine maintenance. Lastly, as was discussed in Section 2.1, the competition in the European market is relatively small which opens doors to lots of potential customers in the offshore wind energy market.



Figure 2.3: SWOT Analysis of the PeliCrane

2.3.3. Weaknesses

Regarding the weaknesses, the dependence on the weather conditions shall not limit the flexible logistic planning since the drone shall be designed to be able to handle 6 bft wind speeds. Looking at atmospheric conditions measured at the meteorological stations on the North Sea coast for reference, the mean wind speeds are 7.8 m/s (measured at 18.5 m height in Ijmuiden) and 7.5 m/s (measured at 15.0 m height in Hoek van Holland)[18]. This measured mean wind speed is verified to represent the atmospheric conditions offshore by means of comparison between offshore measurements and these averages [18]. Converted to Beaufort the average wind speed equals 4 bft, which is much lower than the 6 bft wind speed for which the drone is designed. This shows that the drone will be able to fly in the average encountered weather conditions and thus this weakness will only influence the operations during extreme weather conditions. Another characteristic of the drone that can be seen as a weakness is the limited amount of range. However, this can easily be solved by planning the operations accordingly. The drone will be able to reach the wind turbines 3 times faster than the current solutions do, therefore there is much time left over to recharge by landing on a vessel, or to quickly swap batteries. The most important weakness that should be accounted for is the lack of brand presence. Even though the competitions in the European market is relatively small, the brand awareness will make sure that the reputation will last. Before the manufacturing of the drone starts, the offshore companies will need to be updated on this new solution for delivering the cargo to wind turbines such that all potential customers are aware of all of the advantages that are mentioned here.

2.3.4. Threats

An important threat to consider is the competition in the drone market. Currently, competition in the European market is relatively small, as shown in Section 2.1. However, this could change if European drone companies shift their focus to the offshore market in the future. Thus, the threat is potential rather than immediate. Additionally, economic fluctuations pose a potential threat. Since this cannot be mitigated, a solid investment plan is essential to ensure the UAV project remains unaffected by such fluctuations. The financial overview in Chapter 9 is a strong foundation for this plan and should be updated to account for future economic changes.

3. Functional Analysis

A functional analysis serves as a tool to identify the functions and tasks to be performed during the mission, as well as the interconnectivity and dependencies between these. This is a critical step in the design process because it offers a clear overview of the system's life cycle, breaking down the process into manageable components and detailing the necessary inputs and outputs for each phase. This analysis comprises two main sections: the Functional Flow Block Diagram and the Functional Breakdown Structure, as detailed in Section 3.1 and Section 3.2 respectively.

3.1. Functional Flow Block Diagram

The first step of a functional analysis involves conducting a Functional Flow Block Diagram (FFBD), which is essential for illustrating the flow and will later be used to specify capability. The diagram depicts all the relevant functions the system must perform during the mission, arranged in chronological order. Figure 3.2 displays the FFBD, which comprises four different levels of detail. The first level, indicated in dark blue, presents the overall process. The second level outlines the various categories of the mission in logical order. Some steps divide into either an AND or an OR junction, indicating either a parallel process or an optional functional path, respectively.

The FFBD provides a visual representation of the sequential steps and interactions involved in the operations of the drone. It outlines the logical progression of tasks and interdependencies between components, enabling the optimisation of operational efficiency and workflow. By analysing the FFBD, insights can be gained into the drone's operations, identifying areas for design improvement and maximising the effectiveness of offshore logistics.

3.2. Functional Breakdown Structure

The Functional Breakdown Structure (FBS) follows from the FFBD, providing a hierarchical view of the mission. This diagram illustrates all the potential steps for the mission, mapping out continuous actions during the mission and subsequent phases. The FBS is shown in Figure 4.2. This hierarchical tree form provides a clear view of each component's specific function, ensuring that each fulfils its role effectively and efficiently, and that the system as a whole can achieve its intended objectives.

In the FBS, the first level outlines the UAS' lifecycle. At the second level, only operations are extensively elaborated upon, as the mission profile is outlined in the FFBD. Then, at the third level, categories such as Emergency Response and Electrical Handling are added, which are not depicted in the FFBD. This is done because the system should be capable of performing these functions, even though they do not occur at one specific point in the nominal mission profile. Furthermore, at the fourth and fifth levels, not every block is represented in the Flow Diagram, for the same reason as mentioned before. Examining the Functional Breakdown Structure helps define tasks clearly, allocate resources appropriately, and ensure the system meets functional requirements for successful logistics operations.

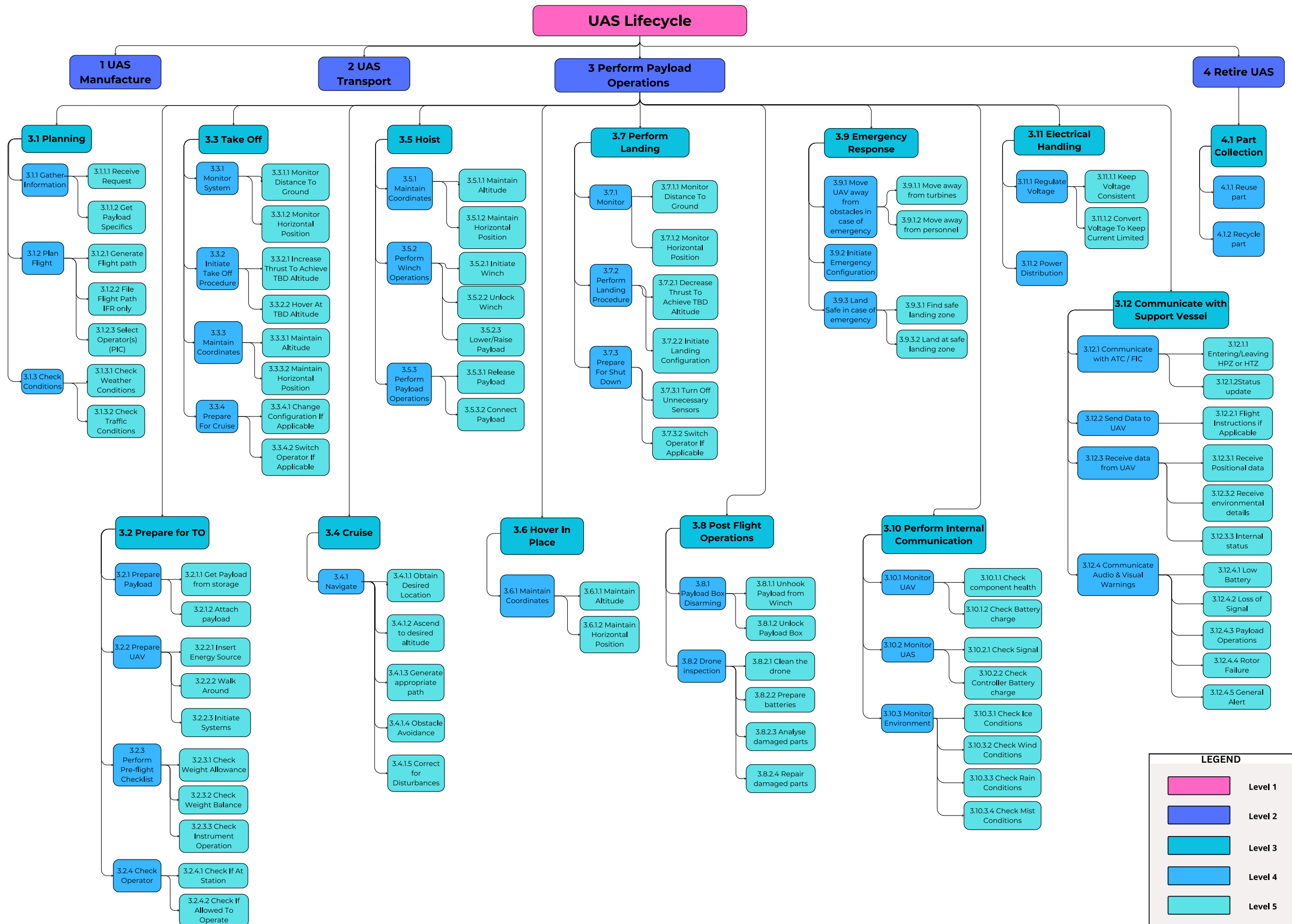


Figure 3.1: Functional Breakdown Structure

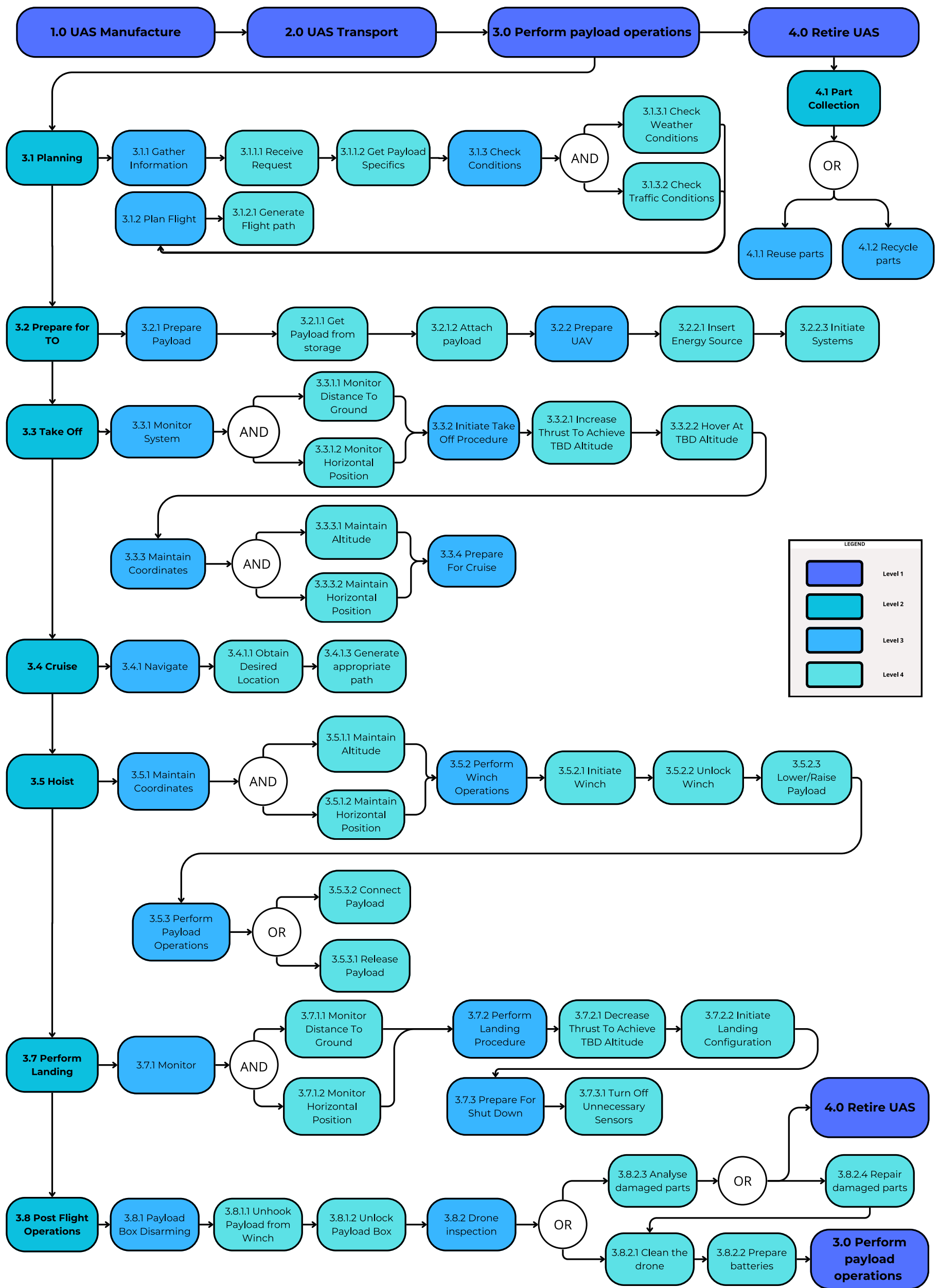


Figure 3.2: Functional Flow Block Diagram

4. Propulsion System

The propellers will need to be able to provide enough thrust such that the drone can execute the mission in the most efficient way possible. The propeller and motor combination will be designed for hover. In order to define the optimal propeller and motor selection, research is conducted on the performance of certain combinations while taking into account that the duct will enhance the performance. The challenging aspect of the design is that the propeller will be four-bladed, which is different from a conventional two-bladed quadcopter. By adding two blades, the rotor size can be decreased and the rotational speed can be lowered. Lowering the rotational speed will make the drone safer, as the tip speed is reduced, and it will reduce the noise of the drone which will increase safety.

4.1. Assumptions

From a detailed trade-off process, it was decided to have a four-bladed propeller design to produce the thrust required for the UAV design. This has been decided because of the lower RPM and therefore lower tip speed, as well as the smaller cross sectional area required for the same amount of thrust. Regarding the range in size, in the previous design phase, using the actuator disk theory, the blade diameter was estimated to be 1.2 m. Serving as a starting point for the propeller selection.

A four-bladed propeller design comes with a practical drawback in the form of propeller availability. Due to the difficulties in manufacturing precise and balanced four-bladed propellers, as well as their uncommon use in UAV design, little to no manufacturers produce four-bladed propellers and provide specifications or details regarding their experimental performance. Moreover, the aim of this design is to have as many off the shelf parts as possible, therefore developing a unique design is not considered.

To however still be able to incorporate a four-bladed propeller design, research is conducted on the feasibility and performance of attaching two propellers together in order to create a four-bladed rotor design. As the stacking distance is very small, compared to the large rotor diameter due to the small thickness of commercially available propellers, the blades are assumed to be co-planar. Therefore, the aerodynamic effects due to this stacking [19] [20] are not considered. Furthermore, these complex flow interactions cannot be solved analytically and require CFD simulation, which is beyond the scope of this project.

Apart from the blade interaction, the assumptions used regarding the propulsion system are given in Table 4.1. Categorising the effect of each of these assumptions is difficult due to the complex aerodynamic interactions beyond the scope of this design. These assumptions act as a way to simplify the design process.

Table 4.1: Assumptions Propulsion System

Identifier	Assumption
ASM-PS-01	The components of the propulsion subsystem are all rigid and show no change in aerodynamic characteristics.
ASM-PS-02	The environmental conditions (density, temperature, viscosity, etc.) the drone operates in are constant and equal to ISA at sea-level conditions.
ASM-PS-03	The thrust and moment coefficient of the propellers do not vary with increasing RPM. [21]
ASM-PS-04	The drone is aerodynamically equivalent to a cuboid. [21]
ASM-PS-05	The drag coefficient of the drone in all directions is equal to 0.80.
ASM-PS-06	The thrust acts perpendicular to the propeller at all pitch angles.
ASM-PS-07	The aerodynamic interference effects of stacking two, two-bladed propellers are not considered
ASM-PS-08	The aerodynamic interference effects between propeller blades are not considered.
ASM-PS-09	The flow is considered to be incompressible
ASM-PS-10	Effects of inflow velocity due to UAV speed are not considered
ASM-PS-11	The aerodynamic interference effects between the propeller blades and drone fuselage (except the ducts) are not considered.

4.2. Theoretical propeller performance

As mentioned in Section 4.1, limited information is available on the experimental performance of four-bladed propellers, causing the conventional straightforward approach of selecting a motor-propeller combination based on given performance specification [22] cannot be used. Therefore, an approach derived from theoretical aerodynamics relations has to be used. These theoretical relations first have to be developed. For this, a method derived from blade element theory is used [21]. In this method, the thrust and torque of a propeller can be calculated based on given constants and blade parameters. The thrust is given as:

$$T = C_T \rho \left(\frac{RPM}{60} \right)^2 D_p^4 \quad (4.1)$$

$$M = C_M \rho \left(\frac{RPM}{60} \right)^2 D_p^5 \quad (4.2)$$

with D_p being the propeller diameter, C_t and C_m being the thrust and moment coefficients respectively which can be calculated as:

$$C_T = 0.25\pi^3 \lambda \zeta^2 B_p K_0 \frac{\epsilon \arctan\left(\frac{H_p}{\pi D_p}\right) - \alpha_0}{\pi AR + K_0} \quad (4.3)$$

$$C_M = \frac{1}{8AR} \pi^2 C_d \zeta^2 \lambda B_p^2 \quad (4.4)$$

The constants from Equation 4.3 and Equation 4.4 are given in Table 4.2 and are based on aerodynamic and geometrical properties [21].

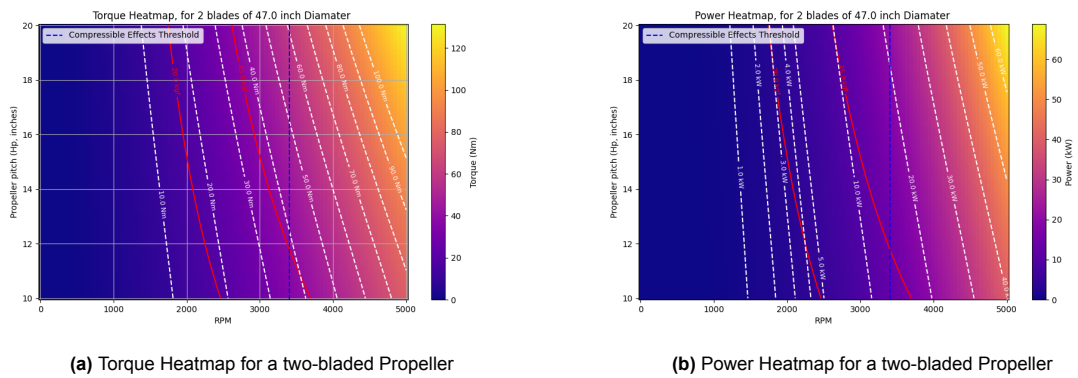
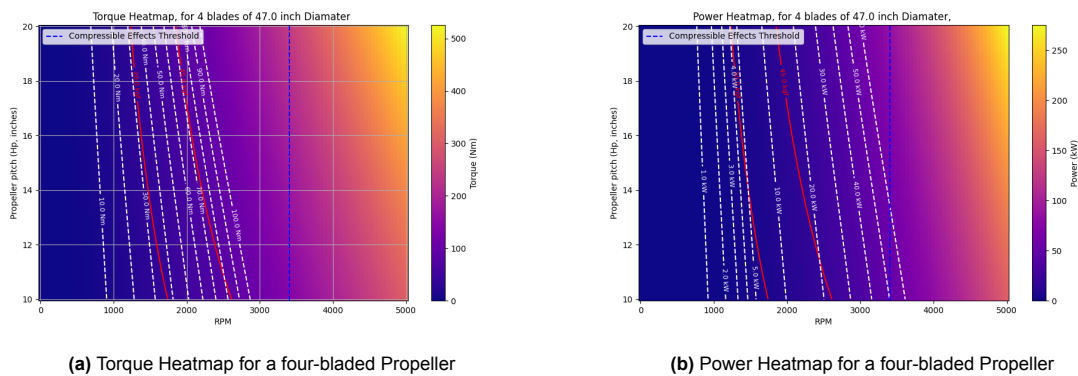
Table 4.2: Aerodynamic Constants [21]

Constant	Value	Explanation
A	5	Aspect Ratio
ϵ	0.85	Oswald Efficiency Number
λ	0.75	Taper Ratio
ξ	0.55	Twist Angle
e	0.83	Span Efficiency Factor
C_{fd}	0.015	Drag Coefficient
α_0	0	Zero-lift Angle of Attack
K_0	6.11	Lift Coefficient

Using this equation, with a fixed diameter, the number of blades B_p , the blade pitch H_p and the RPM can be varied. With this model, the relationship between these variables can be identified. Furthermore, using Equation 4.5, the power required for the propeller can be found.

$$P = \frac{2 \cdot \pi \cdot RPM \cdot T}{60} \quad (4.5)$$

The results can be plotted in the form of a heatmap, as a function of the propeller pitch and RPM, for both a two-bladed propeller and a four-bladed propeller, shown in Figure 4.1 and Figure 4.2 respectively.

**Figure 4.1:** Torque and Thrust Heatmaps for a two-bladed Propeller**Figure 4.2:** Torque and Thrust Heatmap for a four-bladed Propeller

The red lines indicate the thrust required for a T/W of 1:0 and 2:0, which results in a thrust of 22 and 44 kgf respectively. With the weight calculated as per the preliminary weight estimation in the previous

design phase. The dashed lines indicate the isolines with the value indicated at the side. Furthermore, it is found that compressible effects occur at a tip speed of Mach 0.7 [23]. This is plotted as the dashed blue isoline, where the propeller performance is significantly reduced.

The area between the dashed red lines therefore indicates the theoretical design space for the propeller selection, indicating the combination of pitch and RPM possible to meet the T/W requirement. Furthermore, comparing Figure 4.1 and Figure 4.2 it is evident that lower RPM can be achieved for the same T/W requirement, confirming the desired result. However, this occurs at a higher torque and power required, as the propellers need to perform more aerodynamic work.

4.3. Verification and Validation

In order to verify this method, the analytical results as seen in Figure 4.1 and Figure 4.2 are compared against available propeller and motor test data [22] [24] [25]. The results of this comparison are tabulated in Table 4.3. Δ_T is the difference between simulation and experimental results thrust (%) and Δ_M is the difference between simulation and experimental results torque (%).

Table 4.3: Difference in Propeller Thrust and Torque

Diameter (inch)	Pitch (inch)	RPM	Δ_T	Δ_M
57	19	1230	1.22	54.72
42	14	1510	22.59	97.71
34	11	1920	-8.23	15.78
48	17.5	1792	21.61	61.04
36	11	1608	-7.74	22.08
47	18	1320	8.80	53.93
40	13.1	1843	1.35	53.75
56	20	1091	17.47	69.49
20	6	2158	13.83	70.14
24	8	2455	-12.58	-18.32
21	6.3	1859	-1.54	51.32
Total average			4.3	48.3

From this validation it is evident that while the analytical and experimental results for thrust coincide, the results for torque, and thus the results for power are off by an approximate factor of 1.5. This can be explained by the assumptions taken with respect to the aerodynamics constants Table 4.2. The method used [21] is verified for smaller scale propellers, and therefore these aerodynamic constants are verified for smaller scale propellers. Aerodynamic effects introduced with larger scale propellers are therefore not taken into account in these constants. Therefore, while serving as a good indication of the relative performance difference between two and four-bladed propellers and the relevant design space, the results cannot be used directly for exact propeller and motor selection.

Instead a different approach based on relations in Equation 4.3 and Equation 4.4 together with available propeller experimental data will be used to omit the influence of the aerodynamic constants. This approach will be further explained in Section 4.5.

4.4. Duct Design

In the previous design phase, it was decided that the propellers will be ducted for safety. A duct, while adding weight and drag, can increase the efficiency of the propeller by generating lift when accelerating the velocity of the airflow over the duct inlet and diffusing the rotor wake. The main parameters affecting the performance of a generic duct design are shown in Figure 4.3. As can be seen, a duct generally consists of a duct inlet, a throat in which the propeller shall be positioned and a diffuser with a certain diffuser angle. In order to realise a duct design which positively enhances the performance of the propellers, the duct will need to be shaped in detail while taking into account the aerodynamic effects. It is decided to optimise the efficiency gain of the duct, while making sure that the additional weight is as little as possible.

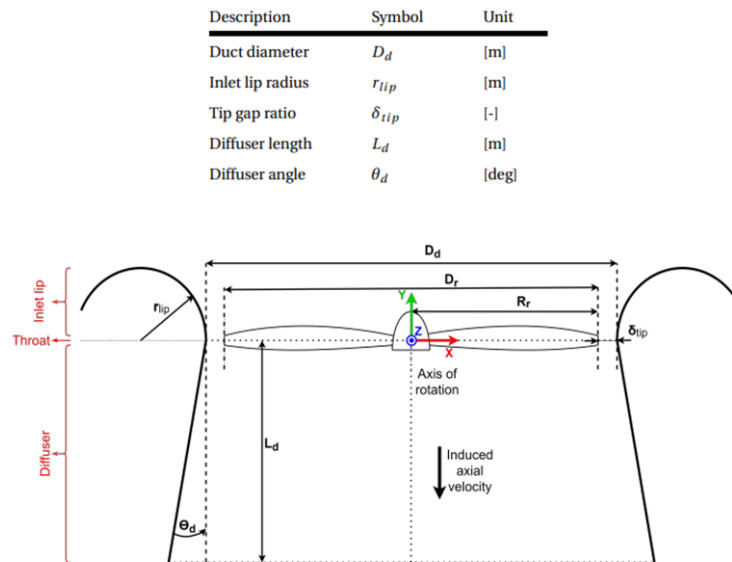


Figure 4.3: Duct Design Parameters [26]

One parameter that can be defined already is the tip clearance, represented by the tip gap ratio δ_{tip} . This clearance will need to be as small as possible such that there will be as little space as possible for potential tip vortices. These tip vortices occur without a duct because of the pressure difference between the top and bottom side of the propeller, and will cause efficiency losses [26]. Typical propeller blades have a taper, where the root chord is thicker than the tip in order to have a lower pressure difference between top and bottom blades of the propeller at the tip, reducing the prevalence of tip vortices. Ducted propellers therefore do not require this taper, and therefore can be made (nearly) straight, increasing the total lift production. However, the focus on off-the-shelf components, and the lack of straight propellers at this size available means this is not considered.

The limiting factor for the clearance will thus not be aerodynamic effects, but rather structural tolerances such that the rotor blade will maintain sufficient distance from the duct throughout all potential loading scenarios.

4.4.1. Inlet

Regarding the inlet of the duct a lot of variations of the design can be found. Several experiments where the duct inlet is shaped elliptically [27] or the entire duct is shaped like an airfoil [28], with inherent advantages and disadvantages specific to the design. The common benefit is the additional thrust is generated by the duct inlet, where air is accelerated along the inlet, lowering the pressure and generating lift similarly to an airfoil, as can be seen in Figure 4.4. Apart from that, it creates a consistent inflow velocity in situations with variable amounts of wind.

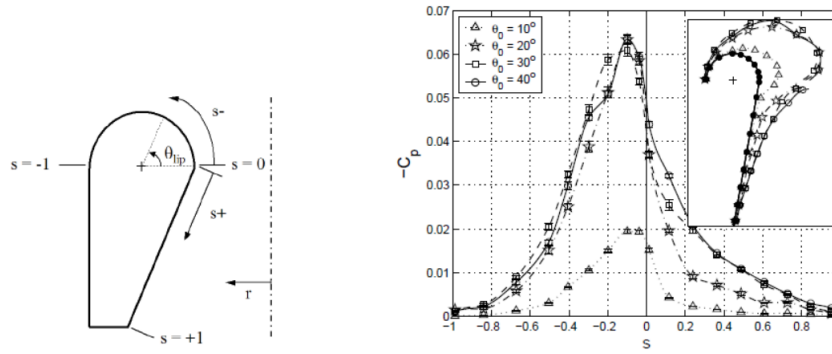


Figure 4.4: Pressure Distribution of a Duct [29]

The efficiency gain for the duct design specific to this UAV design is difficult to determine analytically, as complex numerical simulations (CFD) are necessary to properly model the flow interactions inside and outside the duct. Therefore literature has been consulted in order to find an ideal duct design. As explained, the duct inlet provides the acceleration to the air entering the duct, providing a lift force. The inlet should be shaped in such a way that the resultant lifting force points in axial direction.

In terms of influence on performance, the accelerated inflow velocity will lower the effective angle of attack of the blade, visualised in Figure 4.5. This can be related in terms of trigonometric relations, such that the exact influence on the propeller performance can be determined. This will be explained in great detail in Section 4.5 together with the discussion of the effects it has on the chosen propellers.

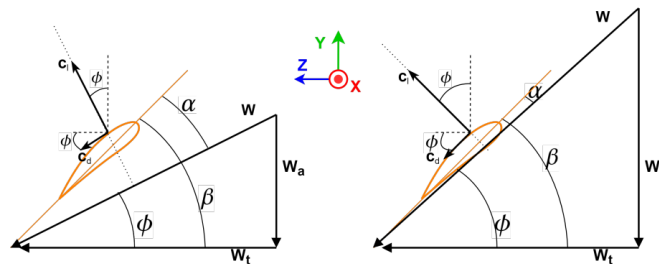


Figure 4.5: Effective angle of attack decrease[26]

4.4.2. Diffuser

The diffuser section, below the propeller increases the efficiency of the propeller by restricting the contraction of the rotor wake. According to actuator disk theory, the wake of an open rotor has an increased velocity than that of a ducted rotor, where the diffuser restricts the contraction of the rotor wake. This is associated with a decrease of kinetic energy and increased pressure and therefore less power lost by the rotor disk. Furthermore, the small clearance between the rotor blades and diffuser wall reduces the prevalence of tip vortices, reducing pressure losses of the propeller blades and increasing the propellers efficiency [26]. The performance gain from the diffuser section can be determined through application of propeller disk theory and conservation of momentum laws, and can be given as [29]

$$\frac{P_{iDR}}{P_{iOR}} = \frac{1}{\sqrt{2 \cdot \sigma_d}} \left(\frac{T_{DR}}{T_{OR}} \right)^{3/2} \left(\frac{A_{OR}}{A_{DR}} \right)^{1/2} \quad (4.6)$$

with i for ideal, DR Ducted Rotor, OR Open Rotor, and σ_d the expansion ratio, given as:

$$\sigma_d = \frac{\text{Duct Exit Area}}{\text{Duct Throat Area}} \quad (4.7)$$

It is clear that the larger the expansion ratio, the better the ducted rotors performance. The expansion ratio is proportional to the diffuser angle and the diffuser length. However, it is decided that in order to not introduce a significant amount of additional drag during cruise, the diffuser length is limited by the overall thickness of the drone. On top of this additional weight is introduced, negatively impacting the hover performance.

Using a simplified cuboid model of the drone, it is found to calculate the drag using a simplified cuboid model as assumed in Table 4.1 with an angle of attack of 30° and a flight velocity of 20 m/s, requires 5% more power during cruise each time the diffuser is extending 0.1 m beyond the thickness of the drone.

As can be seen in Figure 4.6, the power efficiency gain of including a diffuser in an unducted rotor design is plotted as a function of the diffuser angle theta and diffuser length DL, as per the conventions shown in Figure 4.3.

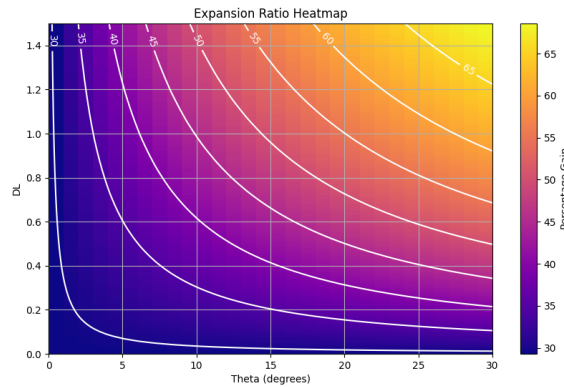


Figure 4.6: Power Efficiency Gain

The white isolines in Figure 4.6 show the percentage gain in power. It is evident that for the same angle increasing the length by the 0.1m stated before results in an efficiency gain of less than 5%. The large diffuser angle required to have the beneficial performance gain at identical diffuser lengths would introduce the risk of flow separation within the diffuser section, introducing turbulent vortices significantly reducing performance [26].

From these considerations, it is decided that the duct diffuser should be limited to the drone body thickness, and to avoid the risk of flow separation the diffuser angle should remain zero. An added benefit of this is that the low pressure region introduced by the duct would introduce a net force in opposite direction to the propeller axial lift force, reducing performance [29]. Having the diffuser walls at a zero angle would have no such negative contribution.

4.4.3. Final Duct Design

A duct design that meets these criteria, is the one visualised in Figure 4.7 [27]. This duct has an elliptical inlet, and a relatively small diffuser section at a diffuser angle of 0° . This design can be scaled up to the size of the current UAV, with a rotor diameter of 1.15 m. The performance gains can therefore be also applicable to the large scale drone [30]. In order to scale the design, the relations with respect to the propeller radius, R, are visualised in Figure 4.8. The exact values of the parameters that are visualised in Figure 4.7 are specified in Table 4.4.

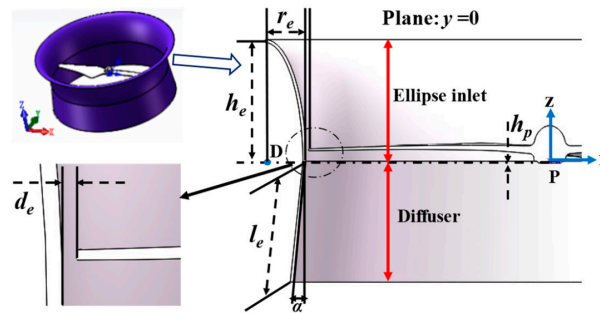


Figure 4.7: Duct Geometrical Parameters [27]

Table 4.4: Duct Geometrical Parameters

Dimension	Symbol	Value
Tip Clearance	D_e	0.005 m
Rotor Height	h_p	0.0 m
Inlet Radius	r_e	0.096 m
Inlet Height	h_e	0.216 m
Diffuser Length	l_e	0.144 m
Diffuser Angle	α	0.0°

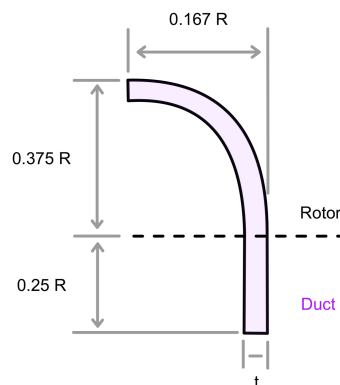


Figure 4.8: Duct Design

Finally the duct design is shown as a 3D render in Figure 4.9. This design has a specified, single rotor thrust increase of 24.5% when compared to a single unducted rotor of same configuration. Therefore, our drone will have a total gain in thrust of a more conservative 20%. This performance gain will be used for propeller selection in Section 4.5. Moreover, the exact material will be decided and discussed in Chapter 5 together with the specifications in terms of weight.

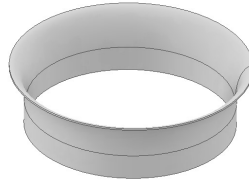


Figure 4.9: Duct Design 3D Render

4.5. Propeller Selection

As was explained in Section 4.1, the propellers will be designed for hover during which the T/W ratio is 1:0. The preliminary diameter of the propellers was set to the range of 45-56 inch, which equals 1.14-1.42 m. Using the theoretical conclusions made in Section 4.2, either a stacked two-bladed propellers or four-bladed propellers can be selected based on available performance measurements. As mentioned before, the direct results as specified in Figure 4.2, cannot be used due to the inaccuracy found in torque calculations. Instead relations between variables in Equation 4.1 and Equation 4.2 are used.

4.5.1. Two Sets of Two-bladed Propellers

All propeller types tabulated in Table 4.5 are two-bladed propellers, as there are simply no four-bladed propellers available commercially, of the specified size range apart from one type which will be discussed in detail in the Subsection 4.5.2. The respective types specified in Table 4.5 contain two numbers within their type names. The first number is the propeller diameter and the second one the propeller pitch, both indicated in inches.

In order to be able to judge the performance of combining these two-bladed propellers, these specifications need to be related to those of four-bladed propellers. This was done using the relation between the number of blades and the thrust and torque, as stated in Equation 4.1 and Equation 4.2 respectively. These relations contain coefficients C_t and C_m that show a linear relation between the number of blades, B_p and the thrust, T, and a quadratic relation between the number of blades and the torque, M:

$$T \propto B_p \quad (4.8)$$

$$M \propto B_p^2 \quad (4.9)$$

Therefore, using the specifications of a certain two-bladed propeller, it is assumed that the thrust and torque for the four-bladed propeller can be estimated by doubling the thrust and quadrupling the torque. With this newly obtained thrust, the RPM can be lowered such that the thrust will be halved again and will just be sufficient to reach a T/W ratio of 1:0 with the new four-bladed propeller. This is in line with the power maps visualised in Figure 4.1 and Figure 4.2. Using the relation, Equation 4.1, it can be seen that the RPM is quadratically related to both the thrust as well as the torque.

$$T \propto RPM^2 \quad (4.10)$$

$$M \propto RPM^2 \quad (4.11)$$

The RPM that was necessary for the two-bladed propeller to provide the thrust will therefore be scaled by $\sqrt{0.5}$ to a lower value, and provide the same amount of thrust with twice the number of blades. In a similar way, using the relation Equation 4.11, the torque also decreases by half.

This is in line with the expectations as the number of blades that need to be rotated is two times as high but the RPM was lowered again.

Using this new RPM and torque, the power required for combining two, two-bladed commercially available propellers can be determined using known two-bladed propeller data with the aforementioned approach. Equation 4.5. The values are shown in Table 4.5.

Table 4.5: Specifications Combined two-bladed Propellers

Type	RPM	Power Required [kW]
CF FLuxer 47 x 13 matt [31]	1633	3.7
HW 48 x 17.5 Inch Foldable Propeller [32]	1521	4.2
T-Motor 47 x 18 CF [33]	1464	4.1
Xrotor UAV 56 x 20	1076	3.2

From Table 4.5, it becomes clear that the biggest diameter will require the lowest amount of power with the lowest RPM, however requiring the highest torque. This very high torque value requires a very powerful motor, which is relatively heavy, for rotating a propeller at such low RPM's. This means that when the diameter becomes too large, a too large motor is required. Therefore, the maximum propeller diameter will be set to 47 inch.

Moreover, once the duct design, presented in Section 4.4, will be positioned around the propeller there will be a gain in lift force of 20%. With this gain in lift force the propeller can be optimised by either reducing the diameter, lowering the RPM even more or increasing the pitch. Reducing the diameter and increasing the pitch are the best options as lowering the RPM further will cause the propellers to rotate at such a low RPM that the propellers will not function efficiently anymore. Moreover, the torque produced will be disproportionally high, such that a very heavy and large motor will be required to provide enough power. A more powerful motor to provide this torque would result in an increased weight of 14% (MAD M50C60) [22], and will therefore counteract the efficiency gain from the duct. With this it can be concluded that only lowering the RPM is not a viable option for optimising the ducted propeller.

Another method for optimising after the placement of the duct, is to decrease the diameter of the propeller. According to Equation 4.1 and Equation 4.2, the thrust and torque are related to the diameter, D_p , in the way given in Equation 4.12 and Equation 4.13 respectively. It becomes clear that when the propeller diameter would be twice as small the RPM will need to be four times as high in order to generate the same amount of thrust. In order to keep the RPM as low as possible while making sure that the propellers still function efficiently, the diameter shall be as big as possible with 47inch being the maximum value it can reach. The optimisation shall thus consist of taking 47inch as a starting point and optimising for the best combination of pitch and RPM for the diameter.

$$T \propto RPM^2 \cdot D_p^4 \quad (4.12)$$

$$M \propto RPM^2 \cdot D_p^5 \quad (4.13)$$

Therefore, while keeping the diameter and RPM fixed, the pitch will need to be increased in order to keep the effective angle of attack constant as can be derived from Equation 4.3. The main issue with increasing the pitch for the existing two-bladed propellers within this range of diameter size is that there are only a very limited amount of propellers in the requested diameter range. Therefore, it will not be assumed possible to change the pitch on an existing off-the-shelf propeller. The experimental specifications of the CF Fluxer 47 x 13 matt [31] propeller will be used for comparison with the four-bladed propeller option that will be discussed in Subsection 4.5.2.

4.5.2. Off-the-Shelf four-bladed Propeller

Apart from combining two two-bladed propellers, the manufacturer E-PROPS has been found to produce four-bladed propellers of the desired diameter range with a wide variety of pitches.[34] These

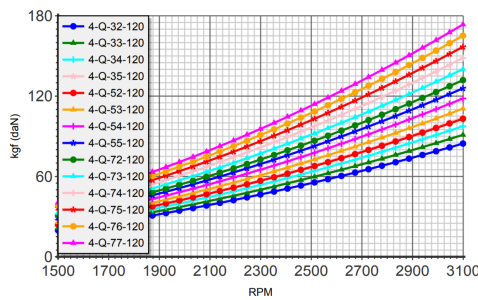
specifications provide crucial insights as to how the pitch could be increased and the diameter decreased once the influence of the duct is taken into account. As the specifications do not provide exact information on the propeller pitch, the results of the 47 x 13 inch propeller tabulated in Table 4.5 are used for comparison. The graphs in Figure 4.10a and Figure 4.10b show the propeller performance, in terms of thrust and torque respectively, for a variety of different pitches. Each line differs 0.5° pitch angle from the line above and below. From the results, a thrust of 22 kgf and torque of 26 Nm at an RPM of 1633, it can be derived that the orange curve 4-Q-34-120 shows the strongest correlation to the previously found combined two-bladed combination. From this graph, the influence of changing the pitch can be obtained as E-PROPS states that the graphs differ 0.5° in pitch angle from each other.[34]

At this point, the duct will be positioned around the four-bladed propeller which will cause the incoming flow velocity to increase while passing through the inlet. The determination of this increase in velocity is calculated using the inlet geometry by the method described in Subsection 4.4.1 and visualised in Figure 4.5. This increase in inflow velocity can be related to the effective angle of attack by means of the trigonometric relation given in Equation 4.14, with θ_{prop} defined as Equation 4.15 [21]:

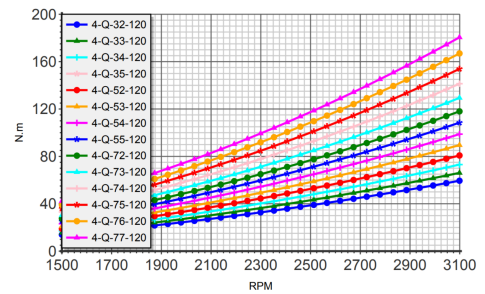
$$\alpha_{prop} = \theta_{prop} - \arctan\left(\frac{V_{inflow}}{\omega \cdot r}\right) \quad (4.14)$$

$$\theta_{prop} = \arctan\left(\frac{\text{pitch}}{\pi \cdot D}\right) \quad (4.15)$$

The relation from Equation 4.14 shows that increasing the angular velocity will increase the angle of attack of the propeller, α_{prop} . Meanwhile, increasing the inflow velocity, V_{inflow} , which happens when the propeller becomes ducted, will reduce the angle of attack encountered by the propeller. Another important conclusion is that increasing the pitch will increase the angle of attack of the propeller, which can be used to counteract the lower angle of attack caused by the duct.



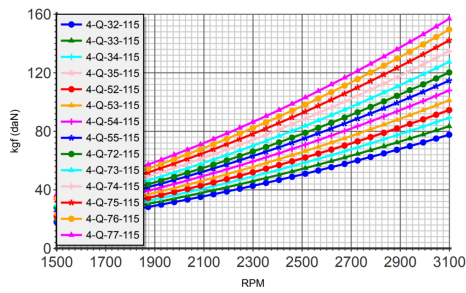
(a) Thrust four-bladed Propeller with 1.20 m Diameter [34]



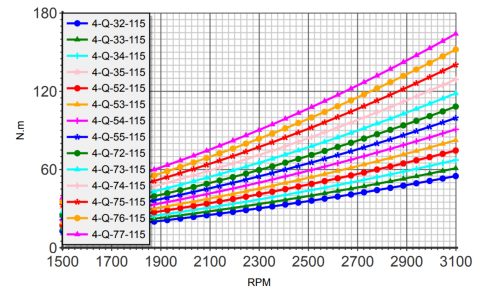
(b) Torque four-bladed Propeller with 1.20 m Diameter [34]

Figure 4.10: Specifications for a four-bladed Propeller with 1.20 m Diameter [34]

Taking into account that the diameter of 120 cm can be decreased slightly, the analysis has been performed again for a diameter of 115 cm. The pitch can be increased for this slightly smaller four-bladed propeller option, of which the graphs shown in Figure 4.11 are used. Considering the propeller initially was set to 47 inch, the optimisation is performed for one step smaller. Therefore, the diameter is set to 115 cm with a pitch of 17 inch, which corresponds to the orange graph 4-Q-53-115. The results are tabulated in Table 4.6.



(a) Thrust four-bladed Propeller with 1.15 m Diameter [34]



(b) Torque four-bladed Propeller with 1.15 m Diameter [34]

Figure 4.11: Specifications for a four-bladed Propeller with 1.15 m Diameter [34]

The power required is still very high due to the high pitch that caused a lot of torque. Therefore, the pitch can be lowered in order to optimise for minimum power required. In the end, a pitch of 15inch give the best results as can be seen in Table 4.6, this corresponds to the pink graph 4-Q-35-115. This resulted in a lower power required which can be lowered slightly more by lowering the RPM such that the thrust is exactly 22 kgf again, these results are visualised in bold in Table 4.6. The lower RPM causes the torque to lower as well and with that a smaller motor can be chosen which is beneficial for the overall weight.

Table 4.6: Optimisation Results Propeller Selection

Diameter [m]	Pitch [inch]	NON-DUCTED				DUCTED			
		RPM	Thrust [kgf]	Torque [Nm]	Power Required [kW]	RPM	Thrust [kgf]	Torque [Nm]	Power Required [kW]
1.2	13	1633	29.8	21.6	3.69	1491	24.8	18.0	2.81
1.15	17	1500	28.8	18.9	2.97	1369	24	15.8	2.26
1.15	15	1525	28.8	16.5	2.64	1392	24	13.8	2.00
1.15	15	1525	28.8	16.5	2.64	1322	22	12.6	1.76

4.6. Motor Selection

In order to find the best motor for the chosen propeller, an analysis has been done on the amounts of power that potential motors can deliver and at which respective throttle setting. This research is shown in Table 4.7, together with their masses. The most important aspect is that at the RPM that the propeller spins, the torque matches the propeller torque from Table 4.6. From Table 4.7 it becomes clear that without the ducts this would be the MAD M50C60 PRO IPE motor, which is very heavy compared to the other options.

Table 4.7: Research on Potential Motors Unducted Quadrotor

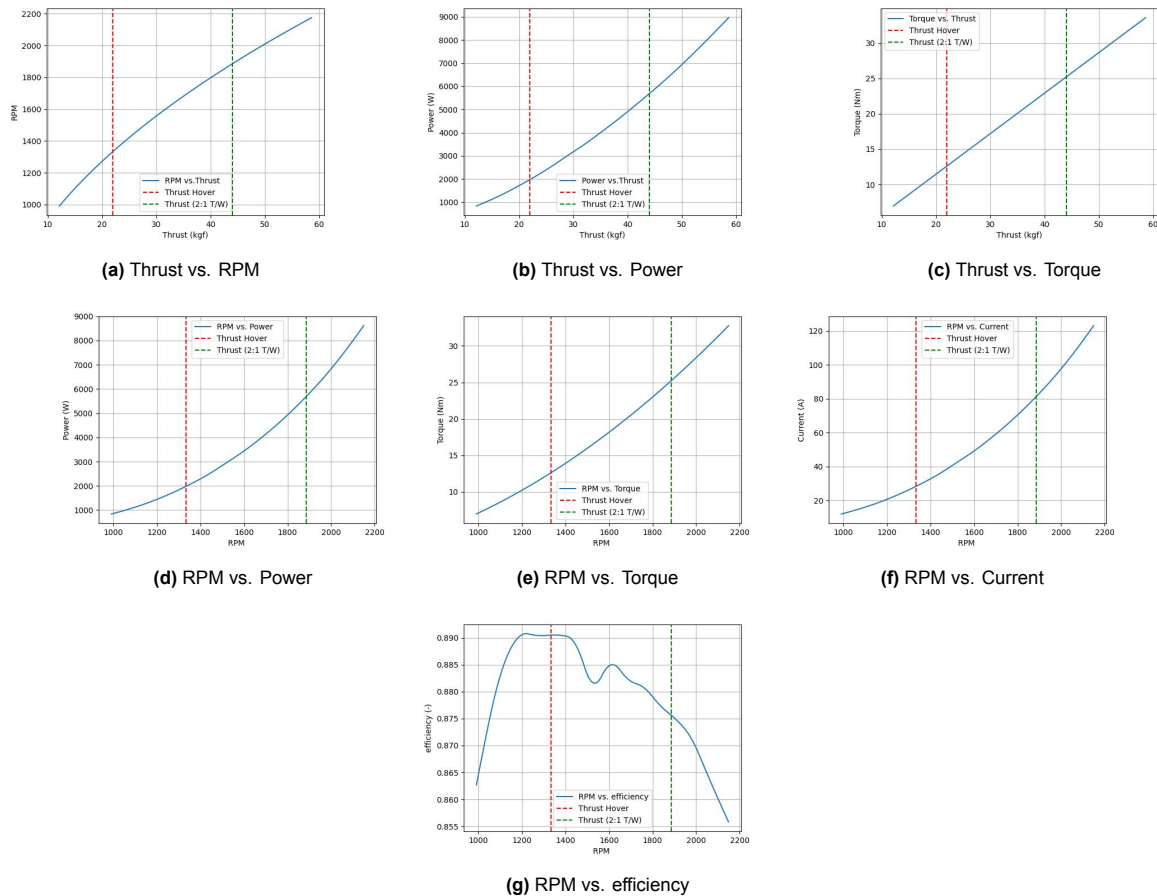
Type	RPM	Torque [Nm]	Throttle	Mass [kg]
M50C35 [22]	1643	15.6	45%	4.33
Xrotor X13-18s [35]	1611	15.8	54%	3.28
MAD M50C60 PRO IPE [22]	1615	24.5	45%	7.20
M90C60 EEE [22]	1653	74.7	50%	12.7
M40C30 [31]	1662	9.47	40%	3.46

However, Table 4.6 shows that once the duct is in place, the RPM can be lowered to 1322. Therefore, the motor selection changes as now the XrotorX13-18s is the best fit, which has a lower mass and will improve the efficiency of the design.

Table 4.8: Research on the Potential Motors for Ducted Quadcopter

Type	RPM	Torque [Nm]	Throttle	Mass [kg]
XrotorX13-18s [35]	1311	12.49	44.0%	3.28
MAD M50C60 PRO IPE [22]	1455	20.0	37.5%	7.20
M50C35 [22] [36]	1493	22.6	50.0%	4.33

For the chosen motor, the specifications can be visualised. It is important to note that the motor should be able to provide a T/W ratio of 2:1 in order to have the required control authority. The results for the Xrotor X13-18S have been plotted in Figure 4.12, where the red dashed line indicates a 1:1 T/W (22 kgf) and the green dashed line a T/W of 2:1 (44 kgf).

**Figure 4.12:** Motor Specifications XrotorX13-18s

4.7. Sensitivity Analysis

In order to determine the sensitivity of the final motor selection to varying parameters such as weight, the model developed in Section 4.2 can be utilised. As evident from Figure 4.1 and Figure 4.2, increasing the drone mass would require a higher thrust and shift the propeller pitch and RPM, design space more to the right. Requiring higher RPM/pitch at higher torques, necessitating a larger motor, further increasing weight. Furthermore, the effect of changing other parameters has been discussed in Section 4.5, where the motor was selected based on the sensitivity of thrust, torque and power on blade diameter, RPM and blade pitch.

With the current motor selection however (Xrotor X13-18s) and consulting Figure 4.12, it is evident that the motor is possible of providing a larger thrust if necessary. This would shift the red and green dashed

line further to the right. While less efficient and drawing more power, the mass limit where the motor would no longer be able to meet the 2:1 T/W requirement can be found by multiplying the maximum thrust output of the motor-propeller combination by a factor of two. The maximum thrust, as can be seen in Figure 4.12, the maximum thrust output of one single motor is 55 kgf. Meaning the upper limit for UAV mass is 110 kg, to still meet the 2:1 T/W requirement. The effect of varying mass on UAV performance will be discussed further in Section 8.3.

4.8. Budgets

In order to make sure that an accurate estimation can be made of the overall mass, cost and power budget of the drone, the budget needs to be defined per subsystem. For the propulsion subsystem this entails two main components, the motor and the propellers. The duct will be added to the budget of the structures subsystem in Section 8.1. The specifications of the motor was found online, but the details of the propellers were not published. Therefore, contact was set up with the EPROPS company by means of e-mail through which the respective mass and cost were communicated as can be seen in Table 4.9. The power required of the propellers is calculated in the way it was described in Section 4.5 and is based on the hover T/W ratio of 1:0.

Table 4.9: Mass Budget Propulsion System

Component	Unit Weight [kg]	Amount	Total Weight [kg]	Cost [EUR]	Power [kW]
Motor	3.28	4	13.1	3,200.00	2.0
Propeller	0.92	4	3.68	3,520.00	1.8

5. Structures and Materials

This chapter explores the structural design and material choices. It begins with an assessment of possible configurations, followed by the identification of potential materials for integration into these configurations. The selected materials are then incorporated into the structure. Each component's selection is evaluated, along with the attachments between different structural components.

5.1. Configuration Selection

Building on the quadcopter configuration selected earlier in the design process, and the previously analysed aerodynamics performance, seen in Chapter 4, multiple structural configurations can now be considered. In order to select the most efficient design, that will have the highest structural resistance, four different designs are considered. These all have fully ducted propellers, which allow for a closed structure in which the batteries are placed in between the ducts. In these configurations the dimensions of the payload box and the central box for the electrical components remain the same. The dimensions of these components are 50x50x50 cm and 50x50x20 cm respectively. With the payload box volume of 0.125 m³, the payload density is about 200 $\frac{\text{kg}}{\text{m}^3}$. This means that any substance/liquid of 25kg with a density higher than this will fit in the proposed volume. For solid objects, this depends on the geometry. For the dimensions of the central box, that houses the electronics, the dimensions were based on two factors: it must align with the height of the batteries and it must align with the size of the payload box.

In Figure 5.1, the four configurations are presented. The main difference between these four designs are the rod arrangements. The top row designs include ducts that match the 20 cm height of the central box, creating a uniform surface. The top left design incorporates four rods attached to the central box, while top right consists solely of ducts. In the first design, the rods bear the majority of the structural load, whereas in the second design, the ducts are responsible for load-bearing. For the two bottom configurations a distinction when compared to the previous one is found in the rods, which are inserted into the gaps between the central and payload boxes. The first configuration features rods in a square configurations, with two central rods in a cross pattern. In contrast, the second configuration adopts an 'H' pattern, where the two vertical rods are specifically designed to support the loads of both the upper and lower boxes.

After a thorough evaluation of all the configurations discussed earlier, the design illustrated in Figure 5.1, which includes four crossing rods attached to the central box, was selected as the most suitable. This decision was based on several key factors. Initially, the alternative design, which relied on load-carrying ducts, was considered inefficient. For the ducts to handle significant loads effectively, they would need to be constructed from highly durable materials. This requirement would significantly increase the weight of the UAV, given that the ducts constitute a large portion of the design's surface area. A configuration with load-carrying rods, on the other hand, offers a more balanced approach by providing strength without a corresponding increase in weight, thus optimising the UAV's performance and efficiency. The remaining two options depicted in Figure 5.1 are considered overdesigned; the greater the number of rods, the heavier the weight, and neither configuration offers the ideal load paths.

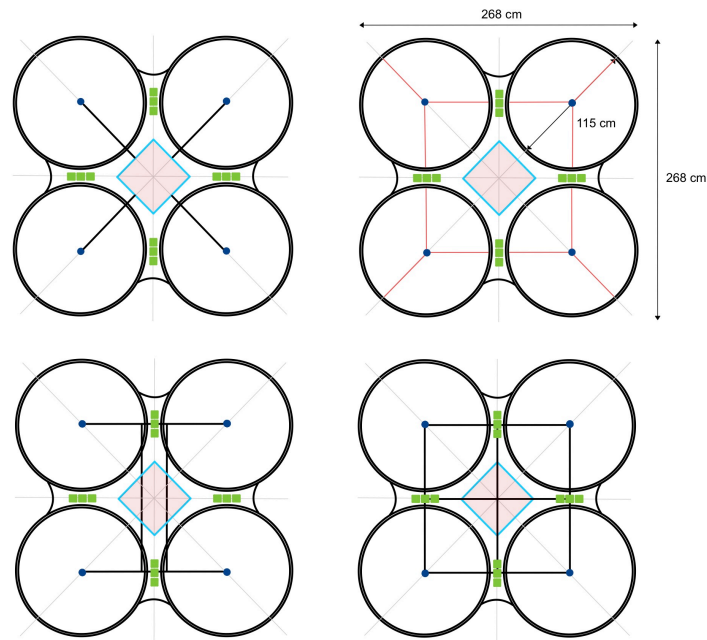


Figure 5.1: Configurations

5.2. Materials

In this section, material selection for the UAV structure is addressed. The primary structural components that require critical material selection include rods, plates, landing gear, payload boxes and ducts. Material options for each component were categorised into metals, plastics, and composites, reflecting the most commonly utilised materials in UAV applications. A preliminary selection focused on commercially available materials that also exhibit corrosion resistance.

The criteria used to evaluate the performance of these materials include density, yield strength, Young's modulus, sustainability, and cost. The performance of each material under these criteria is shown in Table 5.3 for the aluminium alloys, in Table 5.4 for the plastics, and in Table 5.5 for the composites, with the best-performing materials highlighted in green. Note that all properties were provided as ranges, and for each, the worst-case scenario was considered. For example, this means using the smallest value for yield and the largest value for density.

Sustainability was assessed by considering recyclability and the environmental impact during production. The evaluation scales used for these are detailed in Table 5.1 and Table 5.2, along with their respective meanings. Each material was scored based on these criteria, and the average scores are presented in the sustainability column below.

Table 5.1: Levels of Recyclability

Importance	Description
1	Not Commonly Recyclable
2	Recycling Difficulties
3	Often Recyclable

Table 5.2: Levels Environmental Impact

Importance	Description
1	High Environmental Impact
2	Marginal Environmental Impact
3	Low Environmental Impact

Table 5.3: Aluminium Alloy Characteristics

Properties	Density [kg/m ³]	σ_{yield} [MPa]	E [Gpa]	Sustainability	Cost [EUR/kg]	Cost [EUR/m ³]
Materials						
AL2024, O	2800	79	75	2	2.41	6748
AL6061, T4	2730	124	74	3	2.20	6006
AL5052, O	2700	73	74	2	3.80	10260
AL7075, O	2830	120	76	1	7.48	21168

For the selection of plastics it is important to note that these were also pre-selected based on UV resistance. The plastics in Table 5.4 all exhibit excellent UV resistance.

Table 5.4: Plastic Characteristics

Properties	Density [kg/m ³]	σ_{yield} [MPa]	E [Gpa]	Sustainability	Cost [EUR/kg]	Cost [EUR/m ³]
Materials						
Polyvinylidene Fluoride	1708	50	2.53	1	11.30	20114
Polytetrafluoroethylene	2200	22	0.55	1	14.00	30800
Polycarbonate	1180	59	2.21	1	3.38	3980

Table 5.5: Composite Characteristics

Properties	Density [kg/m ³]	σ_{yield} [MPa]	E [Gpa]	Sustainability	Cost [EUR/kg]	Cost [EUR/m ³]
Materials						
Carbon Fibre (copper matrix)	1720	479	71	1	213.00	366000
Glass Fibre (E grade)	2600	2.05	85	2	3.04	7904

Based on the results presented in the tables, definitive conclusions can be made regarding material selection. As detailed in Table 5.3, Aluminium 6061 (AL6061) emerges as the optimal choice, outperforming other materials across most assessed categories. Similarly, from the analysis in Table 5.4, polycarbonate is identified as the superior choice. Additionally, the review of Table 5.5 indicates that carbon fibre offers the best performance among the composite materials looked at. Although glass fibre has more green cells, the very low yield strength is a deal breaker.

5.3. Components

In this section, the components in the selected configuration will be analysed by conducting force and stress calculations to evaluate the loads each component bears. Based on these calculations, the most suitable material will be chosen. This selection process will rely on the top materials previously identified from each category, as detailed in Section 5.2.

5.3.1. Rods

For each component previously mentioned in Section 5.2 a material choice has to be made, these consisted of rods, plates, landing gear, payload boxes, ducts, and propellers. The choices can vary between AL6061, polycarbonate and carbon fibre, as these were preselected.

First bending and shear stress were calculated using an arbitrary thickness. The maximum force ex-

erted on the end of the 73cm rods is assumed to be equal to the maximum thrust. Then by using Equation 5.1 the bending stress can be calculated.

$$\sigma_b = \frac{M}{Z} \quad (5.1)$$

Here the section modulus is denoted by Z and is calculated by using Equation 5.2.

$$Z = \frac{\pi(D_o^4 - D_i^4)}{32D_o} \quad (5.2)$$

Next, the maximum shear stress can easily be calculated by dividing the maximum force by the cross-sectional area of the rod.

To find an equivalent stress, the bending and shear stress need to be combined. This can be done using Equation 5.3.

$$\sigma_{eq} = \sqrt{\sigma_b^2 + 3\tau^2} \quad (5.3)$$

Now the thickness can be iterated until the Unity Check (UC) is at a predetermined value of 0.7. The UC relation can be seen in Equation 5.4.

$$UC = \frac{\sigma_{eq}}{\sigma_{yield}} \quad (5.4)$$

With this thickness, the maximum deflection at the end of the rod can be calculated using Equation 5.5.

$$\delta_{max} = \frac{PL^3}{3EI} \quad (5.5)$$

Where the area moment of inertia is equal to Equation 5.6.

$$I_y = I_z = \frac{\pi(D_{outer}^4 - D_{inner}^4)}{64} \quad (5.6)$$

together with:

$$D_{inner} = D_{outer} - 2t \quad (5.7)$$

The results of these calculations can be seen in Table 5.6. Here the thickness, maximum bending, shear and equivalent stress, maximum deflection and mass are provided.

Table 5.6: Rod Calculations Results

Material \ Parameter	t [mm]	σ_b [MPa]	τ [MPa]	σ_{eq} [MPa]	UC [-]	δ_{max} [mm]	m [g]
Carbon Fiber	0.62	355.12	5.11	355.23	0.70	40.28	132.00
AL6061, T4	3.14	76.99	1.06	77.01	0.70	9.86	1009.00
Polycarbonate	7.77	41.30	0.48	41.30	0.70	159.45	973.00

Several conclusions can be drawn from this. The polycarbonate rod, which deflects by almost 16 cm, was deemed unsuitable due to excessive deflection. While the aluminium rod meets the requirements, it is significantly heavier than the carbon fibre rods. Therefore, carbon fibre has been chosen as the material for the rods. Additionally, carbon fiber rods have the advantage of being readily available off the shelf and easily cut to the required length.

5.3.2. Arm Brackets

The arm brackets are structurally important components since these are the connection points of the rods. These are placed on both sides of the central box and have a hole in to allow the rod to go through. Since these parts will heavily rely on CNC or 3D printing, carbon fibre is not considered.

Because the rods will be placed through the hole of the side panel, bearing stress and shear out need to be considered. The connection of the rods in the side panels can be seen in Figure 5.2, together with a visual representation of the failure modes.

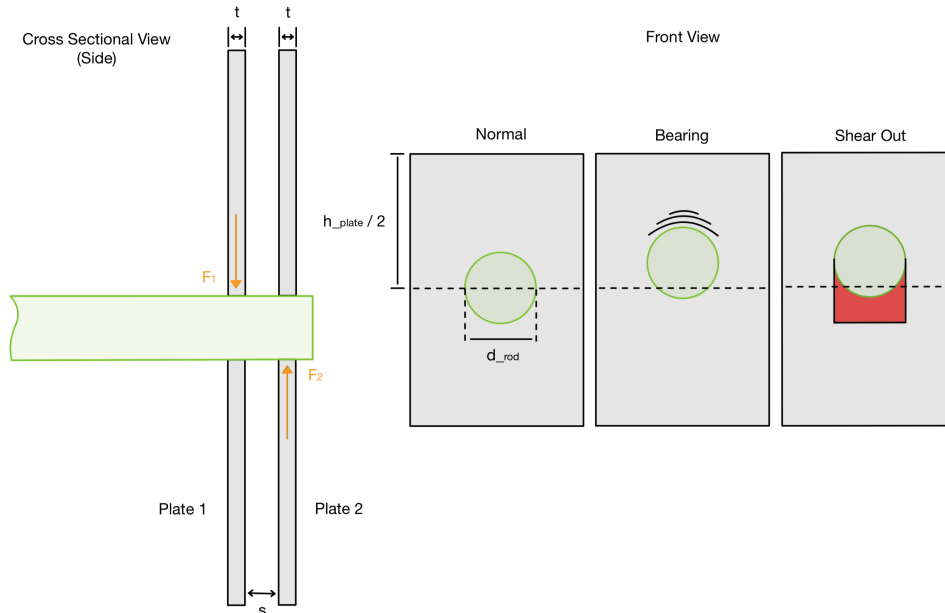


Figure 5.2: Bearing and Shear Out Failures on Arm Brackets

The forces F_1 and F_2 have been calculated using moment equilibrium when the maximum force of 490.5 N is applied at the end of the rod. The Free Body Diagram (FBD) used for these calculations can be seen in Figure 5.3. Then the forces can be calculated using the sum of forces in the y direction and the sum of moments around point A, which resulted in Equation 5.8 and Equation 5.9 respectively. These forces turned out to be 4071.15 N and 3580.65 N respectively. This means that the outer wall will need to be thicker than the inner wall. For these calculations, a distance between the plates of 10 centimeters has been used.

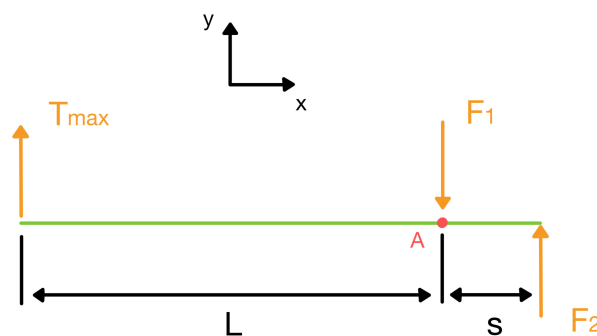


Figure 5.3: Rod FBD

$$\sum F_y^{\uparrow+} = T_{max} - F_1 + F_2 = 0 \quad (5.8)$$

$$\sum M_A^{ccw+} = F_2 \cdot s - T_{max} \cdot L = 0 \quad (5.9)$$

The formulas used for the bearing and shear out are depicted in Equation 5.10 and Equation 5.11.

$$\sigma_{bearing} = \frac{F}{t \cdot d_{rod}} \quad (5.10)$$

$$\tau_{shearout} = \frac{F}{2 \cdot 0.5 \cdot h_{plate} \cdot t} \quad (5.11)$$

Also the critical buckling stress needs to be considered, which can be seen in Equation 5.12.

$$\sigma_{cr} = C \frac{\pi^2 E}{12(1-\nu)} \cdot \left(\frac{t}{d_{rod}} \right)^2 \quad (5.12)$$

Where the Poisson ratio ν can be calculated using Equation 5.13.

$$\nu = \frac{E}{2G} - 1 \quad (5.13)$$

Next, the UC is calculated again using Equation 5.4. For bearing the yield stress can be used, but for shear out the maximum shear stress needs to be determined. The relation between this value and yield can be seen in Equation 5.14.

$$\tau_{max} = \frac{\sigma_{yield}}{\sqrt{3}} \quad (5.14)$$

Now the results for the two plates made out of the aluminium alloy and polycarbonate are given in Table 5.7 and Table 5.8 respectively. Again the thickness of the plates is iterated until a UC of 0.7 is reached for either the shear out or the bearing. However, there is now another situation that needs to be considered, buckling. The applied stress over the critical buckling stress may also not exceed 0.7.

Table 5.7: AL6061, T4

Part \ Properties	$t[mm]$	$\sigma_{bearing}[MPa]$	$\tau_{max}[MPa]$	$\sigma_{cr}[MPa]$	$m[g]$
Plate 1	1.24	71.13	44.46	148.46	21.69
Plate 2	1.10	71.04	44.40	117.59	19.30

Table 5.8: Polycarbonate

Part \ Properties	$t[mm]$	$\sigma_{bearing}[MPa]$	$\tau_{max}[MPa]$	$\sigma_{cr}[MPa]$	$m[g]$
Plate 1	3.31	26.64	16.65	38.05	25.03
Plate 2	3.19	24.62	15.39	35.19	24.07

Several conclusions can be drawn from these results. Aluminium plates can be approximately three times thinner and are lighter than polycarbonate plates. However, in practice, the very small thickness of the aluminium plates poses manufacturing and assembly challenges. To address this, the aluminium plates could be made thicker, but this would lead to overdesign and a significant increase in mass. Therefore, polycarbonate plates appear to be the preferable option.

5.3.3. Ducts

The ducts will be constructed from Extruded Polystyrene Foam (EPF), commonly known as Styrofoam, and wrapped in a layer of carbon fibre sheet. The EPF serves two functions: providing the shape of the ducts and making the UAV buoyant so it is recoverable if it lands in the water. The carbon fibre sheet ensures the structural rigidity of the ducts. The density of the EPF is 33 kg/m^3 , and the carbon fibre sheet weighs 0.353 kg/m^2 .

The dimensions of the ducts are explained and calculated in Section 4.4, and additional parameters that are required for the structural design are illustrated in Figure 5.4.

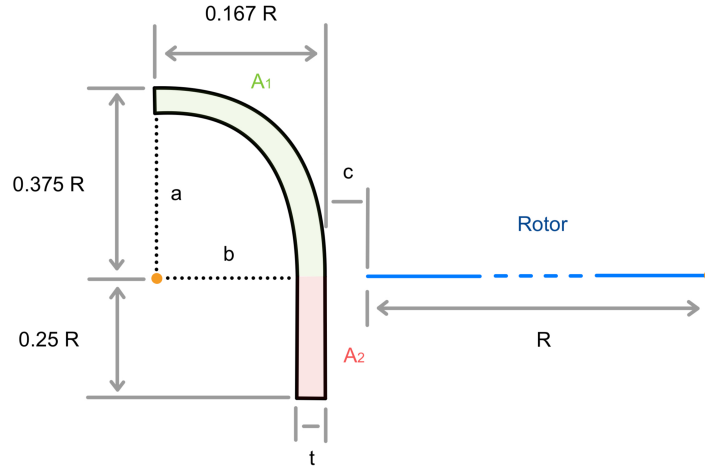


Figure 5.4: Duct Design

As can be seen in Figure 5.4, the size of the duct is determined by the rotor diameter R and the thickness t . Additionally, there will be a clearance c between the duct and the rotor.

To calculate the mass of the duct, the inside area has been divided into two areas, as can be seen in Figure 5.4. A_1 can be calculated by subtracting a quarter of the inner ellipse from a quarter of the outer ellipse. The area of an ellipse can be calculated by multiplying π with the major axis "a" (half of the longest diameter of the ellipse) and the minor axis "b" (half of the shortest diameter of the ellipse). The total inner area can thus be calculated using Equation 5.15.

$$A = A_1 + A_2 = \frac{\pi}{4}(0.375R \cdot 0.167R - (0.375R - t)(0.167R - t)) + 0.25R \cdot t \quad (5.15)$$

Then, the total mass of the styrofoam can be calculated using Equation 5.16.

$$m_{EPF} = \rho_{EPF} \cdot A \cdot 2\pi(R + c + t/2) \quad (5.16)$$

Next, the mass of the carbon fibre outer layer can be determined. The perimeter of an ellipse can be calculated using Equation 5.17.

$$p = 2\pi \sqrt{\frac{a^2 + b^2}{2}} \quad (5.17)$$

To find the total perimeter of the cross-section, add a quarter of the perimeter of the outer ellipse, a quarter of the perimeter of the inner ellipse, and two times the thickness. This calculation is shown in Equation 5.18.

$$p_{tot} = \frac{1}{4} \cdot 2\pi \left(\sqrt{\frac{(0.375R)^2 + (0.167R)^2}{2}} + \sqrt{\frac{(0.375R - t)^2 + (0.167R - t)^2}{2}} \right) + 2(0.25R + t) \quad (5.18)$$

The total mass of the carbon fibre of the ducts can then be calculated using Equation 5.19.

$$m_{CF} = \rho_{ACF} \cdot p_{tot} \cdot 2\pi(R + c + t/2) \quad (5.19)$$

When assuming a duct thickness of one centimetre and a clearance of five millimetres, a preliminary mass of 1.60 kg per duct is calculated. The exact thickness will be determined using Ansys, as manual calculations for the loading of these ducts are considered too complex.

To ensure structural rigidity during flight, the ducts must be securely interconnected. For this purpose, thin, lightweight inter-duct connecting plates have been developed, visualised in Figure 12.17. These plates are made out of polycarbonate, the plastic previously selected for its particularly good ability to resist deformations and lightweight. The choice of polycarbonate allows the plates to be manufactured slim and light without compromising the structure. This design is critical in minimising the overall weight of the assembly. In order to attach this plate to the ducts, as there is very minimal contact area between the two, the best option is judged to be adhesive bonding. Using epoxy adhesives, that have very high load bearing capacity, these can provide strong bonds between aluminium and carbon fiber. These will also need surface preparation before application, such as leaning, abrading, and applying a primer, as this further increases the bonds.

5.3.4. Landing Gear

For the implementation of the landing gear, an initial choice must be made between retractable and non-retractable designs. Both options have their benefits; however, for the scope of this project, a non-retractable design seems more optimal. It is preferred primarily due to its increased simplicity, which enhances reliability and reduces maintenance requirements. This will also result in lower cost and saving weight, due to the lack of retractable mechanisms. For the overall landing gear positioning, tipping point calculations must be performed, in order to obtain the most optimal landing gear location. Figure 5.5 shows how these calculations were performed. The length of the legs are designed to be one meter to ensure payload accessibility from the bottom of the drone.

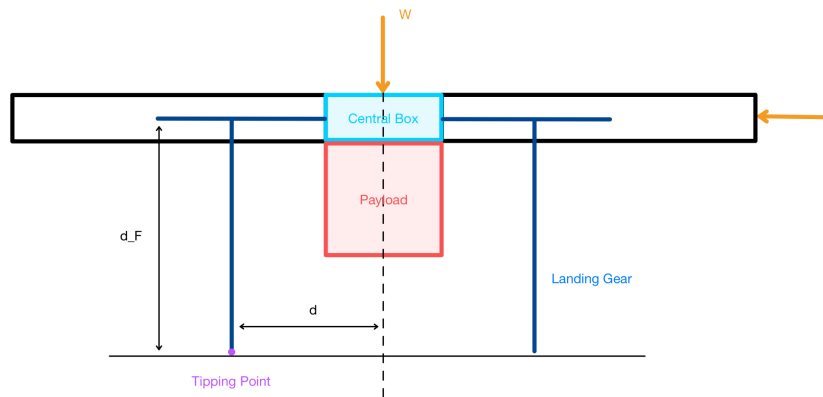


Figure 5.5: Landing Gear Spacing

The force F exerted at the top of the drone consists of a combination of an aerodynamic force caused by a 6 bft maximum wind gust and a bump force of a person. This is represented in Equation 5.20. Here a safety factor of 1.5 has been used.

$$F = 1.5 \cdot \left(\frac{1}{2} \rho V^2 A C_d + F_{Bump} \right) \quad (5.20)$$

Table 5.9: Tipping Force Inputs

Parameter	Value	Unit
ρ	1.225	kg/m ³
V	13.8	m/s
A	1	m ²
C_d	0.8	-
F_{Bump}	20	kg

The tipping criteria can be seen in Equation 5.21. From this, the spacing of the landing gear can be determined.

$$W \cdot d > F \cdot d_F \quad (5.21)$$

This results in a minimum distance d of 0.31 m.

Furthermore, the options of skids and legs were both looked at, however, due to the optimal positioning of the landing gear being a considerable distance from the centre, it was quickly decided that normal standing legs would be more beneficial.

The material has been selected by looking at the compressive and bending stresses and column buckling. The compressive stress can easily be calculated by dividing the force by the area of the rod. The maximum force exerted on each rod of the landing gear is assumed to be the entire weight of the drone. This accounts for the worst-case scenario.

Next, the bending stress can be calculated. For this a friction coefficient between the ground and the landing gear needs to be selected. For this, a value of 0.3 has been chosen. This means that the horizontal force applied at the bottom of the landing gear is 30% of the weight of the drone. Multiplying this force with the length of the landing gear results in the bending moment. Then the bending stress can be calculated using Equation 5.1, where Z is the section modulus which can be calculated with Equation 5.2.

When looking at column buckling Equation 5.22 can be used.

$$P_{cr} = \frac{\pi^2 EI}{L^2} \quad (5.22)$$

The landing gear calculations have been performed on carbon fibre, an aluminium alloy and a plastic. The rods have been given the same outer diameter as the connecting rods of the motors, being 50mm. As can be seen from the results in Table 5.10, the bending stress will be the limiting stress. On this, the UC of 0.7 has again been applied. Then the buckling load has been calculated for all the materials. These are far higher than the maximum applied load of 918 N, and thus not limiting.

Table 5.10: Landing Gear Results

Material Parameter	Carbon Fiber	Al6061, T4	Polycarbonate	Unit
Rod Thickness	1.15	1.49	3.05	mm
Compressive Stress	5.57	4.32	2.18	MPa
Bending Stress	98.03	77.01	41.32	MPa
Buckling Force	75.13	89.72	5.55	kN
Mass	212	434	372	g

Again carbon fibre seems to be the best option. It can have the lowest thickness and even more important, the lowest mass.

5.3.5. Vibrations

This subsection centres on the vibration analysis of the structure and natural frequency calculations. The natural frequency is an important parameter as it determines a components behaviour under dynamic conditions. For designers, it is essential to make sure that the natural frequencies do not match with the operational frequencies of machinery or environmental forces, to avoid resonance. This difference is very important to prevent excessive vibrations that could lead to structural failures. Therefore, it is important to design structures in such a way that they do not operate within or near the natural frequency ranges.

During mission the component that experiences the vibrations the most are the carbon fibre rods. As such the vibrations will only be performed for these. To simplify the vibrations, these are modelled by a spring in the vertical direction, this is because the rods will mainly feel vibrations in the transverse direction, rather than longitudinal, due to the attachment to the central box. This model can be depicted in Figure 5.6. For a simple straight beam, the stiffness k can be estimated using the formula for a cantilever beam seen in Equation 5.23. From the stiffness calculations and using the mass of the rod the natural frequency can be obtained from Equation 5.24 in rad/s, then converted to Hz with Equation 5.25. All these equations use configuration and materials specifications previously described, performing the calculations gives the results shown in Table 5.11.

$$k = \frac{3EI}{L^3} \quad (5.23)$$

$$\omega_n[\text{rad/s}] = \sqrt{\frac{k}{m}} \quad (5.24)$$

$$f_n[\text{Hz}] = \frac{\omega_n}{2\pi} \quad (5.25)$$

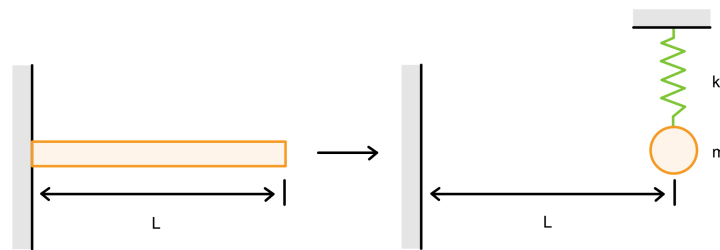


Figure 5.6: Vibrations

Table 5.11: Results Vibrations

Spring Stiffness, K	Natural Frequency, ω_n [rad/s]	Natural Frequency, f_n [Hz]
3.549E+04	84.95	13.52

5.3.6. Payload and Winch System

First a payload box is to be designed for the drone. The main requirements of this box is that it shall have an internal volume of 50x50x50 cm, shall be waterproof, and as light as possible.

The design of the box was inspired by traditional shipping containers. These have similar requirements, only at a much larger scale. They consist of a structural frame in the corners made of L-profiles. The bottom side is also reinforced using stiffeners, to ensure proper load transfer. In a traditional container the sides are made of corrugated sheets, in the drone case this is not necessary due to the smaller size and loads. An overview of a typical structure can be seen in Figure 5.7.

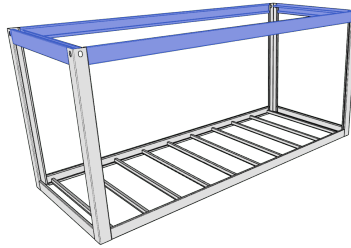


Figure 5.7: Typical Shipping Container Structure

The payload box is designed in a similar way using polycarbonate. This material was chosen over the other options as it is quite easy to manufacture, is cheap, and has quite good strength. The box is built up from L-profiles in the corners and T-profiles as stiffeners on the bottom. The sections have a thickness of 3 mm and a height/width of 15 mm. The sides are covered in a 1 mm plastic sheet. These dimensions are a result of a couple of iterations, where the box was modelled in FEM to verify strength. The current dimensions are nowhere near the theoretical minimum, more optimisation is certainly possible. The current weight of the payload box is about 2.3 kg, further optimisation could easily result in under 2 kg. But due to durability concerns it was decided to not further decrease the thickness. The box can be seen in Figure 5.8.



Figure 5.8: Overview of The Payload Box

On the image it can be seen that 4 padeyes are added in the top 4 corners of the box. These connect to the main winch wire. Please refer to Section 5.4 for more information about the structural analysis of this part. The payload box has a door that slides off to the side, and can be closed with a latch.

Now that the payload box has been considered, an appropriate spool, rope and motor need to be selected for the winch system. The spool will be 3D printed, while the rope and motor will be selected off the shelf. A visualisation of the spool with rope can be seen in Figure 5.9.

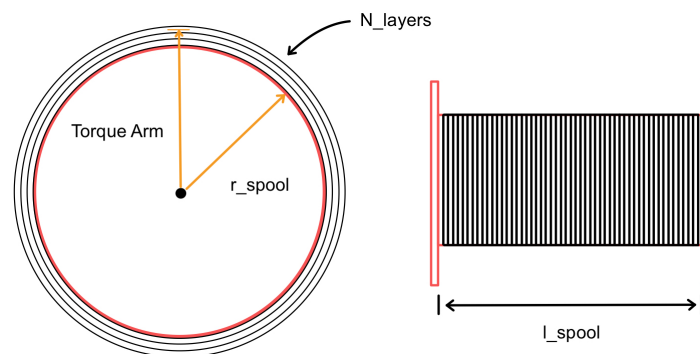


Figure 5.9: Winch Spool

From this figure, a few relations can be described. First, the maximum torque is calculated using Equation 5.26. The torque arm is defined from the centre of the spool to the middle of the last layer of rope, while the force is equal to the payload weight.

$$T_{max} = (r_{spool} + (2N_{layers} - 1) \cdot r_{rope}) \cdot W_{payload} \quad (5.26)$$

Then the length of the rope can easily be calculated by using Equation 5.27.

$$l_{rope} = (\pi \cdot d_{rope} \cdot l_{spool}) \cdot N_{layers} \quad (5.27)$$

For the rope, a polypropylene floating rescue line has been selected [37]. It is strong, lightweight, UV-resistant and has a bright colour for visibility. Also, the 16 strands braided with a parallel core rope ensure it is safe to handle. This 6mm diameter rope has a maximum strength of 450 kg and weighs 1.3 kg per 100 m. At the maximum payload of 25 kg, it has an elongation of 1.90% of its length.

After some iterations, the final design parameters of the winch system are presented in Table 5.12.

Table 5.12: Winch System

Parameter	Value	Unit
d_{spool}	5.0	cm
l_{spool}	20.0	cm
d_{rope}	6.0	mm
N_{layers}	2.0	-
L_{rope}	10.5	m
T_{max}	8.34	Nm
m_{rope}	136.1	g
m_{spool}	32.94	g
δ_{max}	19.9	cm

One important design parameter is the maximum torque that needs to be delivered by the motor. With this value, an appropriate motor will be selected.

To determine if the spool will withstand the applied forces, the maximum shear stress using its dimensions and the maximum torque can be calculated, as shown in Equation Equation 5.28. In this context, J_T represents the polar moment of inertia, which can be calculated using Equation Equation 5.29.

$$\tau_{max} = \frac{T_{max} \cdot r_0}{J_T} \quad (5.28)$$

$$J_T = \frac{\pi}{2}(r_0^4 - r_i^4) \quad (5.29)$$

The maximum shear stress is calculated to 1.10 Mpa, which will result in a UC of only 0.055.

5.3.7. Central Box

After careful review of the design, modifications were made to the central box. Originally, this component not only housed the electronics but also served as the structural core. In the updated design, the dimensions of the central box have been significantly reduced to 50x50x8 cm. Its function has been narrowed down to solely support the structure and accommodate the winch system previously described. A separate electrical box will now be positioned above it to house the electronics. To construct the central box, four polycarbonate sheets will be curved to form the sides, to ensure the box is as lightweight as possible. Directly on top and bottom, these surfaces will be made of AL6061, these are the surfaces that keep the structure together, for these strength is the principal driver in the decision making.

The aluminium plates and the polycarbonate sheets are joint together through box joints. The rods are connected to the central box by first passing through two support panels, pictured in Figure 5.2, these are load carrying and serve as a rigid connection for the rods. These panels are bolted to the top and bottom aluminium plates. The rods also go through a hole created in the four polyethylene sheets. It can be seen that the top and bottom aluminium plates of the box also extend to the sides of the ducts, acting as the primary means of attaching the ducts to the central body. In order to joint the thin edge of the aluminium plate and the surface of the ducts angle brackets or corner braces can be made. This brace can be easily manufactured, by laser cutting a sheet of metal to the appropriate dimensions and can be bent using a press brake. Furthermore, counter sinking can be used to create conical holes for the brace to be screwed to both surfaces.

5.3.8. Electronics Box

For the electronics box, the most critical requirement is waterproofing, as it houses sensitive electronics and any water in the box would result in immediate failure. Since the box does not need to support heavy loads, strength is not a critical factor in its design. Consequently, the team has selected a plastic box made of polycarbonate, which is highly resistant to water and offers the benefit of being lightweight. This box is designed with an octagonal shape, with multiple edges. To ensure a watertight seal on the edges a silicone-based sealant will be applied to enhance the waterproofing. Silicone has excellent resistance to UV and water, making them ideal for the outdoor application of the UAV.

This box is located directly on top of the central box, by drilling holes in both of the meeting surfaces these can be bolted together. Bolted joints, are typically susceptible to water, therefore silicone gaskets are placed between the joining surfaces. These gaskets effectively prevent water infiltration by creating a robust and tight seal around each edge.

5.3.9. Parachute Box

In case of loss of power, the drone drops. In order to quantify the impact velocity the drone, it is dropped from 160 m with an initial velocity of 0 m/s.

For this analysis, the only forces considered are drag and gravity.

$$a = -g + \frac{\rho V^2 S C_D}{2m} \quad (5.30)$$

with C_d of 0.8, a density of 1.225 kg/m^3 and a surface area of 5.9 m^2 .

This is numerically integrated to find the velocity once it hits the ground, this is done using the following equations.

$$a_t = -g + \frac{\rho V_t^2 S C_D}{2m} \quad (5.31)$$

$$v_{t+1} = v_t + a_t \cdot dt \quad (5.32)$$

$$h_{t+1} = h_t + v_t \cdot dt + 0.5 \cdot a_t \cdot dt^2 \quad (5.33)$$

From this it is found that if the drone falls it will impact the ground with 17.3 m/s. This is deemed as too high of a speed for the structure to withstand. As a result a parachute is included in order to slow this down. The parachute selected is the Ultra Cross 100 made by Independence paragliding. The reason for this is that this parachute is significantly cheaper than automatic deployment parachutes made for drones but also has a maximum allowed load of more than the weight of the drone. While still being lightweight.

The Ultra Cross 100 is a reserve parachute with a surface area of 25 m^2 [38]. Using the same numerical integration but with a C_d of 2.2, this is the value of similar parachutes and lines up with the claims of the manufacturer [39]. This results in a sink rate of 5 m/s.

Since this parachute is a reserve parachute, a deployment mechanism has to be designed. Since the parachute has a volume of 3L. It fits in a box of 120x250x100 mm. The parachute is launched from this box using 4 HV-32252 springs by Hermans Veren[40].

Using energy methods, an approximation is made for the launch velocity of this system. To do this Equation 5.34 and Equation 5.35 are used.

$$E_s = \frac{1}{2}k \cdot n \cdot u^2 \quad (5.34)$$

$$E = \frac{1}{2}mv^2 + m \cdot g \cdot h \quad (5.35)$$

where u is the displacement of the springs of 0.015 m, k is the spring constant of 21470 N/m per spring and n is the number of springs. Using these formula's it was found that this configuration launches the parachute upwards with a velocity of 4.5 m/s at 0.5 m above the original position. While drag would reduce this, the velocity should not be reduced to the point where the parachute fails to deploy.

5.4. FEM

To verify the structural integrity under all anticipated loads, a Finite Element Method (FEM) model is developed. Firstly an approach is established for the safety factors, then all loads are defined, and finally the results are shown.

5.4.1. Safety Factor and Standard

A widely recognised industry standard is the NASA Technical Standard 5001 (NASA-STD-5001) [41], which is publicly available. For our structural design, we have chosen NASA-STD-5001, which provides specific safety factors based on the intended usage of the structure. It distinguishes between prototypes (purely for testing, not intended for flight) and protoflight models (copies of the final flight model). Our cargo drone adheres to the protoflight standards outlined in this standard. The safety factors depend on the material. In Table 5.13 an overview is made for the safety factors for different materials for a protoflight structure.

Table 5.13: NASA-STD-5001 Safety Factors

Material	Safety factor on σ_{ult}	Safety factor on σ_{yield}
Metallic Structure	1.4	1.25
Composite Structure	1.5	/

To simplify the calculations and provide additional conservatism an overall safety factor of 1.5 is chosen.

5.4.2. Load Cases and Combinations

This subsection aims to identify all load cases and combinations that the structure might experience during operations. A load case (LC) is defined as a single load experienced by the structure. An overview can be found below in Table 5.14. The load cases presented below do not include the safety factors. These will be applied in the load combinations.

Table 5.14: Overview of Load Cases (LC)

	Description	Load (excl SF)	Point of application	Type of load
LC1	Self Weight	880 N	CG and Ducts	Point and distributed load
LC2	Hover thrust	220 N per arm	End of arm	Point load
LC3	Max thrust	561 N per arm	End of arm	Point load
LC4	Payload weight (incl box)	300 N	Winch	Point load
LC5	Floating load	220 N per duct	Duct	Distributed load
LC6	Max horizontal drag	101 N per duct	Duct	Distributed load
LC7	Max vertical drag	1364 N	Topside drone	Distributed load

The drag comes is calculated for the drone at level flight with a speed of 21 m/s. This simplification corresponds to maximal drag on the side of the duct.

$$D = \frac{1}{2} \cdot 1.225 \cdot 21^2 \cdot (1.16 \cdot 0.37) \cdot 0.8 \quad (5.36)$$

The maximum thrust to weight is 2.55 as described in Chapter 4. In a purely vertical motion this results in a scenario where the drone reaches a speed where the vertical drag is equal to 1.55 times the weight. This is the total drag which is distributed evenly over the whole drone. This case is LC7.

Additionally some load combinations (LCO) are identified. These correspond to the combination of different load cases for different scenarios. These include the safety factors.

Table 5.15: Overview of Load Combinations (LCO)

	Description	Loads	Support
LCO1	Hover	$1.5 \cdot LC2$	At CG
LCO2	Max speed cruise	$1.5 \cdot (LC2 + LC6)$	At CG
LCO3	Winching	$1.5 \cdot LC4$	At arm attachment points
LCO4	Floating	$1.5 \cdot LC5$	At CG
LCO5	Maximal T/W	$1.5 \cdot (LC3 + LC7)$	At CG
LCO6	Parachute recovery	$1.5 \cdot LC1$	Parachute attachment point
LCO7	Resting on landing gear	$1.5 \cdot LC1$	At CG

In total 7 different scenarios are identified for the drone. These correspond to:

- LCO1: The drone is a pure hover, with no wind. Here the drone only experiences the hover thrust while being fixed at the CG.
- LCO2: The drone is flying at it maximal operational speed of 21 m/s and experiences drag in purely the horizontal direction. This is a conservative assumption as in reality most of the drag will be experienced by the propellers and main frame, not ducts.
- LCO3: In this scenario the drone is in a hover and the payload is being winched. Since the structure is already verified for hover in LCO1, only the winching system is verified in this combination. Thus the drone is supported at its CG.
- LCO4: The drone is floating on the water and the buoyancy is assumed to come from the foam in the ducts. Hence the load is applied on the bottom of the ducts with the CG the support.
- LCO5: In this scenario the drone is in a purely vertical motion at maximal thrust. Thus there is the maximal thrust on the arms and drag on the whole body.

- LCO6: This case verifies whether the parachute attachment is structurally sound. Hence the self weight is applied at the CG and the drone is attached by the parachute attachment point.
- LCO7: This load combination mimics the static loads when the drone is landed and resting on its landing gear. It mainly verifies the strength of this landing gear.

5.4.3. FEM Setup

The finite element model (FEM) is simulated in Ansys Mechanical[42] using the static structural analysis tool. Firstly a CAD model is created in Autodesk Inventor as described in Section 8.2. For the FEM only the structural parts are kept in the model, this means that all electronics, motors, propellers, and batteries are removed.

The material properties used in the analysis come from the Ansys Granta Edupack. They correspond to the materials as described in Section 5.2, albeit with more detail.

The model is meshed using a 3D mesh with varying coarseness, ensuring that enough detail is kept in every part. Not applying the same level of detail in every part ensures that the model is not over complicated and improves run time. The contacts or connections between all parts are carried over from the Inventor assembly. These contacts are then checked in Ansys again to ensure proper modelling. An overview of the created mesh and model can be seen in Figure 5.10.



Figure 5.10: Mesh in Ansys Mechanical

The solver is set to mechanical APDL and large deformation analysis is turned off.

5.4.4. Unducted Drone Results

As the ducts are mostly not load bearing, a first analysis is performed without them or their connections. This significantly decreases the complexity of the model, as the carbon fibre and foam would need a very fine mesh due to their small thicknesses.

Firstly LCO1 is modelled, corresponding to the drone in a level hover. It is supported at the bottom plate of the central box with a fixed support. A load of 1320 N is applied on the corners of the 4 arms, resulting in 330 N per arm.

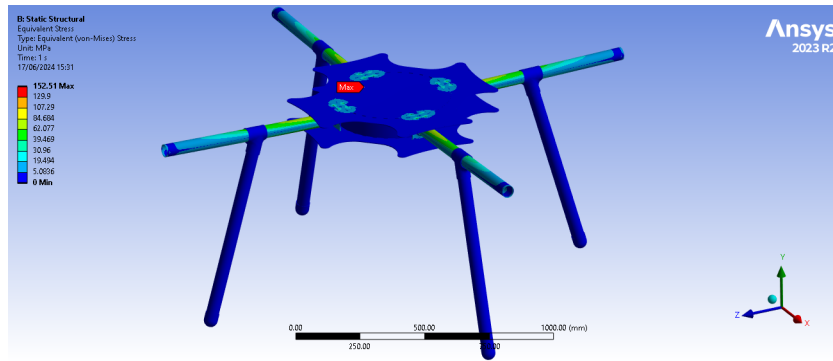


Figure 5.11: Von Mises Equivalent Stress in LCO1

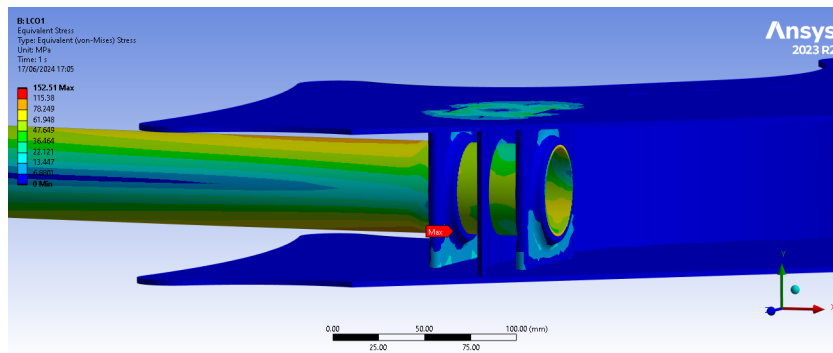


Figure 5.12: Detailed Maximum Von Mises Equivalent Stress in LCO1

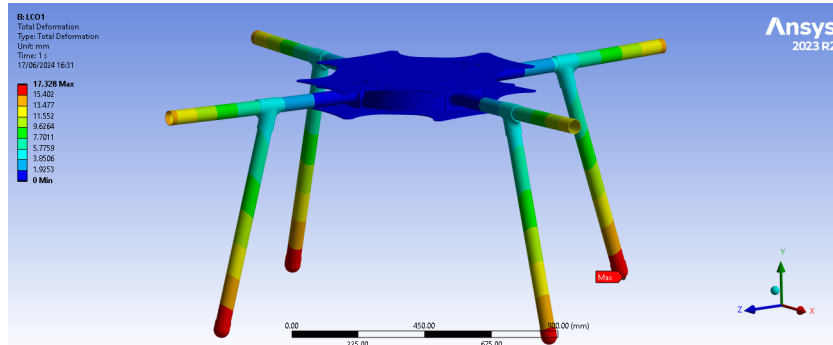


Figure 5.13: Deflection in LCO1

As can be seen in Figure 5.11 and Figure 5.12 there are no stresses which exceed the yield stresses of the materials. The yield of aluminium is 124 MPa, carbon fibre is 479, and polycarbonate is 59 MPa.

The maximal stress in the structure is 152.5 MPa on the carbon fibre rod. This corresponds to a UC of 32 percent. The plastic and aluminium parts also have UC's well below 1. The structure is thus verified for this load case. The maximal deflection is 17.3 mm at the bottom of the landing gear. The location of this maximum is logical as the arms are bending and thus this angle is mostly translated onto the landing gear. This deflection is within acceptable limits for our design, thus no further actions are necessary.

Due to the limited amount of pages in this report, it is decided to not include all results. Only the results of the governing load combinations are shown.

In LCO5, the case with the maximal thrust, the highest loads and thus stresses are present in the arms. This case is ran without the duct and thus the drag, this is conservative as these loads oppose the thrust, and thus the stress will be higher. The results of this case can be seen in Figure 5.14.

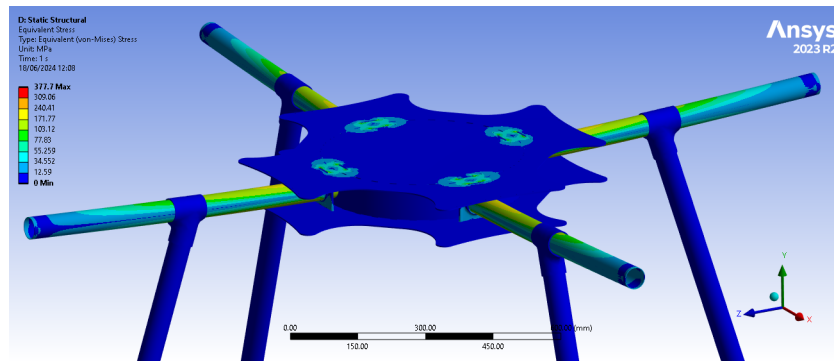


Figure 5.14: Stresses at Maximum Thrust

It can clearly be seen that neither the carbon fibre nor the polycarbonate parts exceed their maximal stresses. This thus confirms the strength of the arms in a worst case scenario. Additionally, in Figure 5.15 the arms can be seen modelled separately as well.

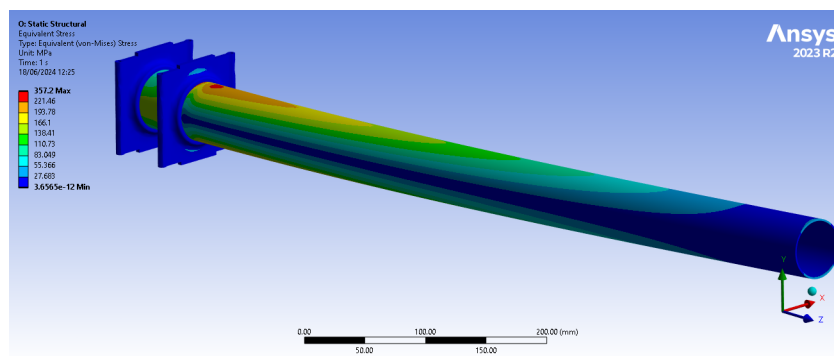


Figure 5.15: Arm Stresses at Maximum Thrust

A part that is interesting to examine individually is the landing gear. As described in Subsection 5.3.4 the governing load case is when the drone comes down onto one leg and experiences a friction load. This corresponds to a vertical load of about 100N and thus a horizontal (friction) load of 30 N. When accounting for the safety factor this equates to 150 N, and 45 N respectively. The results in terms of stress and deflection can be seen in Figure 5.16 and Figure 5.17.

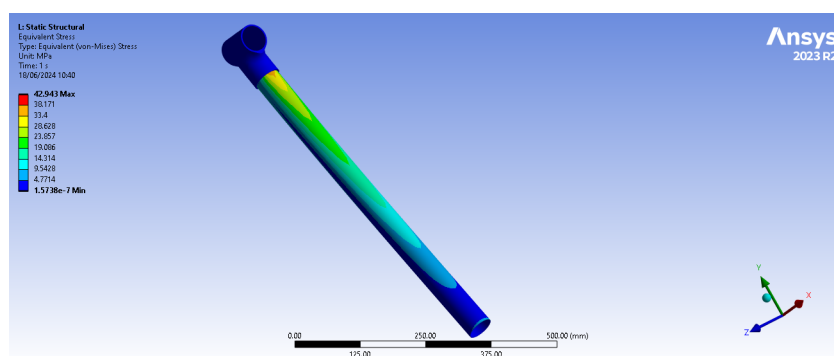


Figure 5.16: Landing Gear Stress

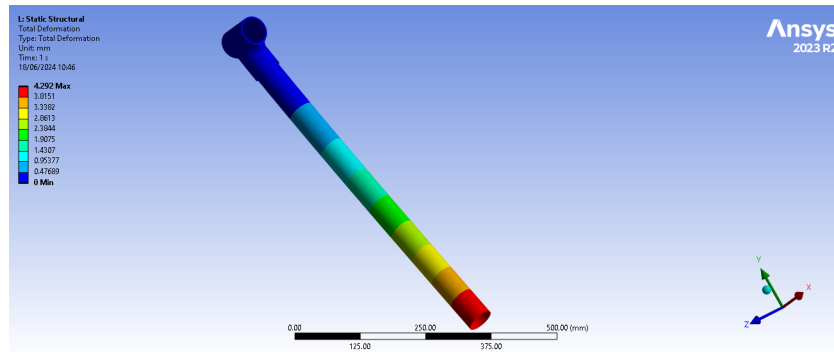


Figure 5.17: Landing Gear Deflection

In the images above it can again clearly be seen that the design does not exceed the maximum allowable stress.

Lastly the payloadbox is modelled. The maximal payload of 25 kg results in a loading of 375N when including the safety factor. This load is applied on the inner surface of the box. The box is supported using fixed supports at the 4 padeyes. The stresses and deflections of the box can be seen in Figure 5.18 and Figure 5.19.

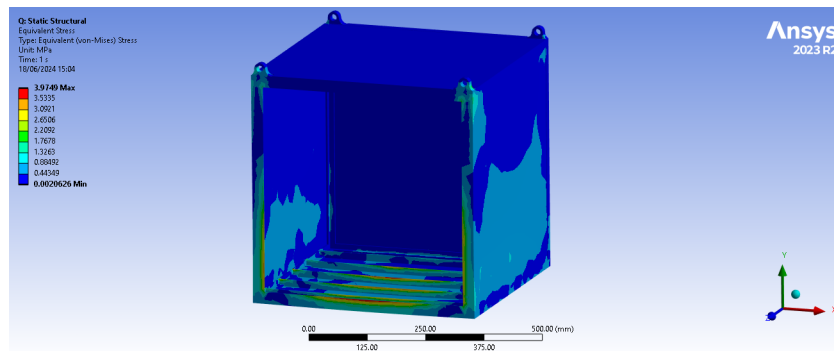


Figure 5.18: Payload Box Stress

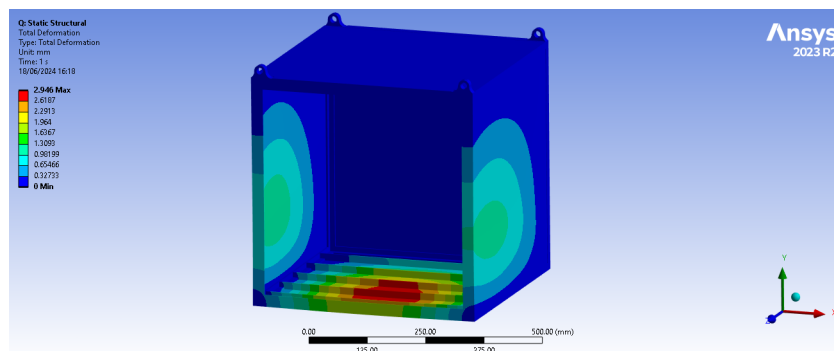


Figure 5.19: Payload Box Deflection

In the above images it can be seen that the payload box is deforming minimally with a 25kg payload and that the stresses are well within limits. The payload box could be further optimised, but for this document it is considered out of scope as it would require much more work for minimal weight savings.

The results presented in this subsection are only the governing results, as presenting all results would exceed the page limit.

5.4.5. Ducts FEM

Due to a high complexity of modelling the carbon fibre duct with a foam core it is decided to model the parts separately. This significantly decreases computational difficulty and enables us to run and iterate the design efficiently. Modelling the parts separately relies on making smart assumptions in how to support and load the part. The main requirement of these assumptions is to make them as simple as possible while maintaining a confidently conservative model.

Firstly the bottom rods of the ducts are checked. These are intended to provide additional rigidity to the duct and are mounted onto the motor. In this structural analysis the motor mount, rod, and duct bracket are checked.

It is conservatively assumed that half of the vertical load onto the duct is taken by this assembly. Both load case 5 and 7 induce a vertical load onto the duct. When comparing the two, it can be seen that LC7 has a higher load of 170.5 N. This corresponds to the total load of 1364 N split onto all 4 ducts and then taking half. When the safety factor of 1.5 is taken into account, the resulting load is 256 N.

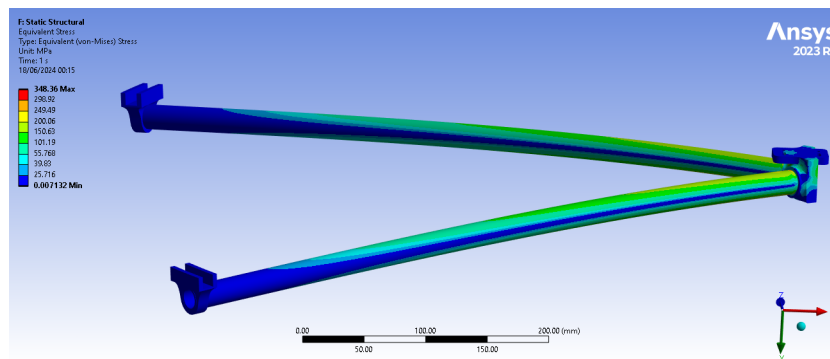


Figure 5.20: Duct Rod Stress

In Figure 5.20 it can clearly be seen that the stresses in the parts do not exceed the maximum allowable stresses for their respective materials. The maximal stress in the carbon fibre rod is about 348 MPa, but this is a very local peak stress (this peak is still within yield). This is most likely due to a modelling defect, the more general maximal stresses are around 200 MPa. The aluminium rod bracket has maximal stresses around 100-120MPa, which is just under the yield of the material.

Secondly the interduct plates that hold the batteries are structurally verified. This is done by supporting the brackets on the side which is secured to the duct, and applying a distributed load over the battery plate. This load corresponds to 150N, which is about 10kg of batteries with a 1.5 safety factor. This is a conservative overestimation, which keeps the model simple. In Figure 5.21 it can clearly be seen that the plastic structure can withstand the loads, as the maximal stress is about 13MPa.

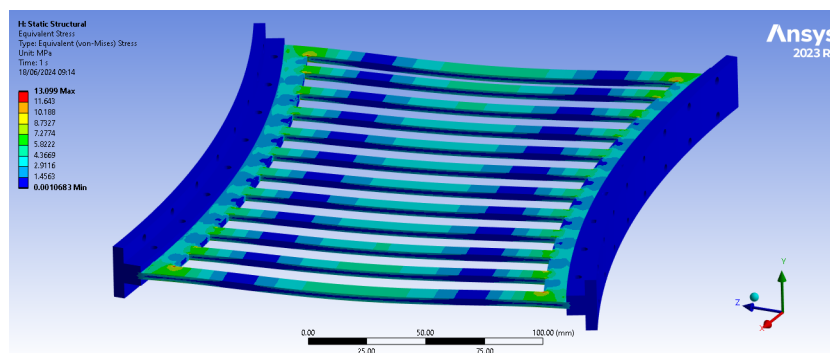


Figure 5.21: Interduct Plate Stress

Additionally the inner foam core of the ducts can be checked with the expected loads. As said before,

modelling the carbon fibre was more complex than expected. Because of this the foam is checked separately, and the assumption is made that these results are conservative for the carbon fibre encased structure.

The ducts are checked for a horizontal load as described in LC7. This is a horizontal load of 101 N, with the safety factor this becomes 151 N. The load is applied as a distributed load along the top of the duct, and the duct is supported at the bottom surface. This mimics the effects of a distributed drag and the duct connections which are all placed on the lower side of the structure. The foam material is expanded polystyrene, with a density of 30 kg/m^3 . This material is again modelled using Ansys Granta. The results in terms of stress and deflection can be seen in Figure 5.22 and Figure 5.23.

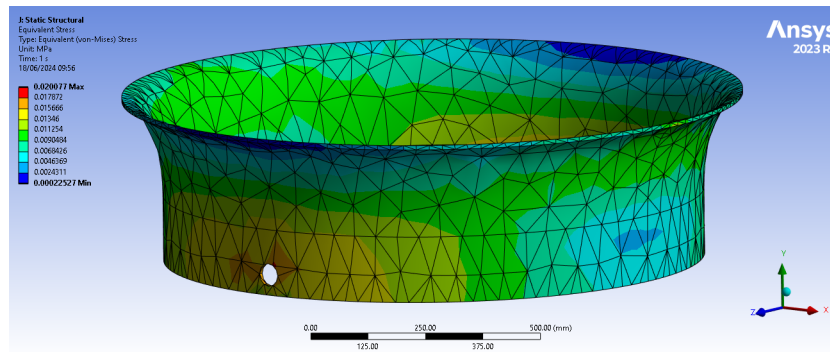


Figure 5.22: Foam Duct Stress

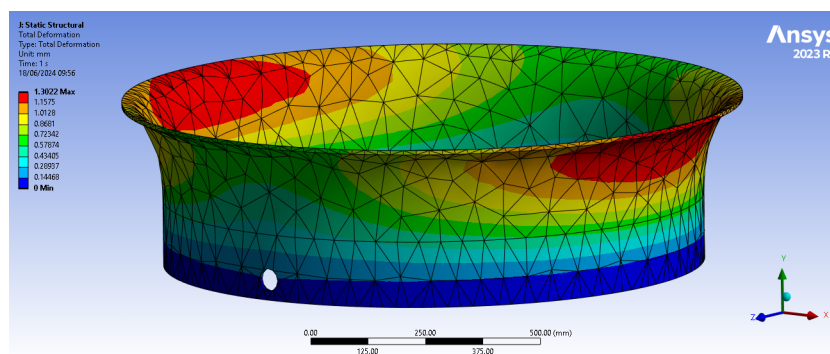


Figure 5.23: Foam Duct Deflection

In terms of stress, the foam is well below its limits in this scenario. The maximal equivalent stress is about 0.02 MPa, this is less than 10 percent of the maximum (0.2-0.25 MPa). In terms of deflection the structure also behaves well. Considering that this structure is missing the extra rigidity of the carbon fibre shell, this again confirms sufficient strength.

5.5. Sensitivity Analysis

For the sensitivity analysis of the structure, thicknesses have been varied. The main components for which the sensitivity analysis has been conducted are the rods and the connecting plates

Figure 5.24 shows how the UC varies with increasing thickness. Under each thickness, the mass of the rod has been provided. The behaviour is as expected, where the slope decreases with increasing thickness.

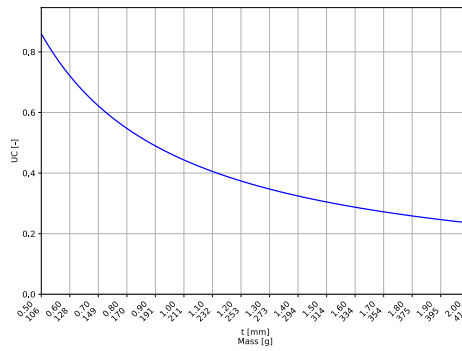


Figure 5.24: UC Evolution of Carbon Fibre Rod

In Figure 5.25, the evolution of the UC with increasing thickness can be seen for the three failure modes. Figure 5.25a and Figure 5.25b show this relation for the plate one and two respectively. Again the relation is as expected, where the buckling failure is the most dominant at low thicknesses.

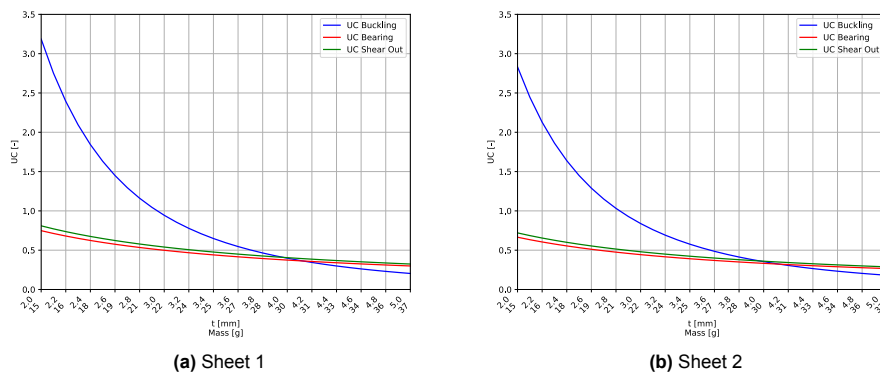


Figure 5.25: UC Evolution of Polycarbonate Sheets

There is a critical thickness at which buckling is no longer the primary failure mode. For plate one, as shown in the figure, this occurs when the buckling intersects with shear-out and bearing failure modes at thicknesses of 3.96 mm and 4.13 mm, respectively. Which are approximately the same thickness for plate two, being 3.97 mm and 4.13 mm.

Finally, the increase in the total mass of the ducts with increasing thickness has been evaluated, as shown in Figure 5.26. The mass of the duct ranges from 5.2 kg to 7.4 kg, representing a significant increase for a one-centimetre increase in thickness.

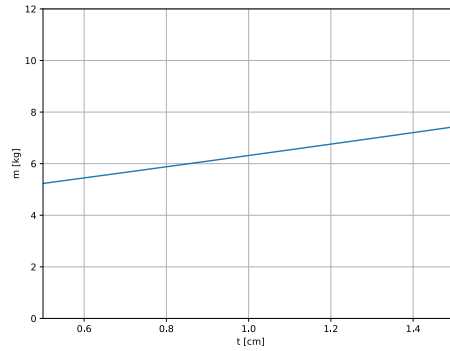


Figure 5.26: Duct Mass Evolution

5.6. Structures Budget

In the end, the cost budget for structures is constructed. It involves the manufacturing costs of the custom parts and purchasing the off-the-shelf components. In Table 5.16 the accumulated costs of the separately manufactured parts can be visualised, with a total cost of 12497.17 EUR. These costs are based on quotes obtained from Xometry [43].

Table 5.16: Custom Components Production Cost

Component	Cost [EUR]
Arm Brackets	253.92
Inter-duct plates	1069.68
Ducts	6500
Landing Gear	294.36
Central Box	1052.46
Electronics Box	1531.75
Motor Connector	371.8
Duct-Rod Connector	55.16
Parachute Box	1104.61
Radar Mounting	213.83
LiDAR Platform	49.6
Total Custom Cost	12497.17

For the off-the-shelf parts, the components that make up the structure are the landing gear rods, the four central arms and the rods found in the ducts, which together accumulate to a total cost of 782.25 EUR. From the off-the-shelf components, the glue also has to be considered, used for assembling components [44]. This adds an additional 114 EUR. In the end the total budget consisting of customary parts, off-the-shelf components and the glue, sums up to 13,393.42 EUR.

6. Electronics

This chapter considers the electronics of the drone and provides a detailed analysis. It starts with a presentation of all low-voltage components, elaborating on their main characteristics and the reasons for their selection in Section 6.1. After this, the high voltage components are selected and sized in Section 6.2. Following this, we discuss the integration process, including communication, data handling, and compatibility considerations in Section 6.3. This leads to an examination and selection of the wiring, culminating in a cohesive electrical system. In Section 6.4 and Section 6.5.

6.1. Low-voltage Electrical Components

This section details the UAV's low-voltage electrical components, covering the flight controller, navigation, communication, collision avoidance, warning systems, power distribution, and winch systems. Each component's specifications and suitability for offshore operations are highlighted, emphasising their roles in ensuring operational efficiency, safety, and regulatory compliance.

6.1.1. Flight Controller

The core component of a drone is a flight controller. It is responsible for managing the subsystems on the vehicle and processing the information. It analyses the vehicle motion and provides control. The selected firmware is ArduPilot as will be further described in Section 7.2. Therefore, compatible autopilots were considered. The one that is commonly used and suitable for UAVs is Cube Orange [45]. This model can be integrated to any published carrier board. The main consideration regarding the flight controller is that the components and subsystems intended to be placed in the drone are compatible with it and can be integrated.

The flight controller contains three IMU sensors (accelerometers/gyroscopes), two barometers and one magnetometer. It is placed on the standard Automatic Dependent Surveillance-Broadcast (ADS-B) IN Carrier Board. As the name suggests, this updated version of the original board is equipped with ADS-B to enhance situational awareness.

ArduPilot, which is run on the flight controller, has limitations regarding the amount of sensors and data processing capabilities. Therefore, the autopilot is connected to Raspberry Pi 4. The computing board is equipped with an 8 GB processor. Some of the electronics, especially rangefinders, are connected to the board. The companion computer and flight controller communicate as described in Section 7.3. This approach allows the signal to be initially processed before being sent to the Cube Orange, overcoming the flight controller's limitations.

6.1.2. Navigation

The GNSS provides the primary navigation means. The selected component is the Here3+ navigating set. It comprises a u-blox M8 high-precision GNSS module receiver, a processor and an IMU sensor (compass, gyroscope, and accelerometer). With a refresh rate of up to 8 Hz, it provides a position accuracy of 2.5 m. It is also water-resistant, which suits the offshore weather conditions. The accuracy of navigation can be increased to 2.5 cm, by using a RTK module. This is included in the navigation set and can be installed as a ground station upon the need of an operator. Due to its critical importance for flight control and stability, the equipment is doubled for redundancy. The IMU system provided with the flight controller is not sufficient because it is placed inside the structure and experiences electromagnetic interference from other electrical components and cabling that disrupt the readings.

The drone is also equipped with a barometer and a pitot tube. The former selected sensor is BME680. It measures the temperature, humidity and pressure with high accuracy. It provides information about the atmospheric conditions and the drone altitude is derived from the pressure according to the atmosphere model. The second sensor measures the airspeed.

The navigation subsystem has two functions. First, it informs a drone operator about the location and orientation of a vehicle via telemetry. Secondly, during the cruise phase, a drone is intended to fly autonomously to the defined location. Navigation delivers information if a vehicle stays on a track and guides it to the destination.

6.1.3. Automatic Dependent Surveillance–Broadcast

The vehicle is equipped with the ADS-B technology to broadcast its navigation data to be tracked in the airspace. This way it conforms the regulations of the civil aviation. Moreover, the drone can receive the information about other aircraft to avoid collision. The flight controller board includes the ADS-B antenna for receiving. However, the separate component TR-1F from Aerobits is selected that can transmit the data. It is described as very compact, low-weight and suitable to integrate the UAVs to the common airspace.

6.1.4. Communication

Communication is provided by the H16 Pro HD Video Transmission System. This set consists of a remote controller and receiver. The onboard element receives the video transmission directly from the camera and sends it to the remote controller. This way, an operator receives the live image of the drone's point of view. The second communication system is provided by RFD868x. It is responsible for transmitting the telemetry and receiving radio commands. The operator uses the remote controller for radio control to provide input to the drone's motion. In case of emergency, the H16 Pro HD Video Transmission System can also convey telemetry. In case of loss of signal, the RFD868x can receive simple commands to engage certain built-in protocols. Both communication systems were ensured to have a range compliant with the drone's mission profile. The H16 Pro HD Video Transmission System sends the signal up to 30 km, and RFD868x up to 40 km. Furthermore, the selected products are certified to be operated in the European Union considering the power transmission regulations. Additionally, the drone is equipped with a Holybro Remote ID system. This Remote ID ensures that the drone can easily be identified by authorities and other airspace users, enhancing safety and compliance with aviation regulations. The Remote ID broadcasts the drone's location and identification details, providing real-time information essential for maintaining situational awareness and operational safety. By integrating these robust communication systems the drone achieves reliable and secure communication, ensuring mission success and regulatory compliance.

6.1.5. Collision avoidance

Although the drone's operational space is mainly the offshore environment, where the airspace is less populated than in other areas, many objects can interfere with the UAV, such as birds, other vehicles, or the wind turbines themselves. For this reason, it is essential to have suitable sensors that provide awareness in all directions and conditions. Conditions can be suboptimal in cases of heavy rain or dense fog, where vision decreases drastically. Effective collision avoidance is critical not only for the safety of the UAV but also for the protection of infrastructure and wildlife. Advanced sensor technologies, such as radar, LiDAR, and infrared cameras, play a vital role in detecting and navigating around obstacles. These sensors must be capable of functioning reliably in various weather conditions and during both day and night operations. Additionally, integrating real-time data processing and machine learning algorithms can enhance the UAV's ability to predict and respond to potential collisions, ensuring more robust and autonomous navigation. By leveraging these technologies, UAVs can achieve higher levels of operational efficiency and safety in offshore environments.

Camera

For this, the first sensor considered is the camera, as it provides real time picture for the operator. When functioning properly it is the main source of navigation as well when controlled by a human. There are several viable approaches for the selection, starting from a phone to a gopro all the way to the most advanced military gimbals. The main considerations here were compactness, weight and ease of integration. The gimbals from Gremsy would have provided quality and reliability, however, the structure is not the most optimal with the large rods used, therefore these options were rejected. The final selection is the SIYI A8 mini by SIYI Technology [46], which has a compact design, with a 180° pitch range and a 320° yaw angle. Around the camera, there is provided a transparent casing that protects the equipment from the environmental factors. Its depiction is shown in Figure 6.1.



Figure 6.1: SIYI Camera With Cover [47]



Figure 6.2: SF40/C by Lightware [48]

LiDAR

LiDAR (Light Detection and Ranging) is employed in the drone for its ability to deliver high-resolution, accurate 3D mapping and distance measurements. By emitting laser pulses and measuring their return times, LiDAR enables precise surface modeling and obstacle detection even in low-light or complex environments. This capability ensures superior situational awareness and navigation accuracy, essential for applications requiring detailed spatial data, such as environmental monitoring, infrastructure inspection, and autonomous flight. LiDARs range in price from very cheap, to super expensive. The team was looking for an optimum between price and performance, which led to choosing the SF40/C from Lightware [48]. This LiDAR has a 360° scanning, 100 m range and a refresh rate of 20,000 Hz, see Figure 6.2.

IR-Lock

An Infrared (IR) Lock system uses an infrared beacon and a drone-mounted IR sensor for precise landing and tracking. The beacon emits IR light that the sensor detects, enabling the drone to calculate the beacon's position relative to itself. This technology allows the drone to land accurately on small or predefined spots, especially useful in low-light conditions or when visibility is obstructed. This is a powerful tool, as low visibility conditions are expected to occur often in the offshore environment. However, it comes at a high price point, especially due to the beacon. It will be useful from an operational point of view, as return to base - which is probably going to be a moving ship- will be made much simpler by utilising this technology. The customers will also have the option to install more beacons, should there be certain locations where the UAV will need to land often.

Unidirectional radar

During landing the IR-Lock provides precise measurements of the UAV's location. However, this is only the case if a beacon is installed. Therefore it must be ensured using a different sensor, that accurate data can be provided about the drone's position. For this several concepts have been looked at, but the radar altimeter was found to be superior, as it fitted perfectly this requirement. The US-D1, an All-Weather Radar Altimeter by Ainstein [49] was selected, as it provides centimetre accurate measurements up to 50 m altitudes, and it operates in all weather conditions as well.

Short range sensors

We aim to use a short-range radar on our drone to enhance obstacle detection and precise landing, especially in environments with poor visibility or complex terrains. Short-range radar provides accurate sensing capabilities that are less affected by lighting conditions or visual obstructions, ensuring reliable performance in diverse operational scenarios. Specifically, we chose the MM5D91-00 60 GHz mmWave radar for its high-resolution presence detection and ability to accurately measure distance and movement. This radar operates by emitting 60 GHz millimeter-wave signals and analyzing their reflections to detect objects and movement within a few meters. Its compact size and low power consumption make it ideal for integration into drones, where space and energy efficiency are critical. Moreover, its effectiveness in varying environmental conditions, such as through fog or dust, enhances the drone's ability to navigate and avoid obstacles reliably. The MM5D91-00 [50] thus provides a robust solution for improving our drone's navigation, safety, and autonomous capabilities.

Radar

Incorporating radar technology into the UAV is essential for improving autonomous navigation and obstacle avoidance, particularly in challenging environments. Radar systems provide reliable detection of objects regardless of lighting conditions or visual obstructions, ensuring the drone can operate safely in diverse scenarios. We selected the MR72 77 GHz Collision Avoidance Radar [51] due to its precise distance measurement capabilities, detecting obstacles up to 80 m with high sensitivity. Its dual-beam design enhances detection accuracy and stability. The radar's compact size, lightweight, and ease of integration make it ideal for our drone, fitting within space and power constraints. Additionally, the MR72's proven performance in applications like plant protection and industrial inspection validates its reliability and effectiveness for our needs.

6.1.6. Warning System

As the operational environment and mission profile demands close encounters between humans and the UAV. Therefore, it is essential to not only have protection around the propellers but also to warn any people around the drone, should the drone malfunction due to any sort of error. For this purpose, several indicator and warning lights will be installed on the drone, as well as an audio warning system. The requirements for these components are generally predefined by regulations and stakeholders.

Based on these requirements the following components were selected:

Indicator Lights

The first method to raise awareness of the drone's position is by equipping it with several indicator lights. The idea is to place 2 lights on each duct that are either constantly on or flashing. One of the 2 indicator lights (on each duct) will be used to signal if there is a motor issue. Indicator lights for the battery status must also be included. Panel Mount Indicators from RS Pro [52] have been selected as they are known for their exquisite reliability and good visibility even in daylight.

NAV Lights

The Firehouse ARC "V" Drone Strobe Spot Light [53] was selected as it meets the UAV regulations effectively. This light provides a strong strobe with high lumen output, complying with the requirement it can emit different colours. Additionally, the light's intensity ensures it is visible under various conditions.

Noise Emitter

The indicator lights and the NAV lights of our UAV are designed to ensure good visibility in both nightlight and daylight. However, the offshore environment can present unpredictable low-visibility conditions, such as heavy rain or dense fog. While our UAV is equipped with several short-range radars capable of determining its position even under these challenging conditions, it is crucial to alert any personnel in the vicinity for safety reasons. This necessity is not only a practical measure but also a requirement dictated by regulatory standards. To enhance measurability and comply with these safety regulations, we have selected the HEX - USB Extension and Buzzer [54] by Cubepilot . This device will provide an additional audible alert to ensure that humans around are adequately informed of the UAV's presence, even in low-visibility scenarios. Integrating this component aligns with our commitment to maintaining high safety standards and adhering to all relevant regulations.

6.1.7. Winch System

The last component is the motor used for the winch system. It is connected to the spool that wraps the line with a payload attached. The motor is selected such that it can provide enough torque. The structural attachments and torque calculation are described in Chapter 5. The chosen component is the 120 W Dc Gear Motor by NBLeison [55]. It is capable of providing a torque of up to 200 kgcm, which is more than sufficient for the required rotational rates for payload delivery.

6.2. High-voltage Electrical Components

Up to this point, the low-voltage part of the electrical system was discussed. Now the high-voltage side will be looked into. This includes the batteries and their management systems. The high-voltage batteries will be used to power the motors through the electronic speed controllers (ESC). Thus the

sizing of these batteries is done based on the required power from the motors. This is checked for both hover and cruise, as this will discover the most critical case. An important point is to always ensure a high enough T/W, as to be able to perform manoeuvres. As discussed in Section 4.6, a T/W of at least 2:1 is necessary.

6.2.1. Hover Requirement

During hover the thrust generated has to be equal to the weight as altitude needs to be maintained. In Section 4.5 the thrust, rpm and torque for hover are shown. The other side of the required power is the electric motor, which was selected in Section 4.6. Here the x13 was selected, from which the electromechanical efficiency was determined from experimental tests [35]. This was done as shown in Equation 6.1. It was taken into account that this efficiency depends on both RPM and torque [56] when determining the relevant efficiency.

$$\eta = \frac{P_{Mechanical}}{P_{Electrical}} \quad (6.1)$$

The mechanical power can be determined from the torque and rpm of the propeller. The electrical power required can then be calculated using electromechanical efficiency. The next step is to calculate the power required for a 30-minute hover. This is easily done by multiplying the electrical power by 0.5, resulting in a required power in kWh. This required power then has to be divided by a factor of 0.8 to reduce battery degradation from a low depth of discharge [57]. From this calculation, a continuous required power of 7.9 kW is found. This then translates to a required battery capacity of 5 kWh.

6.2.2. Range Requirement

The formulas for the thrust and torque and their coefficients [21] seen in Equation 4.1, Equation 4.2, Equation 4.3, and Equation 4.4. are used to determine the relation between thrust, torque, and RPM. This relation, removing all constants, is as shown in Equation 6.2 and Equation 6.3.

$$T \propto RPM^2 \quad (6.2)$$

$$M \propto RPM^2 \quad (6.3)$$

This shows a quadratic relation between thrust and rpm and torque and rpm. From this, it can be deduced that thrust and torque are linearly related. Using these relations the thrust and torque are scaled to the values required for cruise. The values required are found through setting weight equal to the upward component of thrust and drag equal to the horizontal thrust component.

The weight at this point is assumed to be 88 kg as determined during preliminary design. That leaves the drag as an unknown, therefore this will be determined with the method from Introduction to Multicopter Design and Control[21].

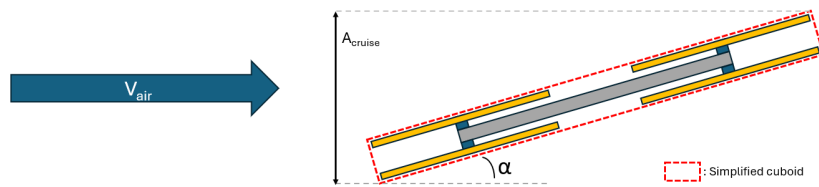


Figure 6.3: Drag Approximation Method

A cross-sectional area is required to calculate drag. This is simplified by using Equation 6.4, as depicted in Figure 6.3.

$$A_{cruise} = W_{cuboid} \cdot ((H_{cuboid} \cdot \cos(\alpha)) + (W_{cuboid} \cdot \sin(\alpha))) \quad (6.4)$$

Furthermore, literature suggests a drag coefficient of approximately 1 for the inclined cuboid [58]. However, the tutor advises applying a factor of 0.8 to accommodate for the slightly better aerodynamics of a UAV compared to a pure cuboid.

$$D_{cruise} = 0.5 \cdot \rho \cdot V_{air}^2 \cdot A_{cruise} \cdot C_d \quad (6.5)$$

It is now possible to calculate the drag experienced by the drone using Equation 6.5, where ρ is equal to 1.225 kg/m^3 and C_d is equal to 0.8. Certain assumptions are taken, like a simplified shape and a simplified drag assumption.

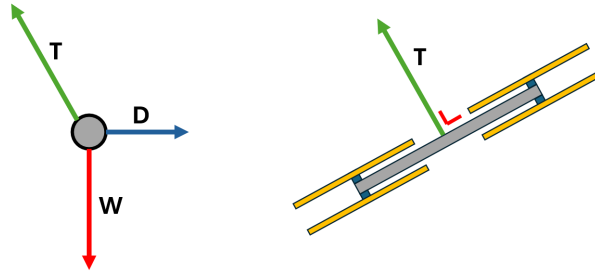


Figure 6.4: Overview of Forces Experienced by Multi-Rotor During Cruise

In Figure 6.4, the free body diagram of the drone during cruise reveals three forces: Drag, Weight, and Thrust. The thrust is acting perpendicular to the drone. During cruise a purely horizontal movement and a 6 bft headwind are assumed, as per requirements, this thus makes the drag act in the horizontal direction opposite to the thrust. The weight points down in the vertical direction. Combining all previous equations with the free body diagram results in Equation 6.6 and Equation 6.7.

$$\Sigma F_x : T \cdot \sin(\alpha) = 0.5 \cdot \rho \cdot V_{air}^2 \cdot C_d \cdot W_{cuboid} \cdot ((H_{cuboid} \cdot \cos(\alpha)) + (W_{cuboid} \cdot \sin(\alpha))) \quad (6.6)$$

$$\Sigma F_y : m \cdot g = T \cdot \cos(\alpha) \quad (6.7)$$

From Equation 6.7 it can be seen that for a chosen thrust setting there exists a corresponding α . Then filling this thrust value and α into Equation 6.6 results in an airspeed. Subtracting the wind speed from this results in a ground speed. The required range obtained from requirements is 5 km. Dividing the range by the speed results in the flight time. Multiplying this flight time with the power required for the given throttle setting results in the expended energy. Once again a lower limit on depth of discharge is set at 20% [21] resulting in a larger required battery capacity. This is repeated for multiple thrust settings to determine the lowest required battery capacity. The lowest power required occurs at a cruise angle of around 60° . At this point, the continuous required power is 21 kWh over an 11-minute time period. This results in a required battery capacity of 5 kWh.

6.2.3. High Voltage Battery Sizing

This then results in two required battery capacities. The highest of the two is the critical situation. This capacity is then divided by the capacity of a single battery to determine the amount of batteries required. These then need to be arranged in series and parallel to provide the right voltage. For the motor selected in Section 4.6 the voltage required is 66.6 V. The selected battery is a 25 Ah 6S battery, which has an average voltage of 22.2 V and a 555 Wh capacity [59]. This battery was selected for its high energy density and convenient form factor. The motors will need 3 batteries in series to deliver the right voltage. This means that all batteries will need to be added in sets of 3. As both hover and cruise require a battery capacity of 5 kWh neither situation is critical. With a single battery capacity of 555, 10 batteries are required. As the batteries need to be in strings of three this dictates 4 strings of 3, resulting in 12 batteries. This does create a slight increase in capacity, but this capacity can be utilised for an increase in hover or range performance.

6.2.4. High Voltage Battery Management System

Lithium-ion cells in series require balancing to avoid unequal discharge, whereas cells in parallel only require precautions to avoid cross-charging (Dong, J. PhD, personal communication, June 3 2024). Cross-charging is where due to a voltage difference, cells with a higher voltage will charge parallel cells with a lower voltage. This is very inefficient and leads to a large loss of capacity. To achieve this balancing an off-the-shelf battery management system (BMS) was selected that functions within the required specifications. For this purpose the JK-B1A24S [60]. This is an active balancer that tracks the voltage of each cell separately. This BMS has a maximum voltage of 100 V and a maximum sustained current of 150 A. Each serial set of batteries will have one of these balancers. The batteries will be connected using the balancing wires already on the batteries, and the BMS and the power lines will be given corresponding connectors.

6.3. System Integration

Having selected all the components, they must be put together into an integral system. This means checking whether each subsystem is getting provided sufficient power, connection types and compatibility of each component. Furthermore, the system must also be placed in the structure, to reveal if there is enough space to house all electrical components.

6.3.1. Electrical Block Diagram

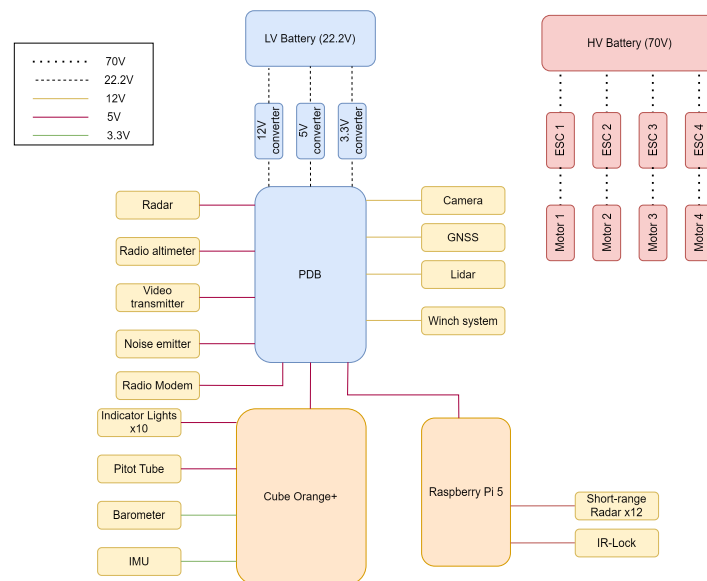
Figure 6.5 shows the electrical block diagram, and the purpose of it is to show the connections within the electronics. As mentioned earlier, both a high- and a low-voltage battery is used, in order to avoid large step downs in voltage. The total power required for the low-voltage system (at maximum power usage) is approximately 100 W, the battery was selected accordingly. The final decision was to implement a PDB. The reason for this is that as can be seen on the diagram, there are a large amount of low-voltage components. Several buck converters would be needed to support all these components, therefore in order to reduce the number of these step downs, the team has made this decision. The idea is that the PDB powers most of the components, however, for low current-draw components, such as the IR-Lock or the external barometer, the controller itself powers it, so that complexity with wiring is reduced.

Low-voltage Battery Sizing

Table 6.1 shows all the voltage and current levels, and subsequently the power levels of each component. As can be seen the total power required is about 100 W, and the total current is around 15 A. The PDB selected is the PM20S-2 by MATEKSYS [61], which can handle an input voltage up to 85 V and has a current peak current limitation of 22 A, which gives a decent safety margin. With these in mind the low-voltage battery can be selected. The main points for consideration are sufficient capacity and current rating. With these in mind a 6S Drone Battery by MAD Components [22] was selected. This battery has a 10 Ah capacity, 0.222 kWh energy storage and 22.2 V voltage. By dividing the energy by the power, it can be found that the operational time of the low-voltage system using this battery is above 2 hours (considering maximum power usage for each component), which is more than sufficient for the mission parameters. The battery has a mass of 0.8 kg, which is quite considerable compared to the mass of the rest of the electrical components.

Table 6.1: Power Breakdown Electronics

Component	Voltage [V]	Current [A]	Power [W]
Flight Controller	5	2.75	13.75
Preprocessor	5	5	25
GNSS	5	0.2	1
Barometer	3.3	0.002	0.0066
Pitot tube	5	0.01	0.05
Telemetry (link)	5	1.5	7.5
RC, telemetry, video	12	2	24
Camera	12	1	12
LiDAR	12	0.5	6
IR-Lock	5	0.05	0.25
Unidirectional radar	12	0.2	2.4
Short range sensors	5	0.1	0.5
Radar	12	0.5	6
PDB	9-85	-	-
NAV lights	12	-	-
Indicator lights	12	0,08	0,5
Noise emitters	5	0,05	0,25
ADS-B	5	0.1	0.5
Winch Motor	12	1.3	15.912
Total	-	15.2	99.75

**Figure 6.5:** Electrical Block Diagram

6.3.2. Components Connection

The components of the electrical subsystem are selected to be high-performance and compatible. All the components and the data buses are indicated in Figure 6.6. The main element is flight controller that receives data and sends the commands to the devices. It is equipped with the 32bit ARM® STM32H753 Cortex®-M7 processor with 400 MHz frequency, 1 MB RAM and 2 MB Flash memory. The second central component is the Raspberry Pi computer with 2.4 GHz frequency and 8 GB RAM. The computational board is connected to the flight controller via the I2C 2 port.

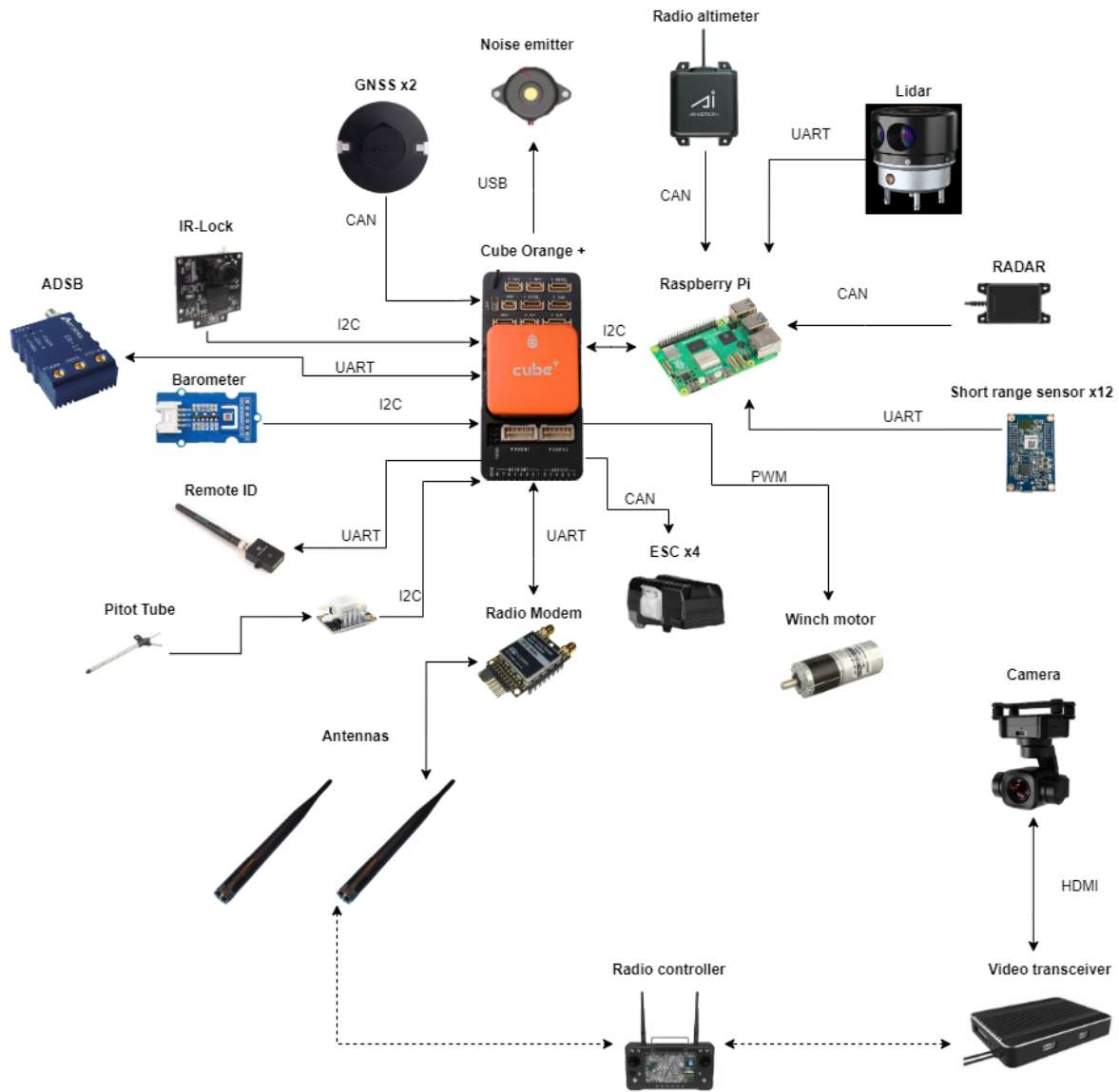


Figure 6.6: Communication and data flow diagram.

The first peripheral devices are two GNSS receivers connected to the autopilot via the GPS 1 and GPS 2 ports. The ports on the Cube Orange+ are shown in Figure 6.7. The GNSS set sends the data on position, velocity, attitude and heading. ADS-B transmits the drone's position and receives the locations of other aircraft. It is connected to the TELEM 1 port.

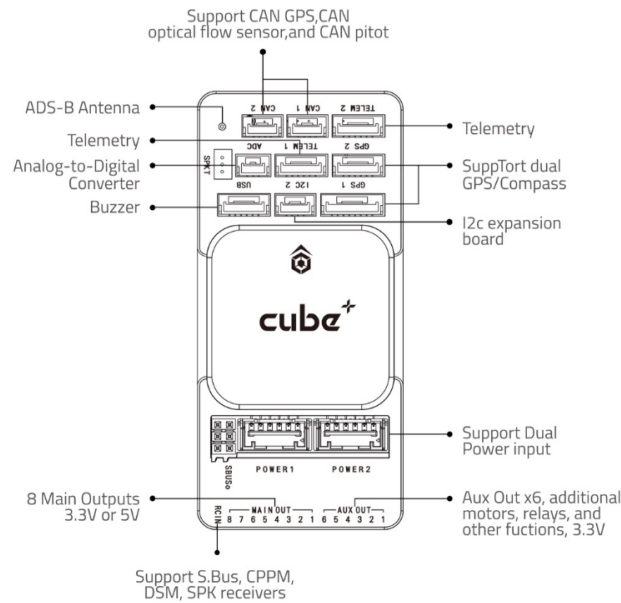


Figure 6.7: Cube Orange+ Connectors.

An I2C extension board is plugged into the CAN 2 socket, allowing for more devices to be attached. These devices are a barometer, pitot tube and IR-lock. The barometer provides primarily pressure used for altitude determination and also humidity and temperature information. The pitot tube conveys the airspeed and the IR-Locks sensor provides the estimated position of the beacon.

Directly to the flight controller, the noise emitter, radio modem and ESCs are connected. The first one is plugged into the USB port and receives simple pulse signals from the board. The ESCs are connected to the pins located on the side of the cube orange. The radio modem is plugged into the TELEM 1 socket. It transmits the telemetry data and receives the radio control signal from the operator. The former concerns information such as drone position, velocity, attitude, altitude and internal indicators. The latter is the input for the drone control. The frequency range of the transceiving system is 868-869 MHz. The data rates are defined by a user and range from 9.6 to 921 kbit/sec on UART and from 4 to 500 kbit/sec on air data transfer.

The radio controller operated by the user is also connected to the camera system. The camera is connected to the video transceiver that sends the video signal to the remote controller. In return, the controller sends the radio control signal for the camera orientation.

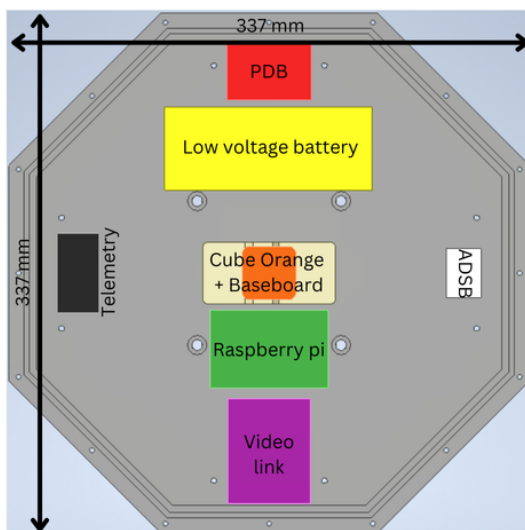
The rangefinders and winch motor are connected via the GPIO interface customary pins to the Raspberry Pi. The board is depicted in Figure 6.8. The radio altimeter and short-range sensors each convey information of the distance to the closest object. The LiDAR creates the point cloud and divides the field of view into sectors. So does the radar. The computing board sends the shortest measured distance to the closest object in each sector. It services the winch motor as well by regulating its speed.



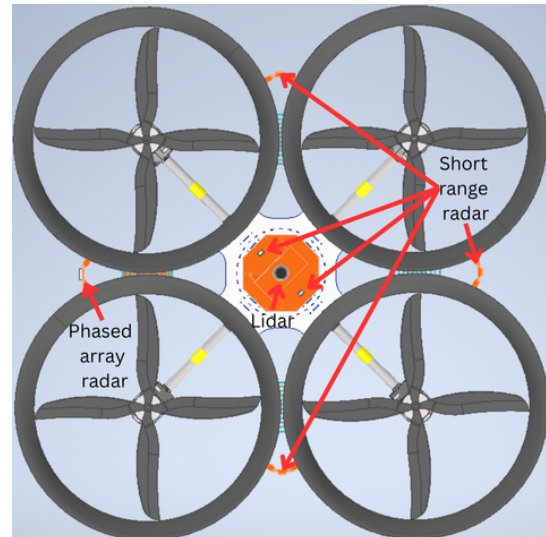
Figure 6.8: Raspberry Pi 5.

6.3.3. Placement in the Structure

The majority of the electronics are placed inside the watertight electronics box. The components are spaced out to improve the weight distribution, which can be seen in Figure 6.9a. This also reduces the amount of interference between the transmission equipment and the power lines. The flight controller is placed in the centre of the box, as this lines up with the centre of gravity of the UAV, improving the performance of the inertial measurement units in case they are required. The low-voltage battery is attached to a bracket to allow easy removal for recharging. The Raspberry Pi is placed close to the flight controller as it will communicate a lot with the flight controller. This is useful as longer cables negatively affect signal strength. The ADS-B, telemetry and video link are each at the edge of the box to reduce cross-interference and improve transmission strength. The PDB is placed far from all other electric systems to reduce electromagnetic interference to those systems.



(a) Top View of Electronics Box



(b) Top View of Sensor Layout

Figure 6.9: Internal and External Top Views

In Figure 6.9b and Figure 6.10 the physical locations of the sensors have been indicated. The locations have been chosen to avoid interference from high-voltage lines to safeguard low signal noise. The LiDAR is located high to avoid the structure from obscuring its field of view. The camera is located on the bottom near the front to allow good vision in the forward and down directions as these are most crucial in standard operation. The altimeter is given a clear field of view to given reliable altitude

measurements.

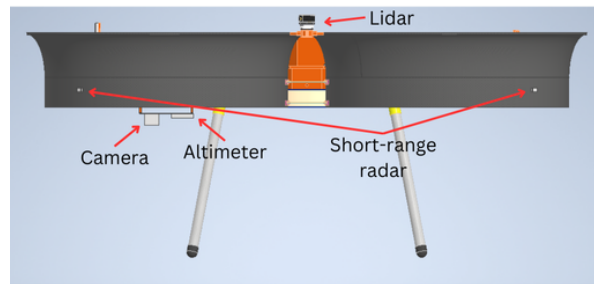


Figure 6.10: Side View of Sensor Layout

As can be seen in Figure 6.11a, the sensors are placed such that a full 360-degree view in the horizontal plane is achieved in any visibility condition. For this use is made of radars as they work in most weather conditions. In good weather, the top-mounted LiDAR can provide incredible detail in a full 360° plane, up to 100 meters away. In the forward direction, a phased array radar offers high accuracy in a narrow, but tall field of view as seen in Figure 6.11. This radar has a range of 80 meters and is the main rangefinder during cruise. The altimeter can measure up to 50 m, which is plenty for landing. Outside this range, the altitude will be determined using a combination of GNSS and barometers.

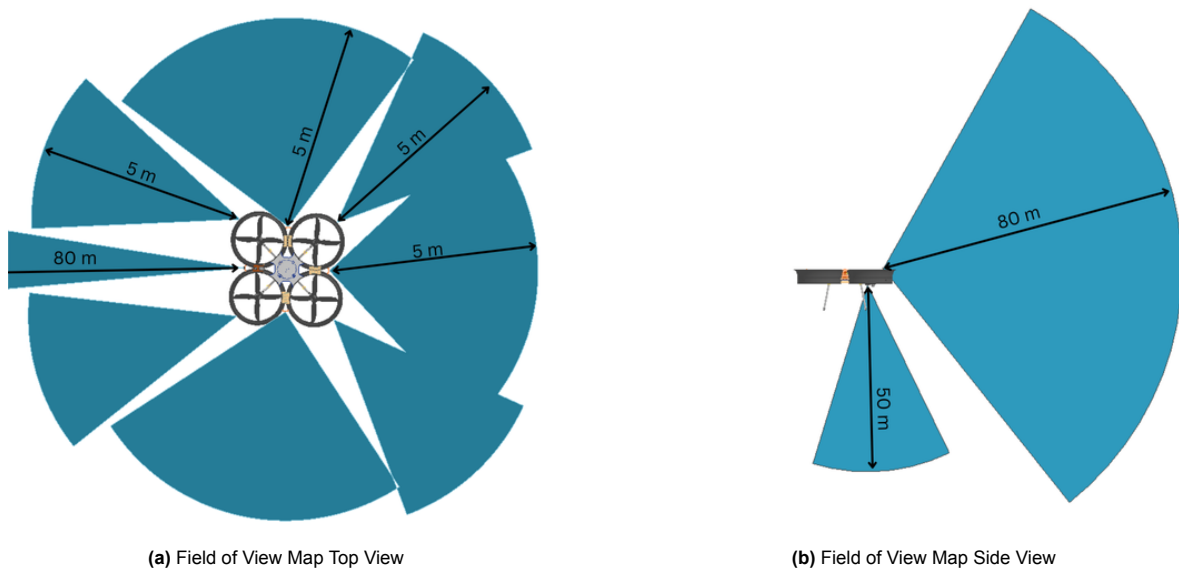


Figure 6.11: Internal and External Top Views

6.3.4. Electronics Budgets

Table 6.2 provides a comprehensive overview of the various components utilised in the communication and data flow systems for the flight control, navigation, collision avoidance, power, warning, and winch systems of the drone. Each component is listed with its corresponding selection, weight, cost, and quantity. This detailed breakdown is essential for understanding the material requirements and budget allocations, ensuring efficient and effective integration of all necessary systems for optimal drone performance. It also serves as a reference for future budget allocation, as most of the parts are off-the-shelf, meaning that estimating the price point of the electrical system can be done quite accurately.

Table 6.2: Communication and Data Flow Diagram

Component	Selection	Weight [g]	Cost [EUR]	Amount [-]
Flight control				
Flight Controller	The Cube Orange+ Standard Set	73	345	1
Preprocessor	Raspberry pi sc1112	46	75	1
Navigation				
GNSS	Here 3+ RTK GNSS/GPS combo	52	290	2
Barometer	Grove – Barometer	9	25	1
Pitot tube	Pixhawk Px4 Digitale	20	80	1
Communication				
RC and telemetry	RFD 868	15	300	1
Video transmission	H16 Pro HD Video Transmission System	90	1800	1
Collision avoidance				
Camera	SIYI A8 mini	95	230	1
LiDAR 2	SF40/C	261	800	1
IR-Lock	IR-lock Sensor	22	350	1
Unidirectional radar	US-D1: All-Weather Radar Altimeter	110	460	1
Short range sensors	MM5D91-00	10	33	12
Radar	77GHZ Collision Avoidance Radar MR72	90	300	1
ADS-B	TR-1F	14	1250	1
Power system				
PDB	Matek PM20S-2	63	50	1
Low voltage battery	6S drone battery by MAD Components87	1700	250	1
Warning system				
NAV light	Firehouse ARC "V" Drone Strobe Spot Light	20	50	1
Indicator light	RS PRO Red Panel Mount Indicator	5	14	10
Noise emitter	HEX - USB Extension and Buzzer	15	10	1
Winch system				
Motor	6-10W Dc Gear Motor	600	430	1
Total		3317	7921	41

6.3.5. Wiring

As the system has been completely described and placed within the structure, the last thing to take a deeper look into is the wiring of the system. The main goal here is to estimate the weight of all the cables and to have a plan for cable management. As the motors operate on a high voltage, wires for these power lines should be separated from the rest, so the electromagnetic interference does not cause disturbances in the low-voltage signals. Should this be unavoidable, proper insulation shall be used on the according wires.

High-voltage

The high-voltage wiring system for our UAV is designed to handle the substantial current demands of the motors while ensuring safety and reliability. According to the motor datasheet, each motor requires a wire that can withstand a current of 200 A. Based on the recommendations of the battery manufacturer, the AWG8 cable has been selected. This cable has a current rating of 50 A. For longer periods it can handle up to 472 A, and for shorter bursts up to 2.5 kA, which shall be sufficient for our UAV.

Considering the UAV has four motors, and the cables have to be routed first to the centre and then to the motors through the arms, we require approximately 6 m of this wire. This 6 m has to be doubled as there also has to be a ground connection, and then doubled again so that each battery is connected to both batteries next to them, as this would ensure a parallel configuration. The total wire length is 24 m, and an extra meter is allocated for unforeseen issues. The specific density of the AWG8 wire is around 74 g/m. The total mass would be 1.85 kg, however, some mass shall be allocated for insulation as well, it has been decided to allocate a 25% margin, which makes it a total of 2.3 kg for the high-voltage wiring. Given the small diameter of the wires, they will easily fit through the tubes. If a solid plate obstructs the path, small holes can be drilled to allow the wires to pass through without compromising the structural integrity of the UAV.

As there is a large length of high-voltage wire, it is important to check the voltage drop and power loss. AWG8 wire has a length-specific resistance of $2.061 \frac{\text{m}\Omega}{\text{m}}$ [62]. The shortest distance from battery to motor is 1.2 m, resulting in a resistance of 2.47 m Ω . The longest distance is 2.4 m, resulting in a resistance of 4.95 m Ω . This would lead to a voltage drop between 0.37 V and 0.74 V. This results in a 1 to 2 percent power loss at the highest current draw.

Additionally, proper cable management ensures the wires are secured along the arms using cable ties and clips to prevent movement and wear due to vibrations during flight. This setup protects the wires from external elements and minimizes the risk of tangling or interference with other components. Using high-quality connectors will further ensure the integrity of the high-voltage system, allowing for easy maintenance and replacement if necessary. This comprehensive approach ensures that the UAV can perform its intended missions effectively and safely.

Low-voltage

The low-voltage wiring system of our UAV is crucial for ensuring efficient power distribution and reliable communication among various components. For the low-voltage components, we use AWG22 and AWG24 wires. The AWG22 wire, with a diameter of approximately 0.644 mm and a current capacity of up to 7 A, is suitable for power distribution to components such as the flight controller, sensors, and communication devices. The AWG24 wire, with a diameter of about 0.511 mm and a current capacity of up to 3.5 A, is used for data transmission lines like I2C and UART connections due to its balance between flexibility, strength, and adequate current capacity for lower-power components. In terms of weight estimation for the low-voltage wires, we need to consider both the AWG22 and AWG24 wires used throughout the UAV. The AWG22 wire has a specific mass of approximately 29 g/m, and the AWG24 wire has a specific mass of about 19 g/m. Estimating the total length of wiring required for the UAV, including connections to all sensors, communication devices, and power distribution, we anticipate using approximately 20 m of AWG22 wire and 15 m of AWG24 wire. This results in a total weight of around 580 g for the AWG22 wire (20 m x 29 g/m) and 285 g for the AWG24 wire (15 m x 19 g/m). Therefore, the combined weight of the low-voltage wiring is approximately 865 g. This conservative estimate ensures that the UAV's design accounts for the necessary wiring weight, contributing to an overall balanced and efficient system.

Maintaining signal integrity is crucial for data transmission. To minimise signal degradation, it is essential to keep data wires as short as possible and avoid running them parallel to high-power lines to prevent electromagnetic interference. Proper cable management ensures efficient and tidy wiring. All wires are neatly routed along the UAV's frame, avoiding sharp bends and potential pinch points that could damage the insulation. Wires are secured using cable ties and clips to prevent movement and wear due to vibrations during flight. Power wires and data wires are routed separately to minimise electromagnetic interference, ensuring that power distribution does not interfere with data transmission. Wire lengths are kept to a minimum to reduce resistance and potential voltage drops. Excess wire is avoided, but if necessary, it is neatly coiled and secured to prevent interference and maintain a clean build. Wires running through the UAV's arms and other structural parts are protected with appropriate sleeving or tubing to prevent abrasion and potential damage. If a solid plate obstructs the path, small holes are drilled to allow the wires to pass through without weakening the structure.

The PDB is centrally located to minimise the length of power wires to the components, ensuring efficient power distribution. The flight controller and sensors are mounted in positions that allow short and direct connections to the PDB and each other, with the flight controller centrally placed to act as the main hub

for all connections. Communication devices, such as the Radio Modem, are positioned to ensure minimal signal loss and interference, with wires routed to avoid crossing high-power lines.

6.4. Sensitivity Analysis

Sensitivity analysis is a critical step in the design and optimisation of the drone's electrical and power systems. By systematically varying key parameters, we can understand the impact of these changes on the drone's performance, efficiency, and reliability. This analysis helps identify the most sensitive aspects of the system, guiding design choices to ensure optimal operation under a range of conditions. In this section, we will focus on three specific areas: battery capacity and energy consumption, wire gauge and electrical losses, and an important environmental factor: temperature.

Battery Sizing

Here we aim to investigate how changing the battery capacity influences the hover time. Increasing the battery capacity results in more energy available, however more batteries mean more weight - both battery weight and structural and wiring mass. Therefore it is expected that the battery capacity can not be increased to infinity as at some point the weight would overpower the added energy, and the motor also has limitations. The relations were added into Python and then the capacity was incrementally increased. Figure 6.12 shows the resulting graph, the increased structural weight is also taken into account by adding a 50% margin to the weight added by the battery, which can be considered to be linearly increasing as the same battery is added over and over again in parallel.

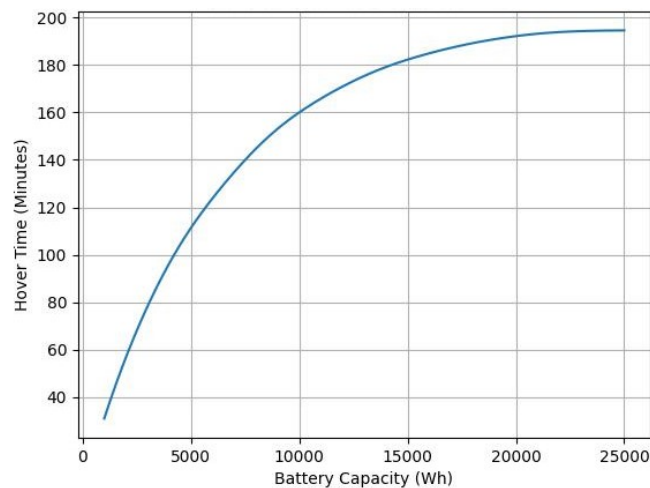


Figure 6.12: Hover Time - Battery Capacity

Temperature

There is not a lot of data available about the specific motor and battery that the UAV is using how they react to change in temperature. Therefore it can not be evaluated qualitatively, however some research can be done. Based on [63], it can be said that generally these electrical UAVs are more sensitive to low temperatures, rather than high temperatures. As mentioned in the paper, at low temperatures, there is a significant loss of performance, and under -25°C the UAV was completely inoperable. Above 60°C performance loss was not as large, however components were more likely to suffer damage from charge-discharge cycles than in normal operational conditions.

6.5. Verification and Validation

Verification and validation are essential to ensure the high-voltage electrical components of the drone meet the design requirements and perform reliably. This section outlines the methods used to verify and validate the battery system, management systems, and power requirements during hover and cruise.

6.5.1. Hover Requirement

To verify the hover requirement, the thrust generated by the motors must equal the drone's weight to maintain altitude. The mechanical power for hover is calculated from the propeller's torque and RPM, while the electrical power is determined using the motor's electromechanical efficiency:

$$\eta = \frac{P_{\text{Mechanical}}}{P_{\text{Electrical}}}$$

Experimental efficiency data for the x13 motor will be validated against manufacturer specifications. The power required for a 30-minute hover, adjusted for battery degradation, was found to be 7.9 kW, translating to a battery capacity of 5 kWh. This was confirmed through simulations and practical tests under expected load conditions.

6.5.2. Range Requirement

The range requirement validation involved ensuring the thrust and torque relationships with RPM followed quadratic relations. The relation between thrust and RPM in Equation 6.8 and torque and RPM in Equation 6.9

$$T \propto N^2 \quad (6.8)$$

$$M \propto N^2 \quad (6.9)$$

These relationships are verified through theoretical calculations. The drag force, calculated using:

$$A_{\text{cruise}} = W_{\text{cuboid}} \cdot ((H_{\text{cuboid}} \cdot \cos(\alpha)) + (W_{\text{cuboid}} \cdot \sin(\alpha)))$$

$$D_{\text{cruise}} = 0.5 \cdot \rho \cdot V_{\text{air}}^2 \cdot A_{\text{cruise}} \cdot C_d$$

can be validated through computational fluid dynamics (CFD) simulations and wind tunnel tests. The required power for cruise, calculated as 21 kWh over an 11-minute period, can be validated through test flights and energy consumption monitoring.

6.5.3. High Voltage Battery Sizing

The high-voltage battery sizing was based on the highest power requirement scenario. The sizing was performed by simply matching the required energy calculated above with the battery capacity. As this is a simple division it was checked multiple times by multiple people to ensure proper working.

7. Control and Stability

This chapter discusses the stability of the design, by means of a control system. It starts with an analysis of inherent stability of a quadcopter in Section 7.1. After it is made clear an autopilot is needed, the firmware is discussed in Section 7.2. The companion computer configuration is described in Section 7.3, and the overall software structure is depicted in Section 7.4. Then, in Section 7.5 and Section 7.6 the simulated models are described and results are shown. Finally, in Section 7.7 and Section 7.8 results are verified and validated, and a sensitivity analysis is performed.

7.1. Stability

For stability of the system, Figure 7.1 shows the initial stability analysis. As can be seen in Figure 7.1, this system is inherently statically and dynamically unstable, the system should be made stable by RPM control of the propellers. Precise control of the RPM per propeller, can only be performed by a compatible flight controller.

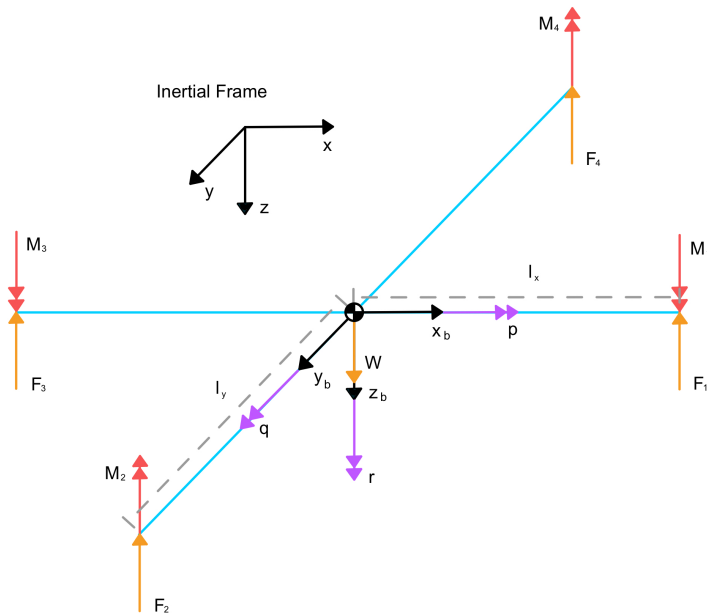


Figure 7.1: FBD

7.2. Flight Controller Firmware

To control the drone and maintain stability, the drone will need a flight controller with compatible firmware. This firmware controls the drone by collecting data from sensors, processing the data with certain controllers and adjusting the speed of each motor via Pulse Width Modulation (PWM) signals to correct orientation and achieve desired movement. In terms of flight controller firmware selection, it is decided to choose for ArduPilot, as it is widely used, and as it is open-source.

7.2.1. ArduPilot Configuration

Arducopter V4.5.3 comes with 4271 configurable parameters out of the box with the option of adding additional custom parameters. Most of these parameters are optional and are only used if a certain device is installed and as such are not relevant in our case.

In analysing the PWM signals to the different rotors, the rotors are numbered and have rotation directions as in Figure 7.2 for the QUAD X configuration that was chosen.

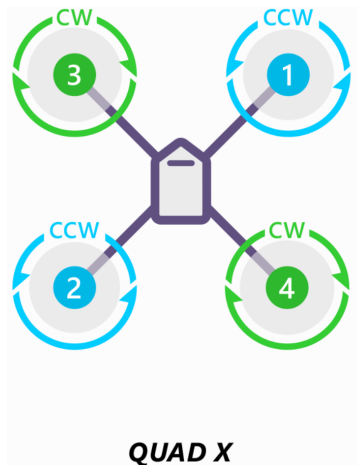


Figure 7.2: Rotor numbering quadcopter [64]

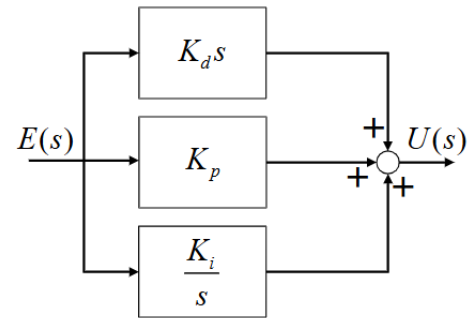


Figure 7.3: PID Controller Block Diagram [65]

7.2.2. Controllers

ArduPilot control system consists of 11 configurable controllers. Of which 6 are proportional controllers and 5 are PID controllers.

PID controllers consist of a Proportional (P), an Integrator (I) and a Differentiator (D) block. These are usually configured as shown in Figure 7.3.

The gain in each component of the controller has a different effect on the output. These can be seen in Table 7.1.

Table 7.1: Effect of Increasing Gain in a PID Controller [65]

+ Gain	Stability	Rise Time	Overshoot	Settling Time	Steady- State error
K_p	Degrades	Decreases	Increases	Small change	Decreases
K_i	Degrades	Decreases	Increases	Increases	Decreases significantly
K_d	Improves for small K_d	Minor change	Decreases	Decreases	No effect (theoretically)

Due to the complexity of tuning a PID controller. They are usually tuned using a heuristic (trial and error) approach [65]. In addition to this, one of the gains is usually fixed to a ratio of another [65]. In ArduPilot's case, the K_p and K_i are kept the same during tuning [66].

Attitude Control

A control loop enables the drone to remain stable and agile, accurately following the pilot's input and compensating for any disturbances in real-time. A loop can stabilise the roll, pitch and yaw in a system designed to maintain drone stability and respond to input commands from a (auto)pilot. Such a process begins with translating the input, converting stick positions into target rates for each axis, with jerk and acceleration conditioning to smoothen out control. Next, these target rates are integrated to form the target position quaternion, representing the desired attitude of the drone. This target attitude is compared to the real attitude, to calculate the error [67].

This error is what is fed into PID controllers for roll, pitch, and yaw. The PID controller computes the corrections needed to minimise errors. Then, the corrections are combined into the motor mixers for adjusting speed of individual motors, to get the RPM to ensure the right attitude. As the system at this point operates with high-frequency PID loops, a low-pass filter is applied to clean sensor data, to ensure precision and stability.

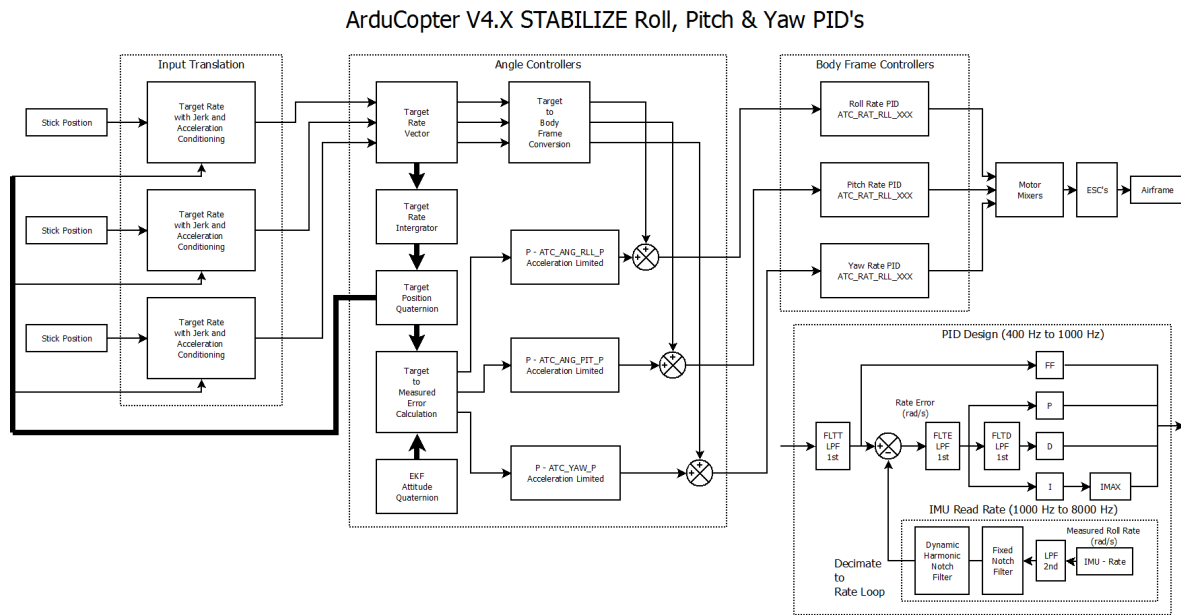


Figure 7.4: ArduPilot Attitude Control Block Diagram [67]

7.2.3. Tuning

The PID controllers used should be tuned per gain for the specific drone used. This can be done in 3 ways: QuickTune, AutoTune and Manual tuning.

QuickTune

QuickTune is an algorithm primarily written by Andrew Tridgell [68]. It slowly increases gains till they are unstable and then lowers them by 60%. This algorithm starts with the roll by tuning the K_d after that it tunes the K_p and K_i . After that it moves on to the pitch in a similar manner and finally it tunes the yaw gains [69].

AutoTune

Autotune is a more in depth algorithm than QuickTune. It tunes the both the P and PID controller for each attitude direction, it also tunes the maximum acceleration and the filters, it can also adjust the feed forward rate for roll and pitch [70]. Autotune can both increase and decrease the gains, however if a vehicle is very unstable it is possible that autotune causes the vehicle to crash. To reduce the likelihood of a crash, an initial tune should be found using Quicktune, after which autotune can be used.

There are some known issues regarding autotune, the main ones that are relevant to our drone are: Autotune can also cause ESC sync issues with low KV motors. Flex in the frame can also result in a bad tune.

Manual Tuning

When autotuning is not available or does not give an acceptable tune, manually tuning the PID parameters is an option. This is done by first lowering K_p , K_i and K_d in steps of 50% till no oscillation are observed [66].

After this the K_d should be increased in steps of 50% till oscillations are observed. Then K_d should be reduced in steps of 10% till the oscillations disappear. After this the K_d should be further reduced by 25%. After this the K_p should be tuned using the same procedure, this should be done while keeping K_i equal to K_p .

The aforementioned procedure should be applied for the roll, pitch and yaw. This procedure should also be applicable to the throttle PID and velocity PID however this is not described by ArduPilot's documentation. Furthermore the proportional controllers for acceleration rate should also be able to be tuned using an approach similar to this.

7.3. Companion Computer

An extra companion computer is needed since autopilot only supports the use of 10 rangefinders. If a 360° rangefinder is used, this single sensor would take up 8 of the 10 slots. Due to requiring more ports than ArduPilot allows, there is a need for a companion computer to merge multiple sensors into 10 or less virtual sensors.

7.3.1. Protocol

The companion computer is connected to the flight computer using an I2C bus and it fakes being a set of 8 rangefinders slaved to the flight computer. On this I2C bus the companion computer mimics the MaxbotixI2C setting that ArduPilot supports, this parameter setting is used for some Maxbotix rangefinders and should be relatively easy to mimic as it is well documented [71]. The flight computer is also directly connected to the sensors using the pins on the companion computer. All sensors connected to the companion computer use UART busses except the main radar which uses can, this results in 13 UART busses and 1 can bus into the companion computer.

The I2C protocol consists of 4 pins, 2 of which are data pins. The other two pins are power and ground. The two data pins are called SDA and SCL. Where SDA carries the data signal and the SCL carries the clock signal. The SDA pin is shared among all devices connected to the bus. Meaning that only one device can communicate at a time. This is managed by a master device asking a slave to transmit data one by one. This configuration allows for multiple devices connected on the same bus. [72]

The UART protocol is similar to the I2C protocol in the number of pins, however the data pins are slightly different. The Rx pin is the receiver and the Tx pin is the transmitter. This allows continues two way communication between the master and slave device. This protocol only supports one master and one slave device on each bus. [73]

The CAN protocol uses the same 4 pins as I2C and UART. Similarly split into 2 data pins and 2 power pins. The data pins are split into CANH and CANL. Unlike UART and I2C the CAN protocol does not use a master/slave setup. Instead all devices transmit and receive on the same data lines. This means that each device has listen on the bus for to find out if it can transmit or not. [74]

With the previously discussed number of devices and the pin counts of the protocols, the required pin count on the companion computer can be calculated. In this instance that is 32 pins.

7.3.2. Pseudo Code

The companion computer requires a custom-built program made for the hardware. Below is a high-level pseudo code designed to provide automated missions by managing sensor data and communication with the flight controller. This pseudo code has been checked by Jarno de Jong, a computer science bachelor student at UvA/VU.

1. Retrieve messages from sensors using programmable pins
2. Decode the values from these messages
3. Sort the obtained values into predefined sectors. (A sector refers to a specific area or zone in the workspace monitored by a group of sensors)
4. Compare the sensor values within each sector
5. Select the lowest value from an enabled device within each sector
6. Send the lowest value from each sector to a dedicated I2C program, as described in Subsection 7.3.1
7. Respond to requests on the I2C bus using programmable pins, providing the most recent range value when asked by the flight controller.

The purpose of this pseudo code is to manage and process sensor data efficiently, ensuring that the flight controller receives accurate information. This enables the implementation of automated missions by providing the flight controller with essential data for navigation and decision-making.

7.4. Software Block Diagram

In order to visualise the the interactions between the software included in the drone, a software block diagram is generated. This diagram is shown in Figure 7.5.

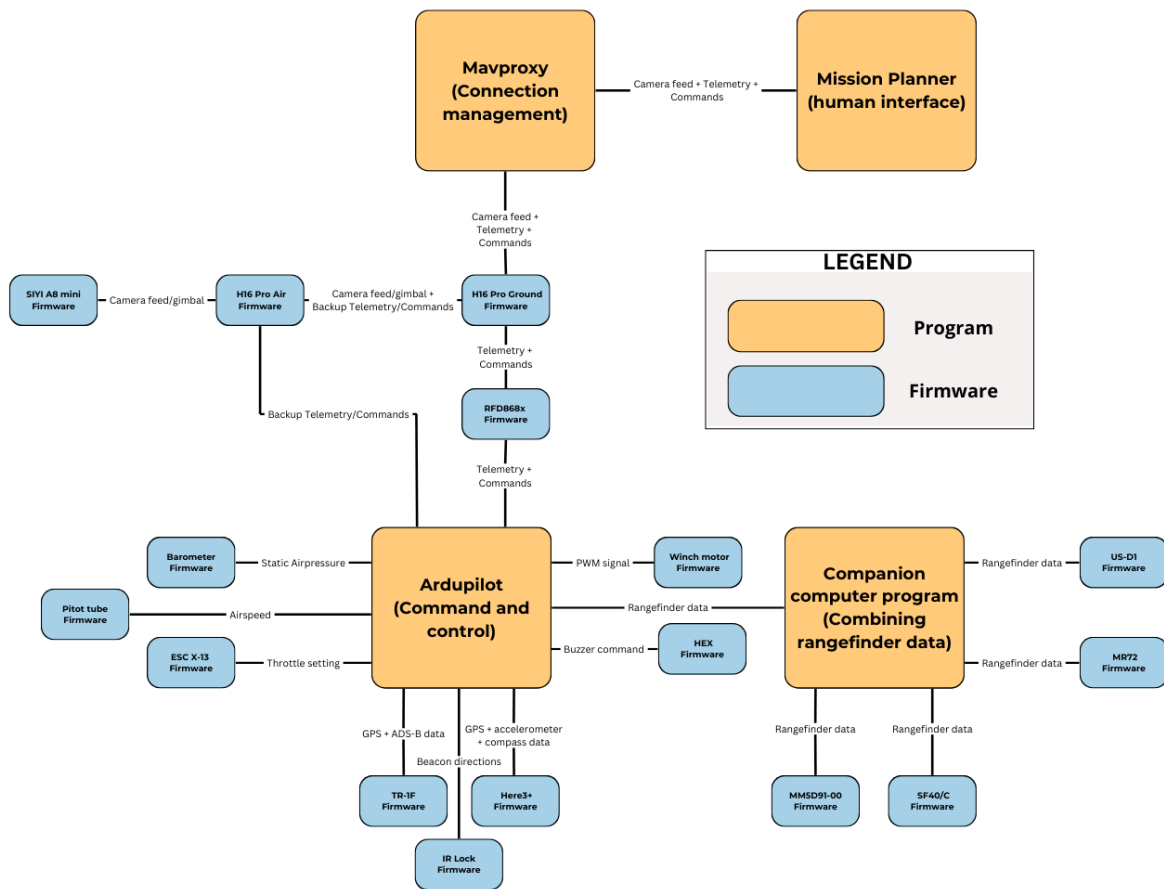


Figure 7.5: Software Block Diagram

Since Figure 7.5 shows the interaction between the software installed on the drone, it can be extremely useful in tracing and debugging any issue that occurs during operation.

7.5. Static Simulation

The static simulation involves the analysis of forces when there are no net accelerations. For Static Simulation the following assumptions are made.

Table 7.2: Assumptions Static Simulation

Identifier	Description
ASP-CTRL-01	The reference frame fixed to the Earth is defined by the North, East, Down (NED) convention and is considered to be an inertial frame
ASP-CTRL-02	The quadcopter is rigid
ASP-CTRL-03	The quadcopter operates within the framework of the International Standard Atmosphere at sea level.
ASP-CTRL-04	In the body-fixed reference frame, the origin is located at the drone's center of gravity.
ASP-CTRL-05	The terms l _{xy} , l _{yz} , and l _{xz} are equal to zero due to symmetry on 2 axes.
ASP-CTRL-06	The propeller's thrust is aligned with the z-axis of the body-fixed reference frame.
ASP-CTRL-07	The weight of the quadcopter acts at its center of mass.

7.5.1. CG Shift

In order to make an estimate of the effect of a shift in CG position in terms of stability a simulation has been conducted. Initially, it calculates the positions and orientations of the four engines relative to the center of gravity and determines the required thrust and torque each engine needs to be in level hover. It iteratively adjusts the power of the engines in small steps countering imbalances to balance the quadcopter in moments and forces, which are shown in Figure 7.6. It ensures the total thrust equals the quadcopter's weight to maintain altitude and the moments around all three axes are zero to keep the quadcopter from rotating.

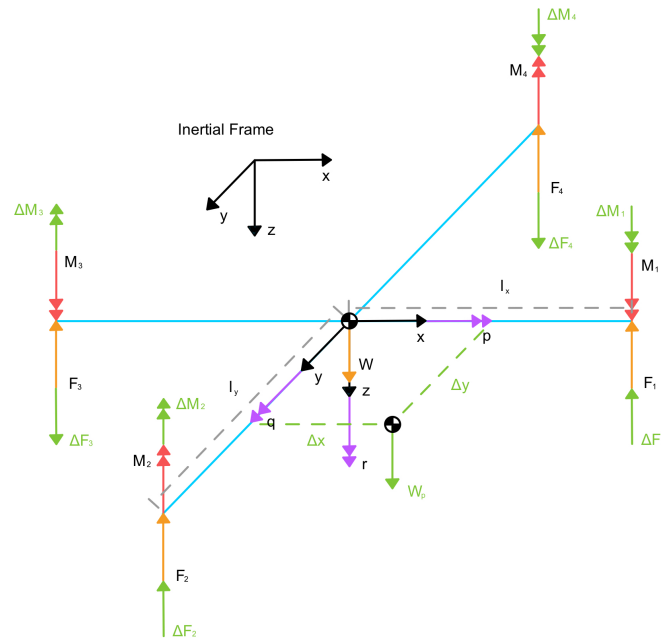


Figure 7.6: Free Body Diagram with Centre of Gravity Shift

Using the thrust per engine, the thrust difference ΔT is calculated using the following formula.

$$\Delta T = T_{max} - T_{min} \quad (7.1)$$

The results of the simulation demonstrates the adjustments of Thrust settings needed for stable flight. The final results of the simulation are shown in Table 7.3.

Table 7.3: ΔT in Relation to CG Shift in x and y

CG shift Δx \ CG shift Δy	0 cm	0.5 cm	1 cm	2 cm	3 cm	4 cm	5 cm
0 cm	0 N	4 N	7 N	14 N	21 N	28 N	35 N
0.5 cm	4 N	7 N	11 N	18 N	25 N	32 N	39 N
1 cm	7 N	11 N	14 N	21 N	28 N	35 N	42 N
2 cm	14 N	18 N	21 N	28 N	35 N	42 N	50 N
3 cm	21 N	25 N	28 N	35 N	42 N	50 N	57 N
4 cm	28 N	32 N	35 N	42 N	50 N	57 N	64 N
5 cm	35 N	39 N	42 N	50 N	57 N	64 N	71 N

As can be seen in the results, the maximum ΔT is 71N. The thrust needed during hover is 216 N per engine, so the difference in engine thrust is quite large. However since the engines thrust to power is relatively constant for small changes in thrust, the lower end of ΔT has a negligible effect on the power needed to operate.

7.5.2. Static moments

The basis of the static moments is the same as that of 7.5.1. The difference is the inclusion of moments around p, q and r. These moments simulate constant disturbances such as having an airspeed.

$$M = \frac{1}{2}\rho V^2 S C_m r \quad (7.2)$$

Using a $C_m = 0.025$, an rotor radius of 0.575 m, an area of 5.9 m and sea level air density of 1.225 kg/m³, the moment can be calculated. Using an iterative approach identical to Subsection 7.5.1, Figure 7.7 can be generated for varying velocity.

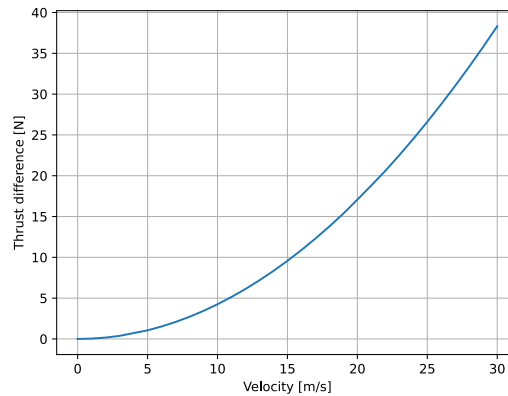


Figure 7.7: Velocity ΔT Graph

Figure 7.7 shows that at higher velocities the change in thrust increases rapidly.

7.5.3. Control resolution

Using the mass moment of inertia and the minimum resolution of the control system. The minimum accelerations that the ArduPilot can set can be calculated. Since a PWM signal can only vary with steps of 1 and this is the resolution ArduPilot uses. This is a throttle change of 0.1%. This results in steps of thrust. The lowest resolution regularly encountered by the drone is during hover,

Due to the two plane symmetry of the drone, the angular acceleration of the drone can be calculated using Equation 7.3, assuming that the drone is two plane symmetric.

$$\dot{\omega} = \frac{M}{I} \quad (7.3)$$

Where M is the moment, I is the mass moment of inertia and $\dot{\omega}$ is the angular acceleration. Using Equation 7.3, the mass moment of inertia and the thrust steps Table 7.4 can be created.

Table 7.4: Control Resolution Angular Acceleration Using PWM

Axis	M [Nm]	I [kg/m ²]	$\dot{\omega}$ [rad/s ²]	$\dot{\omega}$ [deg/s ²]
x	0.62	15.7	0.04	2.3
y	0.62	15.7	0.04	2.3
z	0.08	31.0	0.0026	0.14

Table 7.4 shows that the drone is quite twitchy. Especially considering the PID controller controlling the PWM signal likely overshoots the required PWM value. As such the accelerations of the drone will be much greater. A PWM difference of 10 or 1% throttle would be 10 times the values shown in Table 7.4. As a result of this the protocol used to communicate with the engine was switched to CAN. This change allows for much finer control due to the switch from a 10-bit protocol with PWM to a 32-bit protocol with

CAN [74]. Due to this the control resolution is no longer an issue. Using the new step of four million steps for CAN, Table 7.5 can be generated.

Table 7.5: Control Resolution Angular Acceleration Using CAN

Axis	M [Nm]	I [kg/m ²]	$\dot{\omega}$ [rad/s ²]	$\dot{\omega}$ [deg/s ²]
x	0.00031	15.7	0.00002	0.0011
y	0.00031	15.7	0.00002	0.0011
z	0.00004	31.0	0.0000013	0.00007

Table 7.5 shows that the low resolution issue is indeed resolved by utilising CAN instead of PWM.

7.6. Dynamic Simulation

The dynamic simulation involves the kinematic behaviour of the quadcopter. For Dynamic Simulation the following assumptions are made.

Table 7.6: Assumptions Dynamic Simulation

Identifier	Description
ASP-CTRL-01	The reference frame fixed to the Earth is defined by the North, East, Down (NED) convention and is considered to be an inertial frame
ASP-CTRL-02	The quadcopter is rigid
ASP-CTRL-03	The quadcopter operates within the framework of the International Standard Atmosphere at sea level.
ASP-CTRL-04	In the body-fixed reference frame, the origin is located at the drone's center of gravity.
ASP-CTRL-05	The terms I_{xy} , I_{yz} , and I_{xz} are equal to zero due to symmetry on 2 axes.
ASP-CTRL-06	The propeller's thrust is aligned with the z-axis of the body-fixed reference frame.
ASP-CTRL-07	The weight of the quadcopter acts at its center of mass.
ASP-CTRL-08	The drag is quadratic.
ASP-CTRL-09	The drag of the quadcopter acts at its center of mass.
ASP-CTRL-10	The ground is represented by the x-y plane at zero altitude (z)
ASP-CTRL-11	In the simulation system, acceleration and velocity are constrained to non-negative values when the altitude (z) is zero.
ASP-CTRL-12	The engine responds instantaneously.
ASP-CTRL-13	The angular drag is equal to zero.

7.6.1. Model Description

Two models were developed in different software. At first the model in python was developed, this is an entirely new implementation. As for the second model, this was created using Simulink while utilising prebuild blocks in order to reduce the chance of implementation error. The results of both models can be compared as a verification step since both models use the same underlying theory.

Python

The dynamic drone flight model implemented in Python is based on the following equation of motion shown in Equation 7.4 and Equation 7.5.

$$\vec{V}_{b_n} = \frac{1}{m} \left(-\frac{1}{2} \rho V_{b_n}^2 S C_D + \begin{bmatrix} \Sigma T \\ 0 \\ 0 \end{bmatrix}_n \right) + \mathbb{T}_{BE} \begin{bmatrix} 0 \\ 0 \\ 9.81 \end{bmatrix}_n - \begin{bmatrix} p \\ q \\ r \end{bmatrix}_n \times \vec{V}_{b_n} \quad (7.4)$$

Equation 7.4 implements the thrust, drag and gravity in addition to a term due to the rotation of the reference frames.

$$\begin{bmatrix} \dot{p} \\ \dot{q} \\ \dot{r} \end{bmatrix}_n = I^{-1} \left(L_m \vec{T}_n + \begin{bmatrix} 0 \\ 0 \\ M \end{bmatrix}_n - \begin{bmatrix} p \\ q \\ r \end{bmatrix}_n \times I \begin{bmatrix} p \\ q \\ r \end{bmatrix}_n \right) \quad (7.5)$$

Equation 7.5 implements the moments due to differential thrust, the torque of the engines and a term due to the rotation of the reference frames. L_m is a matrix consisting of the moment arms of the engines. \vec{T}_n is the thrust per engine at time step n .

The dynamic model utilises PWM signals instead of CAN signals for compatibility with the standard SITL's from ArduPilot. PWM settings are converted to an RPM setting using the following equation:

$$RPM = RPM_{max} \cdot \frac{PWM - 1000}{1000} \quad (7.6)$$

With the RPM and Figure 4.12, the thrust and torque are interpolated using an exponential regression.

Due to the rotation of the drone throughout the flight a change in angles between the b-frame and the E-frame will exist. These angles are shown in Figure 7.8.

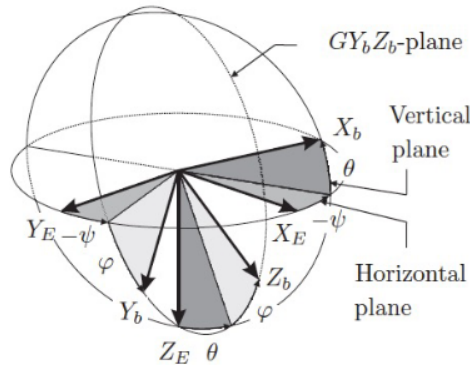


Figure 7.8: Body and Earth frames [75]

In order to rotate between the two frames shown in Figure 7.8 two rotation matrices are created at each time step.

$$H_n = \begin{bmatrix} 1 & \sin \phi \tan \theta & \cos \phi \tan \theta \\ 0 & \cos \phi & -\sin \phi \\ 0 & \frac{\sin \phi}{\cos \theta} & \frac{\cos \phi}{\cos \theta} \end{bmatrix}_n \quad (7.7)$$

Where ϕ is the roll angle, θ is the pitch angle.

$$\mathbb{T}_{BE_n} = \begin{bmatrix} 1 & 0 & 0 \\ 0 & \cos \phi & -\sin \phi \\ 0 & \sin \phi & \cos \phi \end{bmatrix}_n \begin{bmatrix} \cos \theta & 0 & \sin \theta \\ 0 & 1 & 0 \\ -\sin \theta & 0 & \cos \theta \end{bmatrix}_n \begin{bmatrix} \cos \psi & -\sin \psi & 0 \\ \sin \psi & \cos \psi & 0 \\ 0 & 0 & 1 \end{bmatrix}_n \quad (7.8)$$

Where ϕ is the roll angle, θ is the pitch angle and ψ is the yaw angle.

These rotations are then applied in the following equations.

$$\begin{bmatrix} \dot{\phi} \\ \dot{\theta} \\ \dot{\psi} \end{bmatrix}_n = H \begin{bmatrix} p \\ q \\ r \end{bmatrix}_n \quad (7.9)$$

$$\vec{V}_{b_n} = \mathbb{T}_{BE_n} \vec{V}_{e_n} \quad (7.10)$$

$$\vec{V}_{e_n} = \mathbb{T}_{BE_n}^{-1} \vec{V}_{b_n} \quad (7.11)$$

The python model uses a forward Euler integration scheme in order to to the next time step. The time step (dt) used for this integration is 0.01 s. The Euler angles are integrated using the following equation:

$$\begin{bmatrix} \phi \\ \theta \\ \psi \end{bmatrix}_{n+1} = \begin{bmatrix} \phi \\ \theta \\ \psi \end{bmatrix}_n + \begin{bmatrix} \dot{\phi} \\ \dot{\theta} \\ \dot{\psi} \end{bmatrix}_n \cdot dt \quad (7.12)$$

The angular velocity is integrated around the body frame, as shown in Equation 7.13.

$$\begin{bmatrix} p \\ q \\ r \end{bmatrix}_{n+1} = \begin{bmatrix} p \\ q \\ r \end{bmatrix}_n + \begin{bmatrix} \dot{p} \\ \dot{q} \\ \dot{r} \end{bmatrix}_n \cdot dt \quad (7.13)$$

Both the position and velocity are integrated in the E frame as shown in Equation 7.14 and Equation 7.15 respectively.

$$\vec{P}_{e_{n+1}} = \vec{P}_{e_n} + \vec{V}_{e_n} \cdot dt + 0.5 \cdot \vec{V}_{e_n} \cdot dt^2 \quad (7.14)$$

$$\vec{V}_{e_{n+1}} = \vec{V}_{e_n} + \vec{V}_{e_n} \cdot dt \quad (7.15)$$

SimuLink

An overview of the model is shown in Figure 7.9. SimuLink is partially made with prebuild blocks from Mathworks's aerospace blockset.

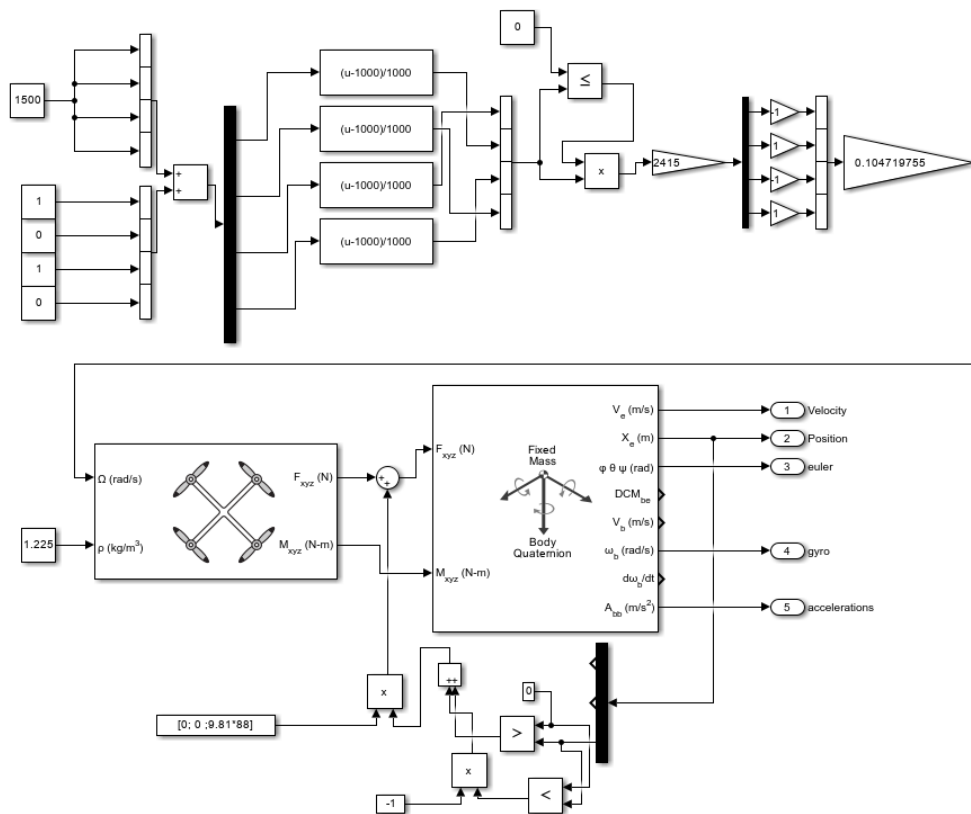


Figure 7.9: Simulink Simulation of the Drone

The top half of the simulation turns the PWM signal into an angular velocity of the rotors. The multirotor block turns the angular velocity into forces and moments. Then the custom block on the bottom manages the ground collision and the gravitational force. These forces and moments are then put into a 6 DOF system that uses quaternions internally. From this velocity position, Euler angles, angular rates and the accelerations are extracted.

The thrust provided by the multirotor block is substantially lower than that of the data it is derived from at the same RPM. As a result the Simulink simulation generally runs at larger PWM values and with different thrust and torques. While the values provided by the Simulink simulation are most likely

wrong the behaviour of the system should be similar to the python program. Additionally the Simulink simulation does not implement drag. As a result the drone does not have terminal velocity, which is a slightly different behaviour than python where this is implemented.

7.6.2. Interfaces

Both python and Simulink have 2 methods of interacting with the simulation. The first method is programming either constant PWM signal, pre-set time varying PWM signal or a custom controller. The second method is connecting ArduPilot to the simulation. The latter is accomplished using software in the loop integration with a JSON protocol [76].

7.6.3. Scenario description

To analyse the dynamic behaviour of the system, the different rotors are numbered as in Figure 7.2. The following different user case scenarios are considered in Python and SimuLink:

- Takeoff; increase PWM signals over all four engines
- Pure roll, pitch, and yaw; variate PWM signals of two engines to create a pure axis rotation moment
- Multiple axes rotation; disturbances over multiple axes
- Hover followed by one engine inoperable; increase PWM signals over all four engines and then reduce PWM signals over all four engines. Then set PWM signal of one rotor equal to zero.

To be able to create the pure axis rotations, adjusted PWM signals are created. For z-axis rotation, rotor 1 and 2 are given an increased signal as defined in Figure 7.2. For x-axis rotation, rotor 1 and 4 are given an increased RPM, and for y-axis rotation rotor 1 and 3 are given increased PWM signals.

7.6.4. Scenario results

The simulation will be run in both Python and Simulink. These results are given below.

Python

In python, the following results are shown. The first take-off scenario shows the behaviour for constant PWM signals equal to 1600, which corresponds to a 60% throttle for minimal thrust for takeoff, in Figure 7.10 and Figure 7.10. In this case, the quadcopter ascends to cruise altitude in 50 s and uses 0.125 kWh for this manoeuver. If the drone needs to ascend in 16 s, the PWM signal needs to be increased by 50.

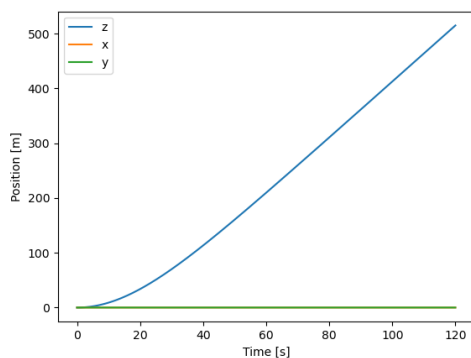


Figure 7.10: Takeoff Position Plot

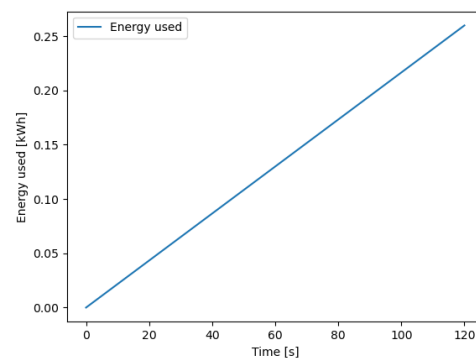


Figure 7.11: Takeoff Energy Plot

For pure axis rotations, first rotation around the z-axis is analysed. Increasing PWM signal to 1601 for rotor 1 and 2, and keeping PWM signals of rotors 3 and 4 constant at 1600, will result in a pure z-axis rotation, as can be seen in Figure 7.12 and Figure 7.13. The behaviour the plot shows matches the expectations, as the constant PWM signal causes an increasing rate and angular drag is assumed to be equal to zero, as stated in ASP-CTRL-13.

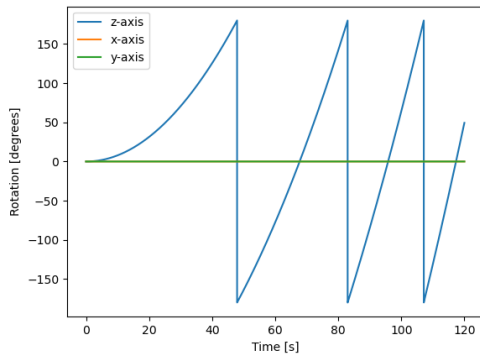


Figure 7.12: Pure z-axis rotation plot

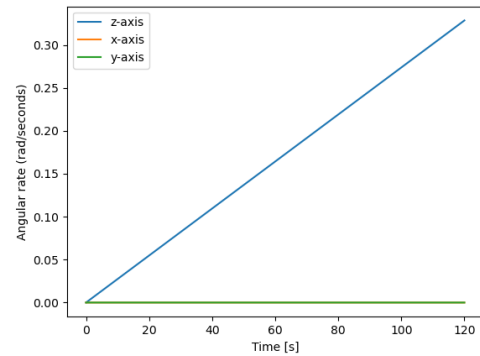


Figure 7.13: Pure z-axis angular rate plot

The second rotation analysed is around the x-axis, which has comparable behaviour to the pure z-axis rotation. Engines 1 and 4 are given an additional PWM signal, so the total PWM signal of engine 1 and 4 being equal to 1601. The only difference of the results is that the angular rate is higher. For the z-axis rotation the additional PWM signals increase the RPM of 2 engines which is the sole reason for rotation. For the x-axis rotation, it shows behaviour for the drone flipping over and at that point the extra thrust created causes the drone to rotate increasingly instead of increasing its altitude. The results are shown in Figure 7.14 and Figure 7.15. This simulation shows what was stated in Subsection 7.5.3 with the exceedingly high accelerations for a single PWM step.

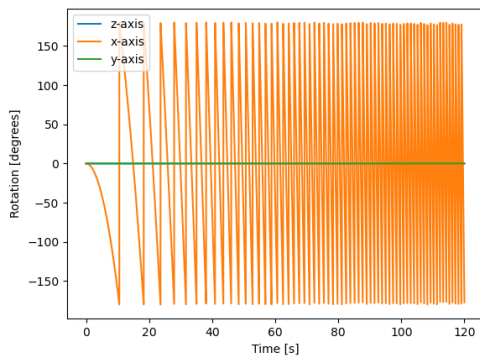


Figure 7.14: Pure x-axis rotation plot

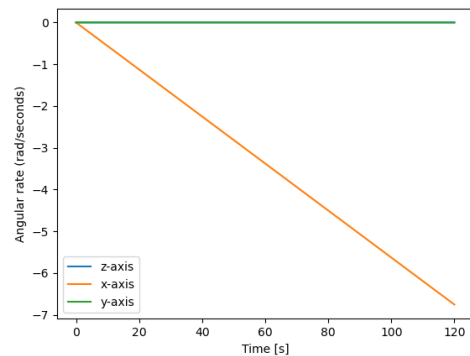


Figure 7.15: Pure x-axis angular rate plot

The third pure axis rotation analysed is around the y-axis. Again PWM is increased by 1 for engine 2 and 4. In Figure 7.16 the plot shows normal behaviour until 90° pitch, afterwards however the system shows signs of singularity as by the nature of the Euler transfer equation (7.7), causing the system to enter a chaotic state. The singularity however only influences the rotation, not the angular rate, and so it shows the same behaviour as for the x-axis plot, shown by Figure 7.17.

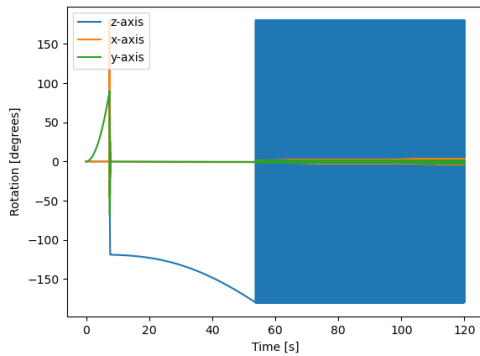


Figure 7.16: Pure y-axis rotation plot

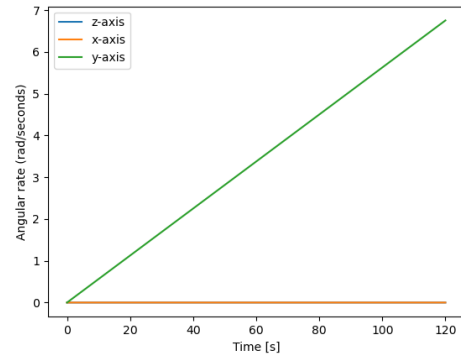


Figure 7.17: Pure y-axis angular rate plot

The system could have disturbance over multiple axes, so to test that the same thrust setting is applied as for the z-axis (2 PWM on rotor 1 and 2), plus an additional PWM increase of 0.001 signal on rotors 2 and 3 to cause a very small x-axis rotation for 120 s. This step should be possible with the switch to CAN due to the increased resolution. These axes are chosen as they do not show singularity effects. The behaviour is depicted in Figure 7.18 and Figure 7.19. The rate increases for the z-axis as the PWM signal is large, and the x-axis rate shows small oscillatory deviations. The trajectory is a spiral with decreasing radius, as the increasing yaw rate stabilises the roll.

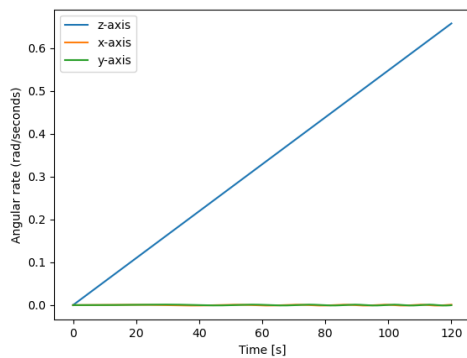


Figure 7.18: Multi-axes rotation rates plot

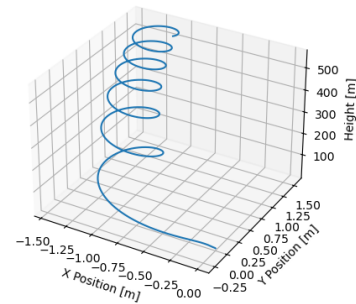


Figure 7.19: Multi-axes trajectory plot

The final scenario depicts take-off - hover - one engine inoperable. The first plot, Figure 7.20, shows the position of the drone. Until 5 s, PWM is 1620, equivalent to 62% maximum RPM. Then for 5 s, it decreases speed, afterwards it hover for 12 s on 60% throttle at 20 m altitude. At that instant, the one engine inoperable scenario starts. First the drone increases altitude for safety reasons, it does this until 160 m altitude which is the a limitation due to air risk which is elaborated later in Figure 10.3. To achieve this manoeuvre without flipping over, the drone increases the throttle of rotors 1 and 2 (or rotors 3 and 4 if either of the former is inoperable) to 90%, while shutting down the other two. This action induces a z-axis rotation, which escalates to an angular rate of 27 rad/s, as illustrated in Figure 7.21, due to the assumption of no angular drag as per ASP-CTRL-13.

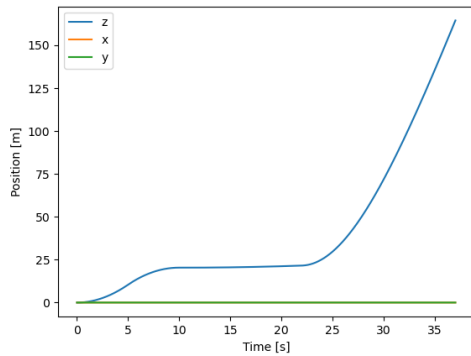


Figure 7.20: One engine inoperable position plot

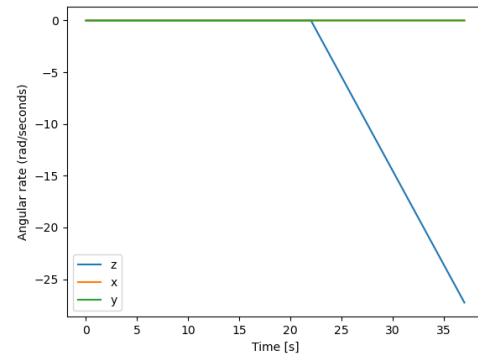


Figure 7.21: One engine inoperable rotation rate plot

The results of the previous results show that the model has no problem with most operational procedures. The singularity at 90° pitch is an important constraint. Furthermore, the spin rate in case of one inoperable engine is to be taken into consideration for the parachute. While a slight spin rate is favourable for parachute deployment, 27 rad/s is too high. However at the service ceiling it stops increasing yaw rate. For future recommendations, the angular drag of the model should be further investigated.

SimuLink

Simulink, part of the MATLAB toolbox suite, is used for simulating and analysing the dynamic model of the drone, utilising its specialised toolboxes for aerospace and control systems. Simulink is used for verification and testing, facilitating continuous testing and validation throughout the development process.

For Take-off, the behaviour is depicted in Figure 7.22. This shows similar behaviour to the Python model.

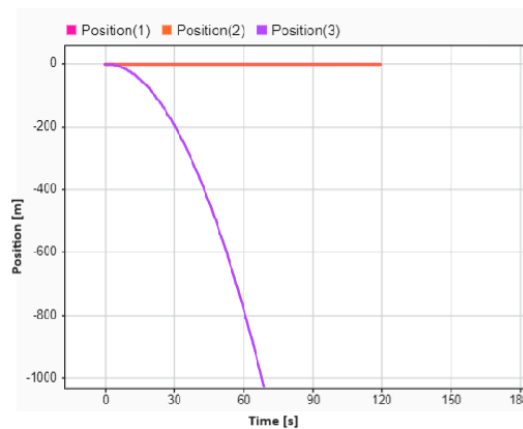


Figure 7.22: Takeoff position plot SimuLink

Pure x-axis rotation is shown in Figure 7.23 and Figure 7.24. Same behaviour, roll (euler(1)) rate continuously increases at a constant rate.

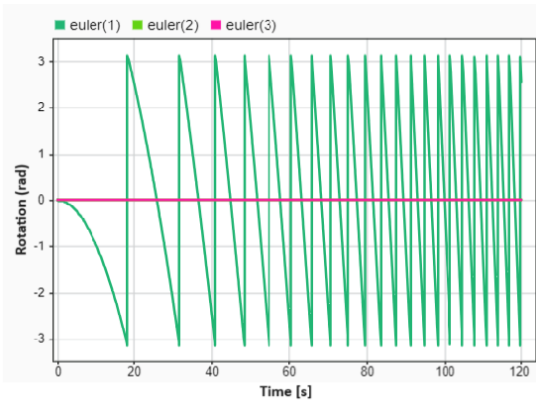


Figure 7.23: Pure x-axis Rotation Position Plot SimuLink

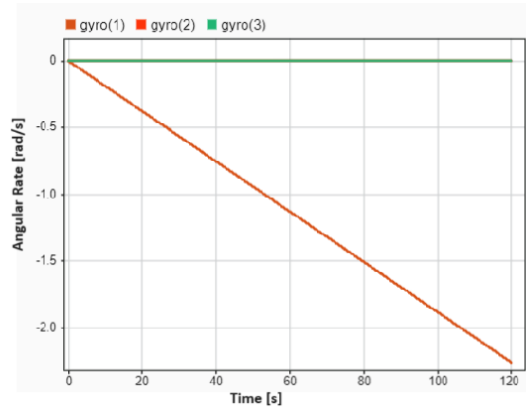


Figure 7.24: Pure x-axis Rotation Angular Rate Plot SimuLink

Pitch behaviour becomes chaotic from 90° , because of singularity.

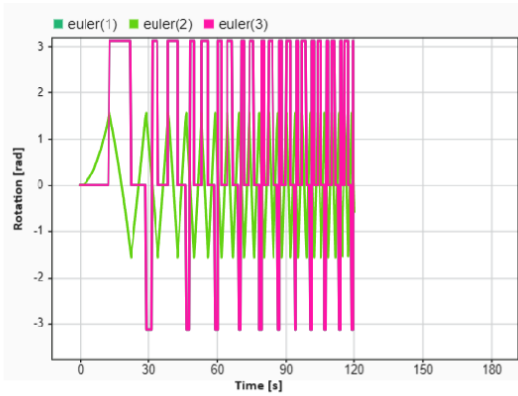


Figure 7.25: Pure y-axis Rotation Position Plot SimuLink

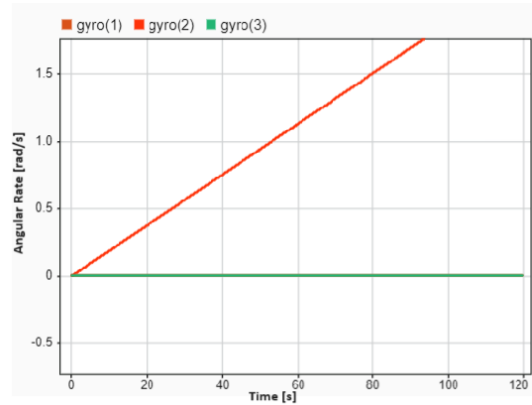


Figure 7.26: Pure y-axis Rotation Angular Rate Plot SimuLink

Z-axis angular rate increasing at a lower rate than x-axis angular rate, as most extra generated thrust used for increasing altitude.

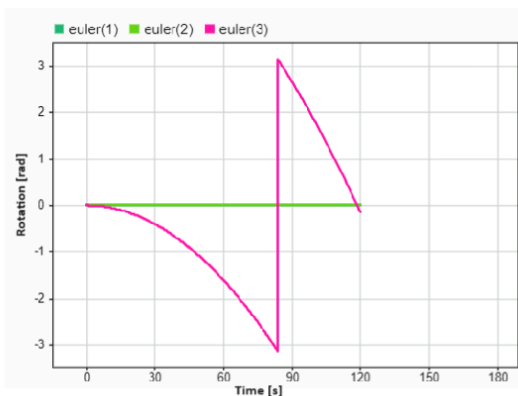


Figure 7.27: Pure z-axis Rotation Position Plot SimuLink

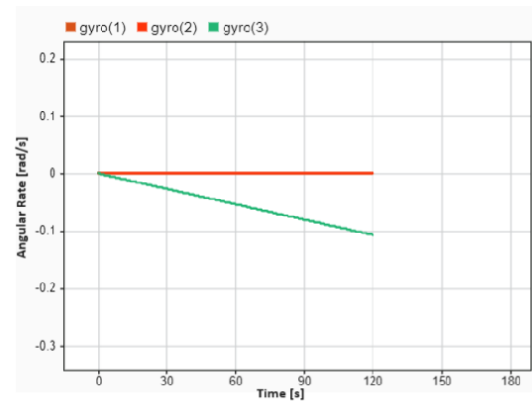


Figure 7.28: Pure z-axis Rotation Angular Rate Plot SimuLink

The previous scenarios show the same behaviour as before. Multiple axes analysis could not be per-

formed in SimuLink as it does not show comparable behaviour in thrust levels and as such is difficult to match.

ArduPilot

Finally, connecting the simulation to ArduPilot, Mavproxy and Mission Planner, the system can be tested out. This showed that the default gains of ArduPilot are unable to keep the drone stable. It is likely that Another likely possibility is that this result is due to the EKF falsely identifying a sensor failure due to the constant 0 sensor data at the start of the simulation and as such ignoring the some of simulations input. This behaviour was consistent for both python and Simulink. This combined with the SITL only being configured for PWM control, results in the unstable behaviour. It is likely that during flight tests the drone can be tuned into a stable configuration.

7.7. Sensitivity Analysis

Sensitivity Analysis is already implemented in the sections of this chapter. For example the CG shift result in ΔT shows this. Control analysis is primarily done to perform sensitivity analysis on certain performance characteristics. However these analysis have their own inputs, due to the computational expense of running the dynamic models multiple times, sensitivity analysis is only performed on the static models.

CG shift

Since the CG shift thrust difference is computed in an iterative manner it is quite computationally expensive to run. The two primary inputs to this analysis are the mass and the engine arms. In general, longer arms reduce the ΔT , while the mass has the opposite reaction where increasing the mass leads to larger ΔT

In Table 7.7 the mass and engine arms are varied with a CG shift of 5 cm in both x and y. This CG shift was the most critical of the analysed CG shifts in Table 7.3.

Table 7.7: ΔT in Relation to CG Shift in with a CG at $\Delta x = 0.05$ m and $\Delta y = 0.05$ m with Changing Mass and Moment Arms

Engine arm [m]	Mass [kg]				
	75	80	88	90	95
0.7	74 N	79 N	87 N	89 N	94 N
0.8	65 N	69 N	76 N	78 N	82 N
0.86	60 N	64 N	71 N	72 N	76 N
0.9	58 N	62 N	68 N	69 N	73 N
1	52 N	55 N	61 N	62 N	66 N

Table 7.7 shows that an increase in the total mass of the drone can easily be countered with n increased engine arm. It also shows that even in the largest case identified in Table 7.3, the increase to ΔT is relatively small even with a mass increase of 12 kg.

Static Moments

Unlike the CG shift, the static moment analysis can be approached with an analytical scaling factor. This is due to all parameters adjusting ΔT in a proportional manner. The scaling factor can be calculated using Equation 7.16.

$$SF = \frac{SC_m l_0}{l S_0 C_{m_0}} = 5.83 \cdot \frac{SC_m}{l} \quad (7.16)$$

Where SF is the scaling factor, the subscript 0 indicates the values used during the first analysis, S is the area, l is the engine arm length and C_m is the moment coefficient. From the equation it follows that an 10% increase in area leads to a 10% increase in ΔT if the other parameters do not change. The same holds true for the moment coefficient. The engine arm has a slightly different relation, here if the arm increases with 10% it causes a decrease of 9% in ΔT if the other parameters do not change.

Control resolution

With the control resolution an approach similar to the sensitivity analysis approach taken for the static moments can be taken. The scaling factor can be calculated using Equation 7.17.

$$SF = \frac{l \cdot I_0}{I \cdot l_0} \quad (7.17)$$

Where I is the mass moment of inertia and l is the moment arm. Equation 7.17 shows that increases in the arm length increase the twitchiness of the drone, while increases in the mass moment of inertia decrease the twitchiness. A much bigger influence would be to switch to a different protocol than CAN as the steps in thrust are mostly dominant.

7.8. Verification and Validation

As discussed in Section 7.6, two numerical models were developed. The Simulink model primarily uses premade blocks in order to reduce implementation errors. While the thrust of the multirotor block appears unreliable. The general behaviour of the system is used to check the Python model which exhibits the expected thrust levels. As shown in 7.6.4 the single axis motions are nearly identical in behaviour. The behaviour is also checked with the expected motion. Both of prior mentioned actions are verification, unfortunately no validation could be performed on the models at this time due to a lack of similar real world data. However the model itself is assumed to be validated, as it is an extensive open source model used extensively in industry for control of drones.

As for the static models, both the CG shift and static moment are randomly checked to see if the thrusts generate a net 0 force in z and net 0 moments. The behaviour of the models during both the analysis and the sensitivity analysis is checked with the expected behaviour. Both of these are verification checks. In order to validate the models the prototype could be used as an unbalanced payload could be attached for the CG shift and a forward flight could be used for the static moment. The control authority's validity balances on the two plane symmetry. This could be checked by looking at the final tune of the prototype. A final step of verification was to check model input errors and to run the code on different time instances.

7.9. Control summary

From a general free body diagram, it is found that drones are unstable by nature. Due to this a flight controller is required to stabilise the system. The flight controller that is chosen is ArduPilot.

Due to a limitations of ArduPilot with regards to the amount of rangefinders, a companion computer is introduced. This companion computer merges the readings from all rangefinders into ten virtual sensors, which is the maximum amount ArduPilot supports.

Static analysis is performed with regards to a CG shift and a constant moment. It is found that CG shifts smaller than 2 cm in both directions can be neglected. Larger CG shifts can cause a significant difference in throttle settings and thus an increase in power used. During static moment analysis, it is found that in forward cruise the moment due to aerodynamic effects on the duct is close to negligible at low speed but ramps up at higher speed. However due to the elevated thrust to achieve these speeds the thrust difference is still negligible.

The last static analysis performed is the control resolution. From this it is found that the CAN protocol should be used for engine control since PWM control suffers from a low resolution.

As for the dynamic analysis, a general takeoff procedure was investigated. From this it is found that at a low 60% thrust setting, takeoff to 160 m maximum altitude takes approximately 50 s, with a 5% throttle increase this drops to 16 s. During the slow takeoff, 0.125 kWh is used for the manoeuvre.

The final dynamic analysis performed is an one engine inoperative scenario. During this manoeuvre the drone ascends to maximum altitude for safety reasons, and then deploys the parachute. From this analysis it is found that in case of an engine failure at 25 m altitude, the drone will spin at 27 rad/s at maximum altitude. In this analysis angular drag is not included. It is expected that angular drag will reduce this spin to a safe level.

8. Final Configuration

Now that each subsystem has been designed, a final overview of the UAV design can be provided. In Section 8.1 the final mass and cost budget are presented. Then in Section 8.2 the final configuration of the UAV is provided using 3D models. Then the performance of the final design is discussed in Section 8.3 and used to verify all requirements are met in Section 8.4.

8.1. Budget Analysis

The final budget is presented in Table 8.1 and Table 8.2

The final structural mass was determined from CAD models of the UAV, to be discussed in Section 8.2 with all the results from Chapter 5. All other budgets have been previously presented in Chapter 6, Chapter 5 and Chapter 4.

Table 8.1: Final Mass Budget

System/components	Unit Weight (kg)	#parts	Total Weight (kg)
Propulsion			16.8
Motor	3.3	4	13.1
Propellers	0.9	4	3.7
Power & Electronics			30.8
Sensors	4.2	1	4.2
Wiring	2.3	1	2.3
High voltage battery	2.0	12	23.5
BMS	0.2	4	0.8
Structures			22.6
Payload + Winch			27.2
Winch motor	2.2	1	2.2
Payload	25.0	1	25.0
Parachute			0.98
			98.3

The final cost budget is presented in Table 8.2, where the structural cost budget is discussed in Chapter 9.

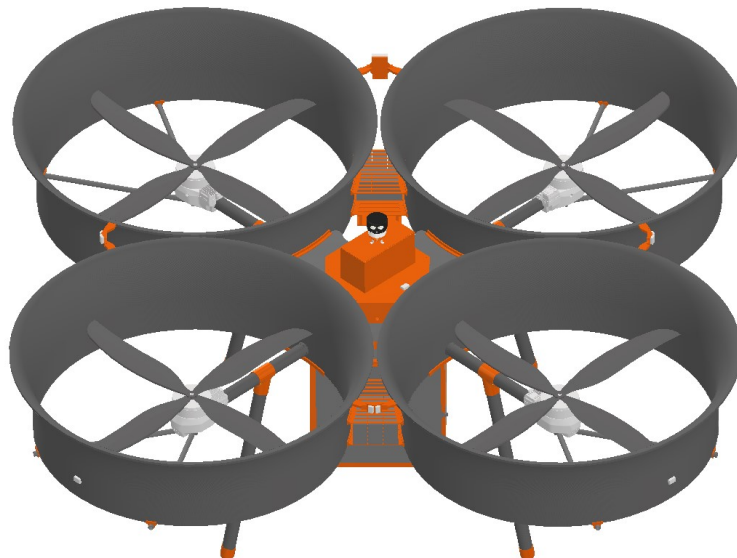
Table 8.2: Final Cost Budget

System/components	Unit cost (euro)	#parts	Total cost (euro)
Propulsion			18476.00
Motor	3,734.00	4	14936.00
Propellers	885.00	4	3540.00
Power & Electronics			14295.20
Sensors and electronics	7,491.00	1	7491.00
AWG8 cabling	11.30	24 (m)	271.20
AWG22 cabling	1.40	35 (m)	49.00
High voltage battery	502.00	12	6024.00
BMS	115.00	4	460.00
Structures			13393.42
Payload + Winch			488.10
Box	0.00	1	0.00
Rope	0.81	10	8.10
Winch motor	430.00	1	430.00
Spool	50.00	1	50.00
Parachute			1118.56
Chute	1,090.00	1	1090.00
Springs	7.14	4	28.56
Total			47771.28 euro 47.77 k euro

8.2. CAD Model

As seen in previous chapters a detailed CAD model was developed. This model was developed in Autodesk Inventor[77]. Additionally an integration with Ansys is available which further increases ease of use and efficiency.

The CAD model consists of over 50 individual parts which are then combined into multiple sub assemblies and/or master assembly. The master assembly of the drone can be seen in Figure 8.1.

**Figure 8.1:** Master Assembly of UAV

The design of this final configuration is a result of the previous chapters where all design decisions were justified. The structure was discussed in Chapter 5, the electronics in Chapter 6, and the mo-

tors/propellers in Chapter 4. Furthermore the design is discussed in great detail in Chapter 12, where the production of each part is discussed.

The model includes all structural parts, propulsion system (Motor, Propeller), batteries, electronics, payload box, and winch. All parts except the motors were modelled by the team.

Due to the short nature of the DSE, it was decided to not yet spend time on detailed drawings for every part. An assembly drawing was created for the complete drone. A BOM (Bill of materials) is also included on the next page to specify which parts are needed together with quantities. This drawing can be found in Figure 8.2.

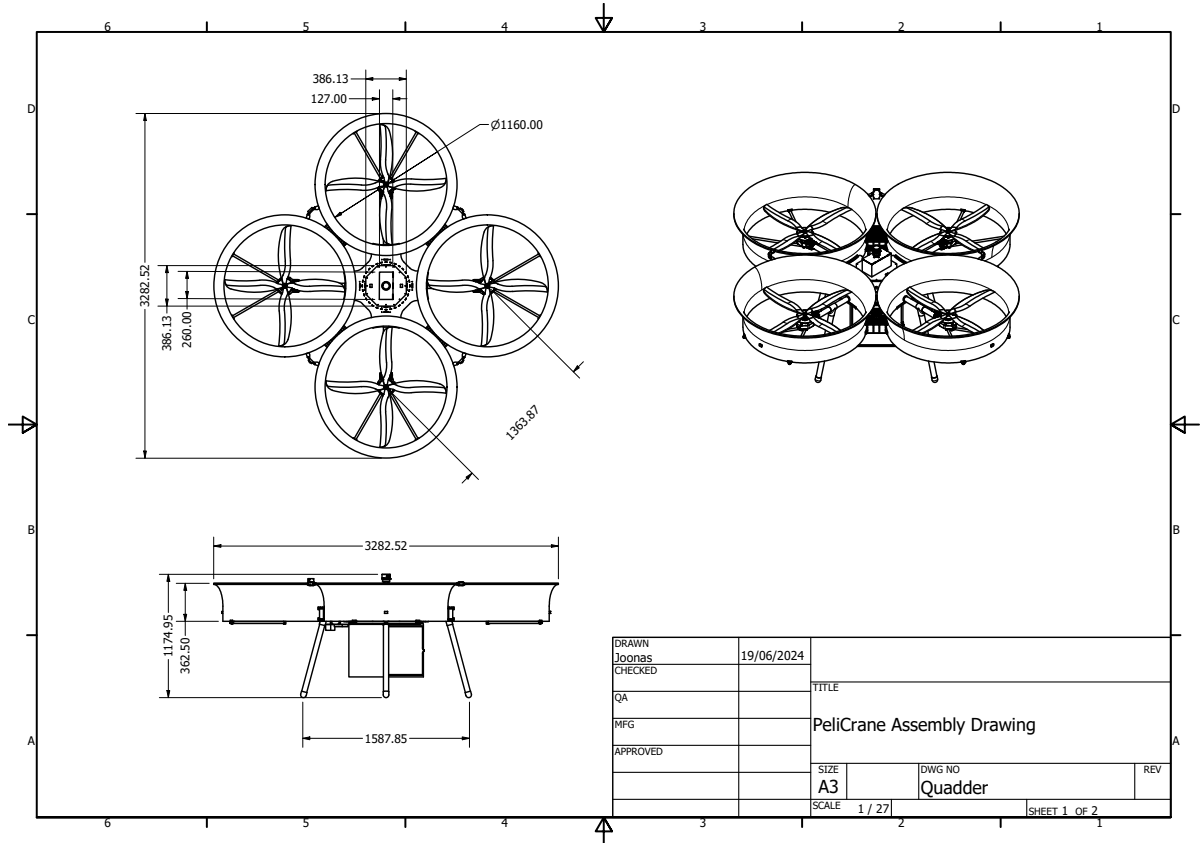


Figure 8.2: Technical Drawing of PeliCrane Assembly

Main Assembly Parts List				
ITEM	QTY	PART NUMBER	MATERIAL	MASS
1	1	Plate with stiffener	Aluminum 6061	3.046 kg
2	8	Arm clamp	Aluminum 6061	0.087 kg
3	4	Arm	GFRC	0.311 kg
4	4	Side panel	Polyethylene, Low Density	0.049 kg
5	4	X13	Generic	
6	1	Top plate with load point	Aluminum 6061	3.044 kg
7	4	42x14_propeller	Generic	0.000 kg
8	1	Winch		0.041 kg
9	4	Landing gear mount v2	Polycarbonate, Smoke	0.092 kg
10	4	Landing gear rod	GFRC	0.183 kg
11	4	landing gear feet	Polycarbonate, Clear	0.022 kg
12	4	Duct Carbon shell	CFRP	1.146 kg
13	16	Inter duct plate connector	Polycarbonate, Smoke	0.049 kg
14	8	Interduct plate v2	Polycarbonate, Clear	0.049 kg
15	4	Duct Foam Inside	Polystyrene, Expanded	0.455 kg
16	4	Duct connection	Polycarbonate, Clear	0.073 kg
17	4	Duct connectio Bottom	Generic	0.082 kg
18	4	Motor connector	Generic	0.025 kg
19	8	Duct Rod	GFRC	0.115 kg
20	8	duct rod connector	Polycarbonate, Clear	0.009 kg
21	1	Electronics_box_full2		2.443 kg
22	1	Lidar_tower	Generic	0.005 kg
23	1	LA-000_092-SF40C-Final-Assembly		1.245 lbmass
24	8	Duct_radar_clip	Generic	0.013 kg
25	1	Main_Radar	Generic	0.093 kg
26	1	Main_Radar_plate	Generic	0.061 kg
27	4	Short_range_duct_sensor	Generic	0.006 kg
28	8	Short_range_sensor	Generic	0.006 kg
29	1	Altimeter	Generic	0.174 kg
30	1	Battery_sensor-plate	Generic	0.086 kg
31	1	Battery_sensor-stand	Generic	0.022 kg
32	1	Camera	Generic	0.210 kg
33	12	6S-25AH	Generic	
34	1	Parachute assembly		0.791 kg
35	4	L_bracket	Generic	
36	3	Short_range_duct_sensor_plate	Generic	0.035 kg
37	1	Payload box assembly		3.099 kg

Winch Parts List				
ITEM	QTY	PART NUMBER	MATERIAL	MASS
1	1	Spool	PC/ABS Plastic	0.025 kg
2	1	PG28BL28	Generic	
3	1	Spool_mount	Aluminum 6061	0.007 kg
4	1	winch_motor_mount	Aluminum 6061	0.009 kg

Parachute Assembly Part List				
ITEM	QTY	PART NUMBER	MATERIAL	MASS
1	1	Parachute outer box	Generic	0.443 kg
2	4	Spring	Generic	0.004 kg
3	1	Inner Parachute box	Generic	0.264 kg
4	1	parachute box top	Generic	0.067 kg

Payload Box Parts List				
ITEM	QTY	PART NUMBER	MATERIAL	MASS
1	1	Payload Box	Polycarbonate, Clear	2.313 kg
2	1	Payload box door	Polycarbonate, Clear	0.783 kg
3	1	Payload box latch	Generic	0.002 kg

DRAWN Joonas		19/06/2024		TITLE PeliCrane Assembly Drawing		
CHECKED						
QA						
MFG						
APPROVED				SIZE A3	DWG NO Quadder	REV
				SCALE	SHEET 2 OF 2	

8.3. Performance Analysis

The performance analysis is performed in order to find the possible mission profiles of the UAV. The range at various wind speeds, hover endurances, and combinations of these are important metrics to consider. These will be based on the batteries, motors and overall size and weight of the PeliCrane. In order to perform these calculations, a number of assumptions are made regarding the drone performance seen in Table 8.3.

Table 8.3: Assumptions Made Regarding Performance

Identifier	Assumption taken
ASM-PF-01	The UAV battery is discharged linearly
ASM-PF-02	The UAV performance is unchanged by environmental factors such as temperature and pressure
ASM-PF-03	The UAV motor works at a constant voltage
ASM-PF-04	The only forces acting on the drone during cruise are drag, weight and thrust
ASM-PF-05	Aerodynamic interactions and moments beside drag are not considered
ASM-PF-06	The center of gravity is equidistant from all propellers
ASM-PF-07	The pitching of the drone is instantaneous
ASM-PF-08	The UAV operates in constant wind conditions of 13.8 m/s, with no gusts.

Using these assumptions, a model can be developed in order to calculate the performance parameters of the UAV.

8.3.1. Hover Performance

During hover, the thrust produced by the UAV is equal to the total weight of the drone. With the total battery energy in kWh found in Chapter 6, the hover endurance t can be simply attained through dividing the total energy available, by the power required for hover, found in Section 4.6. An additional factor of 0.8 is applied to the battery capacity for safety [21].

$$t = \frac{E_{available} \cdot 0.8}{P_{required}} \quad (8.1)$$

Using Equation 8.1, the total hover endurance can be found as a function of the payload mass. This relation is shown in Figure 8.3.

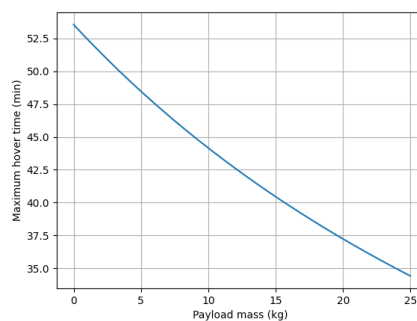


Figure 8.3: Payload mass vs. maximum hover time

8.3.2. Cruise Performance

The forces applied to the UAV are visualised in Figure 6.4. Using this, the relation between the pitch angle θ and the T/W shown in Equation 8.2 can be found.

$$T/W = \frac{1}{\cos(\theta)} \quad (8.2)$$

Equation 8.2 is visualised in Figure 8.4.

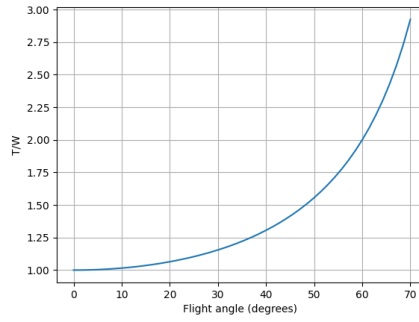
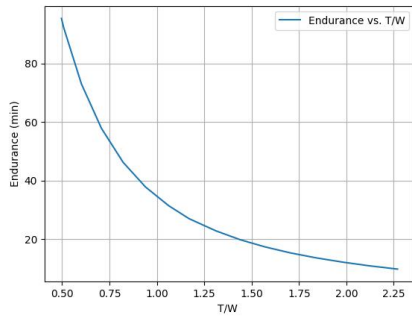
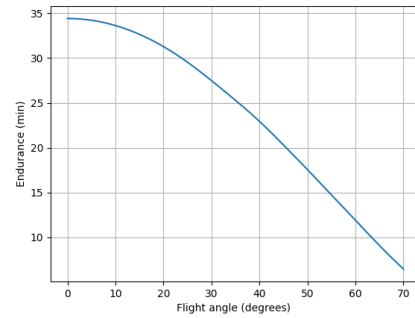


Figure 8.4: Flight angle vs. T/W

With the power required for a certain T/W found in Section 4.6, the endurance as a function of the T/W ratio can be found using Equation 8.1, as well as a function of the pitch angle in as shown in Figure 8.5.



(a) T/W vs. endurance



(b) Pitch angle vs. endurance

Figure 8.5: T/W vs. endurance and pitch angle vs. endurance

Furthermore from Figure 6.4, Equation 8.3 can be found.

$$D = T \cdot \sin(\theta) \quad (8.3)$$

With the drag given as in Equation 8.4.

$$D = 0.5\rho C_d V^2 A \quad (8.4)$$

Where C_d is given as 0.8 and the area of the drone simplified by a cuboid as assumed in Table 4.1.

Combining Equation 8.3 and Equation 8.4, the flight speed of the UAV can be found as a function of the pitch angle as shown in Equation 8.5.

$$V(\theta) = \sqrt{\frac{2W \tan(\theta)}{C_D \rho V^2 A}} \quad (8.5)$$

with the results shown in Figure 8.6

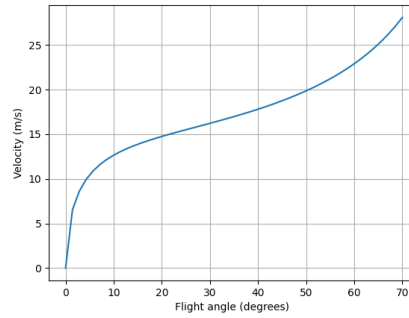


Figure 8.6: Pitch angle vs. velocity

Lastly the range can be found by simply multiplying the velocity at a certain pitch angle by the endurance at given pitch angle.

$$R(\theta) = V \cdot t \quad (8.6)$$

In 6bft head-on wind conditions, Equation 8.6 is modified in order to incorporate the wind speed as shown in Equation 8.7.

$$R = V_{ground} \cdot t = (V_{air} - V_{wind}) \cdot t \quad (8.7)$$

The results for range vs. flight angle are plotted in Figure 8.7 for both conditions.

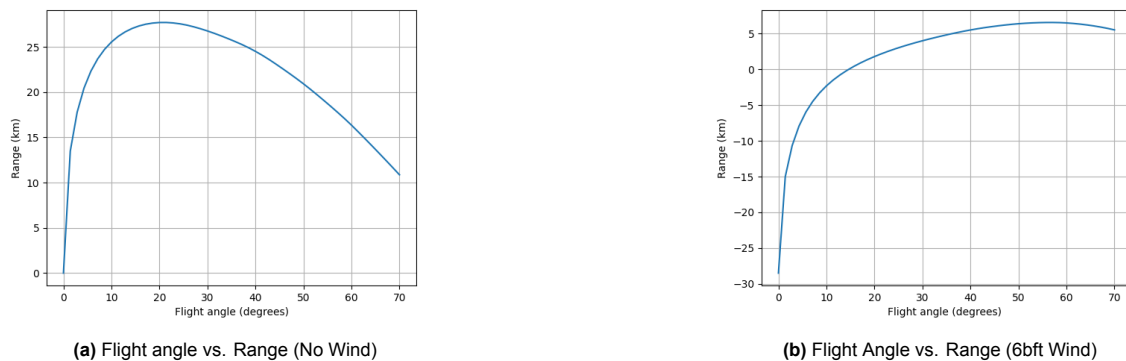


Figure 8.7: Range in no wind and wind conditions as a function of flight angle

It is evident from Figure 8.7 that the optimal flight angle for the no-wind conditions is approximately 20 degrees, while the optimal flight angle for the 6bft wind condition is approximately 55 degrees.

Plotting the relationship between hover time and range, at full 25 kg payload, will give an indication of possible mission profiles, given in Figure 8.8

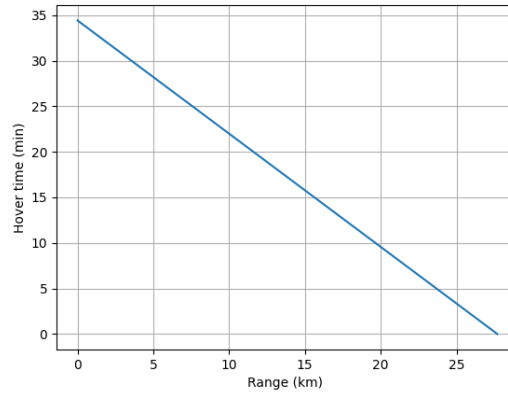
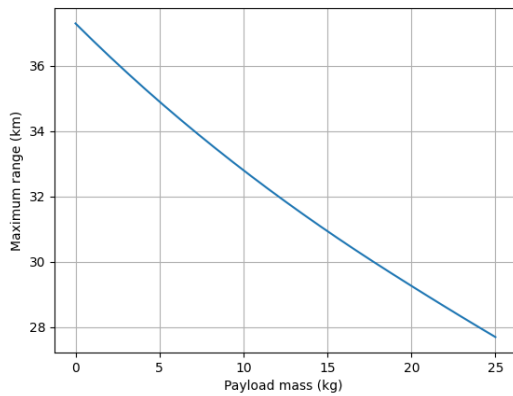
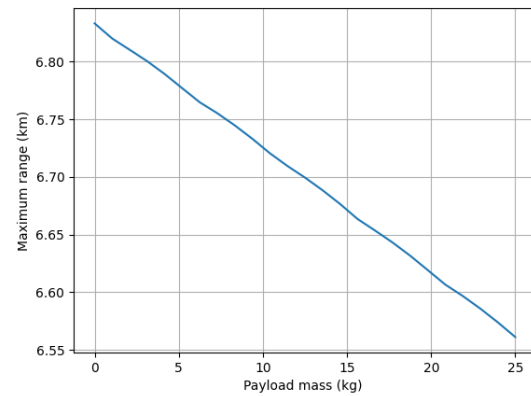


Figure 8.8: Range vs hover time (no wind)

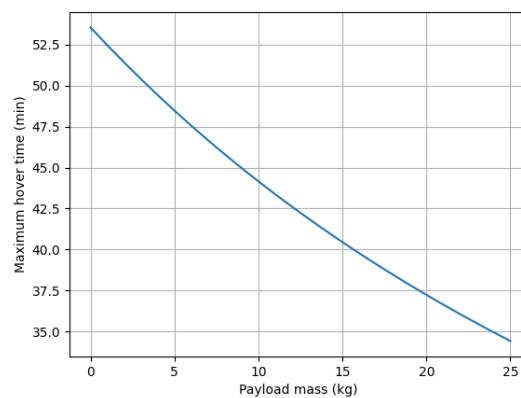
Furthermore, the maximum range as a function of payload mass is given in Figure 8.9, as well as the maximum hover endurance as a function of the payload mass.



(a) Payload Mass vs. Range (No Wind)



(b) Payload mass vs. range (6bft wind)



(c) Payload Mass vs. Maximum Hover Time

Figure 8.9: Comparison of Payload Mass vs. Range Under Different Wind Conditions

8.3.3. Performance Summary

A summary of performance metrics is provided in Table 8.4

Table 8.4: Summary of Performance Metrics

Parameter	Value	Unit
<i>General</i>		
UAV total mass	98	kg
Maximum hover endurance 25kg payload	34.4	min
Maximum hover endurance no payload	62	min
Maximum airspeed 25 kg payload	28.1	m/s
Maximum ferry airspeed no payload	22.5	m/s
<i>No wind</i>		
Maximum range 25 kg payload	27.7	km
Optimal pitch angle 25 kg payload	21.4	degrees
Optimal airspeed 25kg payload	15	m/s
Maximum ferry range no payload	41.2	km
<i>6 bft wind</i>		
Maximum range 25 kg payload	6.6	km
Optimal pitch angle 25 kg payload	57.1	degrees
Optimal airspeed 25kg payload	21.9	m/s
Maximum ferry range no payload	6.9	km

8.3.4. Verification and Validation

As the above results are obtained through use of python, the code has to be verified to be function correctly. The following verification methods were applied Table 8.5

Table 8.5: Performance Analysis Verification

Identifier	Verification method
VER-PERF-01	Check whether results match hand calculations
VER-PERF-02	Check whether optimal pitch angle with zero wind is invariant with mass
VER-PERF-03	Check whether optimal pitch angle varies with mass for the 6bft wind condition
VER-PERF-04	Visually check correct implementation of code
VER-PERF-05	Check correct implementation of motor-propeller specifications
VER-PERF-06	Check consistency of units
VER-PERF-07	Perform dimensional analysis

All of these methods yielded successful results. As the method is developed from a book on drone development [21], it is assumed to be validated.

8.3.5. Sensitivity Analysis

For the sensitivity analysis, it is important to discuss the sensitivity of the model to a varying mass. For this, the results for range and hover endurance as a function of the payload mass can be consulted, there exists a pseudo-linear relation between both mass and range as well as mass and hover endurance, which can also be concluded from the mathematical relations used. Therefore, the model is not particularly sensitive to a varying mass. However it can be noted, as explained in Chapter 4, a mass that is significantly higher would require a heavier motor in order to meet the thrust required efficiently, introducing additional weight, snowballing the mass estimation and decreasing range and hover time significantly. Inversely, a significantly lower mass would require a lighter motor, with the range and hover endurance becoming significantly lower. This would occur at masses below 40 kg, as this is the lower thrust limit of the motor Figure 4.12, and masses above 124 kg, as this would mean the motor is unable to attain a 2:1 T/W ratio considered necessary Figure 4.12. This mass interval is considered to be large enough that it is not considered feasible that the UAV reaches either end of the interval, with the mass budget established in Section 8.1.

The results for this mass interval are shown in Figure 8.10, with all parameters, such as battery capacity and propeller selection invariant except for the total UAV mass.

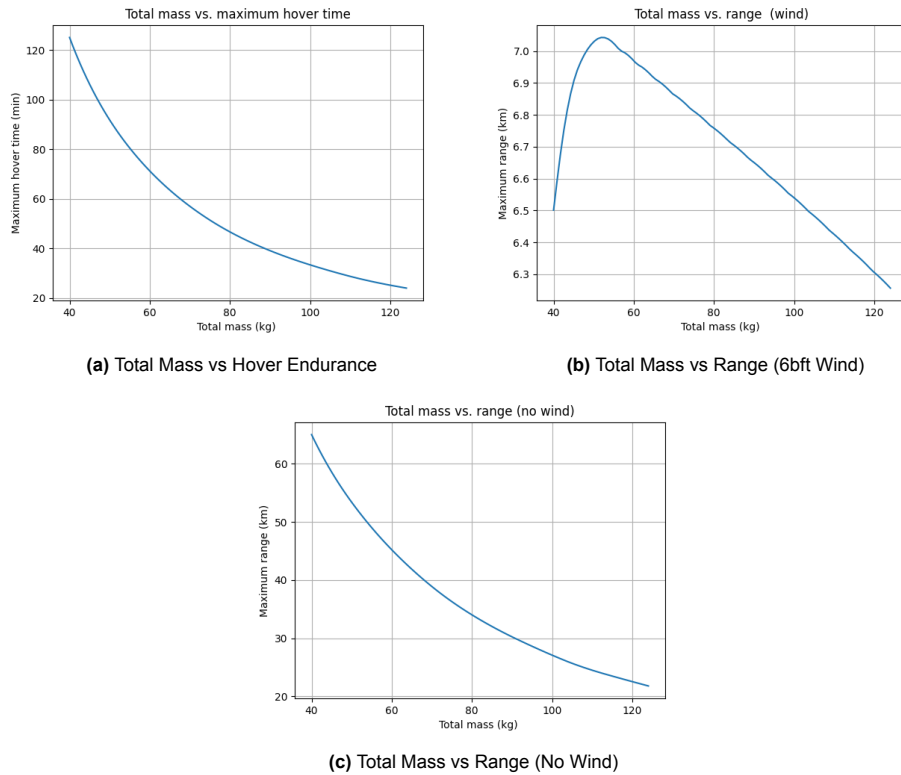


Figure 8.10: Sensitivity Analysis for Performance

As evident, the range and hover are not particularly sensitive to a change in mass. The exception to this is the range in wind conditions, where below approximately 50 kg the UAV experiences a drop in maximum range attainable. This can be explained using Equation 8.5, where a reduction in weight results in smaller velocity, where at approximately 50 kg the velocity of the drone cannot overcome the wind speed efficiently.

8.4. Compliance Matrix

In order to verify that the requirements have been met, a compliance matrix is constructed, showing which requirements have been met (✓), which are no longer applicable (N/A), which are yet to be determined (TBD) and which have not been met (x). This is shown in Table 8.7 for the requirements relating to performing the mission within constraints and Table 8.6 for requirements relating to performing the mission technically. Verifying the requirements was done through comparing the requirements with the results discussed in this report.

Table 8.6: Compliance Matrix, Requirements for Performing Mission Technically

Identifier	Requirements	Compliance
UVOP-STK-01	The UAV shall be able to deliver 25kg payload to wind turbines off-shore	✓
UVOP-SYS-S01-1	The UAV shall be able to carry at least 25kg as payload.	✓
UVOP-SYS-S01-1-STC.1	The structure of the UAV shall be able to support an additional 25 kg of mass in all conditions	✓
UVOP-SYS-S01-1-STC.2	The landing system shall be able to support the weight of the UAV and an additional 25 kg	✓
UVOP-SYS-S01-1-LFT.1	The Lift subsystem shall be able to operate nominally with a payload attached	N/A
UVOP-SYS-S01-1-HST.1	The payload subsystem shall be able to support 25kg in all conditions	✓

UVOP-SYS-S01-1-HST.2	The payload weight shall be verified before every mission	✓
UVOP-SYS-S01-2	The payload shall be able to be securely attached to the UAV	✓
UVOP-SYS-S01-2-HST.3	The payload subsystem shall include a system to secure a 25kg payload of 50x50x50 cm dimensions	✓
UVOP-SYS-S01-2-HST.4	The hoisting subsystem shall have a redundant independent attachment point for the payload	x
UVOP-SYS-S01-3	The UAV shall be able to be controllable with a shift in center of gravity due to different payload contents	✓
UVOP-SYS-S01-3-HST.5	The control subsystem shall be able to adapt to the shift in center of gravity	✓
UVOP-SYS-S01-4	The UAV shall be able to be stable with a shift in center of gravity due to different payload contents	✓
UVOP-SYS-S01-4-STB.1	The stability subsystem shall be able to adapt to a shift in center of gravity	✓
UVOP-SYS-S01-5	The UAV shall be able to lower and raise a 25kg payload onto/off an offshore wind turbine	✓
UVOP-SYS-S01-5-HST.6	The payload subsystem shall be able to raise/lower a 25kg payload 8 m	✓
UVOP-SYS-S01-5-HST.7	The payload subsystem shall be able to release/clamp a payload	✓
UVOP-SYS-S01-5-HST.8	The payload subsystem shall be compatible with current off-shore wind turbine designs	✓
UVOP-SYS-S01-6	The UAV shall be stable during lowering/raising of a 25 kg payload with TBD bft	TBD
UVOP-SYS-S01-6-STB.2	The stability subsystem shall be able to correct for any disturbance autonomously when lowering/raising a 25kg payload	TBD
UVOP-SYS-S01-6-STB.3	The stability subsystem shall be able to keep the drone in the same position relative to the wind turbine with a margin of <TBD>	TBD
UVOP-SYS-S01-6-STB.4	The stability subsystem shall be able to keep the payload from swinging up to <TBD> metres when lowering/raising the payload	TBD
UVOP-SYS-S01-5	The UAV system shall be able to communicate with personnel on the wind turbine	✓
UVOP-SYS-S01-5-COM.1	The ground support subsystem shall be able to communicate with wind turbine personnel	✓
UVOP-SYS-S01-7	The UAV shall be controllable during lowering/raising of a 25kg payload with 6 bft wind	TBD
UVOP-SYS-S01-7-CTR.1	The control subsystem shall be able to change the location of the UAV during hoisting operations with 6 bft wind	TBD
UVOP-STK-02	The UAV shall be able to take off and land from/at existing support ships	✓
UVOP-SYS-S02-1	The UAV shall be able to take-off and land on a moving platform at sea	✓
UVOP-SYS-S02-1-LAG.1	The landing system shall have a track width of 1.1 m	✓
UVOP-SYS-S02-1-CTR.2	The control subsystem shall be able to account for landing on a moving platform under windy conditions	✓
UVOP-SYS-S02-1-STB.5	The stability subsystem shall be able to account for landing on a moving platform under windy conditions	✓
UVOP-SYS-S02-2	The UAV shall be stable during T/O and landing	TBD
UVOP-SYS-S02-2-STB.6	The stability subsystem shall be able to correct for any disturbance autonomously during T/O and landing	TBD

UVOP-SYS-S02-3	The UAV shall be controllable during T/O and landing	TBD
UVOP-SYS-S02-3-CTR.3	The control subsystem shall be able to change the location of the UAV during T/O and landing	TBD
UVOP-SYS-S02-4	The UAV shall be able to fit within the given support ship dimensions	✓
UVOP-SYS-S02-4-STC.3	The UAV shall have a maximum height of 2 m	✓
UVOP-SYS-S02-4-STC.4	The UAV shall have a maximum characteristic dimension of 14m	✓
UVOP-STK-03	The UAV shall be able to hover for at least 30 minutes	✓
UVOP-SYS-S03-1	The UAV shall be equipped with a lifting subsystem that allows for hovering in place for 30 minutes	✓
UVOP-SYS-S03-4-POW.1	The power subsystem should provide 2100 W power during hover	✓
UVOP-SYS-S03-1-LFT.2	The lifting subsystem shall be able produce 92 kgf Lift	✓
UVOP-SYS-S03-2	The UAV shall remain within 0.5 meters of selected position during hover	✓
UVOP-SYS-S03-2-STB.7	The stability subsystem shall be able to correct for any disturbance autonomously during hover	✓
UVOP-SYS-S03-3	The UAV shall be able to accelerate at <TBD> m/s^2 in any direction during hover	TBD
UVOP-SYS-S03-3-CTR.4	The control subsystem shall be able to change the location and attitude of the UAV during hover	✓
UVOP-SYS-S03-3-LFT.3	The lifting subsystem shall be able to vary its lift output	✓
UVOP-STK-04	The minimum range of the UAV shall be 5km	✓
UVOP-SYS-S04-2	The UAV shall remain within 30 meters of flightpath during travel	TBD
UVOP-SYS-S04-2-STB.8	The stability subsystem shall be able to correct for any disturbance autonomously during travel	TBD
UVOP-SYS-S04-3	The UAV shall be able to accelerate at <TBD> m/s^2 in any direction during travel	TBD
UVOP-SYS-S04-3-CTR.5	The control subsystem shall be able to change the location of the UAV during travel	✓
UVOP-SYS-S04-4	The UAV shall have enough power to sustain a 5 kilometre travel distance	✓
UVOP-SYS-S04-4-POW.2	The power system shall be able to provide 3000 W power during cruise	✓
UVOP-SYS-S04-1	The UAV should be able to travel for at least 5 kilometres in any direction in 6 bft wind	✓
UVOP-SYS-S04-1-PRP.1	The propulsion subsystem should be able to provide 160 kgf thrust	✓
UVOP-SYS-S04-1-COM.2	The communication subsystem should be able to communicate for lengths greater than 5km	✓
UVOP-SYS-S04-1-LFT.4	The lift subsystem should provide 1716N lift during cruise	✓
UVOP-STK-05	The UAV shall be equipped with visual and acoustic warning systems to indicate various states of the drone to the personnel nearby	✓
UVOP-SYS-S05-1	The Drone shall be equipped with visual signal subsystems	✓
UVOP-SYS-S05-1-SGN.1	The visual signal subsystem should indicate <TBD> condition	TBD
UVOP-SYS-S05-1-SGN.2	The visual signal subsystem should have a strength of 2800 mcd	✓
UVOP-SYS-S05-1-SGN.3	The visual signal subsystem should be able to produce red and green color	✓

UVOP-SYS-S05-2	The Drone shall be equipped with acoustic signal subsystems	✓
UVOP-SYS-S05-2-SGN.4	The acoustic signal subsystem shall have a strength of 95 dB	✓
UVOP-SYS-S05-3	The drone shall be able to communicate various states autonomously	TBD
UVOP-SYS-S05-3-COM.3	The drone shall be able to identify battery state	✓
UVOP-STK-06	The UAV shall be able to operate autonomously	✓
UVOP-SYS-S06-1	The UAV shall be able to navigate autonomously, given specific commands	✓
UVOP-SYS-S06-1-NAV.1	The navigation subsystem shall be able to autonomously navigate to a given position	✓
UVOP-SYS-S06-1-CTR.6	The control subsystem shall be able to autonomously control the position of the UAV	✓
UVOP-SYS-S06-1-NAV.3	The navigation subsystem shall include a redundancy to allow for functioning after one components failure	✓
UVOP-SYS-S06-2	The UAV shall be able to avoid obstacles autonomously	✓
UVOP-SYS-S06-2-CTR.8	The collision avoidance subsystem shall be able to autonomously identify obstacles	✓
UVOP-SYS-S06-2-CTR.9	The collision avoidance subsystem shall be able to stop the drone autonomously when an obstacle is encountered	✓
UVOP-SYS-S06-2-COM.4	The communication subsystem shall be able to alert the ground station when an obstacle is encountered	✓
UVOP-SYS-S06-2-COM.5	The collision avoidance subsystem shall include a redundancy to allow for functioning after one components failure	✓
UVOP-STK-07	The UAV shall be able to be controlled by an operator from a ground station	✓
UVOP-SYS-S07-1	The UAV shall be able to communicate with the ground station	✓
UVOP-SYS-S07-1-COM.6	The communication subsystem of the UAV shall be able to communicate <TBD> bit/s to the ground station	N/A
UVOP-SYS-S07-1-COM.7	The communication subsystem of the UAV shall be able to communicate with the ground station with a latency of 500 ms	✓
UVOP-SYS-S07-1-COM.12	The communication subsystem shall include a redundancy to allow for functioning after one components fails	✓
UVOP-SYS-S07-1-COM.13	The communications from the communication subsystem shall be secure from 3rd parties	N/A
UVOP-SYS-S07-2	The ground station shall be able to directly control the UAV at a distance of at least 5 km	✓
UVOP-SYS-S07-1-COM.14	The communication subsystem shall be able to receive control commands from the ground station	✓
UVOP-SYS-S07-1-COM.15	The control subsystem shall be able to execute control commands receive from the ground station	✓
UVOP-SYS-S07-1-COM.16	The stability subsystem shall be able to keep the UAV stable while executing control commands	✓
UVOP-SYS-S07-1-COM.17	The stability subsystem shall be able to keep the UAV stable while executing control commands	✓
UVOP-SYS-S07-3	The UAV shall be equipped with a camera subsystem to facilitate a live feed to the ground station	✓
UVOP-SYS-S07-1-CAM.1	The camera subsystem shall have a resolution of at least 8 MP	✓
UVOP-SYS-S07-1-CAM.2	The camera subsystem shall have an FOV of at least <TBD> degrees	N/A

UVOP-SYS-S07-1-CAM.3	The camera subsystem shall be able to look forward and down	✓
----------------------	---	---

Table 8.7: Compliance Matrix, Requirements for Performing Mission Within Constraints

Identifier	Requirements	Compliance
UVOP-STK-08	The system shall be sustainable	✓
UVOP-SYS-S08-1	The system shall not emit more than 900 g toxic products during lifetime	✓
UVOP-SYS-S08-1-PRP.2	The propulsion subsystem shall not utilise an energy source with toxic byproducts	✓
UVOP-SYS-S08-1-HST.9	The payload system shall not utilize any toxic fluids	✓
UVOP-SYS-S08-1-HST.10	The UAV shall contain any leak of hazardous materials from the payload	✓
UVOP-SYS-S08-1-STC.5	The UAV shall not leak more than 0.1 kg of hazardous materials upon a crash landing	✓
UVOP-SYS-S08-2	The system shall be able to be locally assembled from no more than <TBD> parts	TBD
UVOP-SYS-S08-2-LAG.2	The landing system subsystem shall consist of no more than <TBD> parts	TBD
UVOP-SYS-S08-2-PRP.3	The propulsion subsystem shall consist of no more than <TBD> parts	TBD
UVOP-SYS-S08-2-POW.3	The power subsystem shall consist of no more than <TBD> parts	TBD
UVOP-SYS-S08-2-LFT.5	The lift subsystem shall consist of no more than <TBD> parts	TBD
UVOP-SYS-S08-2-COM.18	The communication subsystem shall consist of no more than <TBD> parts	TBD
UVOP-SYS-S08-2-CTR.11	The control subsystem shall consist of no more than <TBD> parts	TBD
UVOP-SYS-S08-2-REC.1	The recovery subsystem shall consist of no more than <TBD> parts	TBD
UVOP-SYS-S08-2-HST.11	The hoist subsystem shall consist of no more than <TBD> parts	TBD
UVOP-SYS-S08-2-MTC.1	The system shall only require tools regularly available on <TBD> site for assembly	TBD
UVOP-SYS-S08-3	The system shall be maintainable	✓
UVOP-SYS-S08-3-MTC.2	The replacement of any component shall take less than <TBD> minutes	TBD
UVOP-SYS-S08-3-MTC.9	The UAV system shall have maintenance performed <TBD> per <TBD>	TBD
UVOP-SYS-S08-3-MTC.3	"Standard maintenance" shall take less than <TBD> minutes	TBD
UVOP-SYS-S08-3-MTC.4	The replacement of any subsystem shall take less than <TBD> minutes	TBD
UVOP-SYS-S08-3-MTC.5	The revision of any component shall take less than <TBD> minutes	TBD
UVOP-SYS-S08-3-MTC.6	The revision of any subsystem shall take less than <TBD> minutes	TBD
UVOP-SYS-S08-3-MTC.7	The inspection of any subsystem shall take less than <TBD> minutes	TBD
UVOP-SYS-S08-3-MTC.8	The inspection of any part shall be non destructive outside of consumables	TBD

UVOP-SYS-S08-4	The system shall consist of at least 50% off the shelf components	✓
UVOP-SYS-S08-5	The system shall be able to be stored within 9 m ³	✓
UVOP-SYS-S08-5-X.X	Subsystem X shall take up no more than <TBD> m ³ (in storage configuration)	N/A
UVOP-SYS-S08-6	The life cycle of the UAV shall be longer than <TBD> years	TBD
UVOP-SYS-S08-6-X.X	The life cycle of the X subsystem shall be longer than <TBD> years	TBD
UVOP-STK-09	The system shall operate in an offshore environment	✓
UVOP-SYS-S09-1	The UAV shall be able to withstand the humid and corrosive offshore environment	✓
UVOP-SYS-S09-1-STC.6	The UAV shall be assessed with ISO 9227 or equivalent.	✓
UVOP-SYS-S09-1-STC.7	The UAV shall be operable after <TBD> h of a salt spray test	TBD
UVOP-SYS-S09-1-STC.8	The UAV shall be inspected for corrosion regularly	✓
UVOP-SYS-S09-2	The UAV shall be able to hover in Beaufort 6 winds	✓
UVOP-SYS-S09-2-STB.9	The stability subsystem shall be able to keep the UAV in the same position in 6 Bft winds	✓
UVOP-SYS-S09-2-CTR.10	The control subsystem shall be able to change the position of the UAV in 6Bft winds	✓
UVOP-SYS-S09-3	The UAV shall be able to travel with a Beaufort 6 wind from any direction	✓
UVOP-SYS-S09-3-PRP.4	The propulsion subsystem shall be able to produce 184 kgf of thrust during travel in 6 Bft winds	✓
UVOP-SYS-S09-3-LFT.6	The Lift subsystem shall be able to produce 1805 N of Lift during travel in 6 Bft winds	N/A
UVOP-SYS-S09-3-STB.10	The stability subsystem shall be able to keep the UAV stable during travel in 6 Bft winds	✓
UVOP-SYS-S09-4	The UAV shall be rated for IPX6	✓
UVOP-SYS-S09-5	The UAV shall be able to survive a lightning strike	TBD
UVOP-SYS-S09-6	The UAV shall be able to operate in temperatures between -10 degrees and 40 degrees	✓
UVOP-SYS-S09-6-ICE.1	The UAV shall be able to resist the effects of icing	TBD
UVOP-SYS-S09-6-PRP.5	The UAV's propulsion system shall be able to operate between -10 degrees and 40 degrees continuously	✓
UVOP-SYS-S09-7	The UAV shall be able to operate in low visibility conditions	✓
UVOP-SYS-S09-8	The UAV shall be able to operate in hail conditions	TBD
UVOP-SYS-S09-8-STC.9	The UAV shall be able to survive hail impacts of at least 1.26 J	TBD
UVOP-STK-10	The system shall cost less than 75,000 € to produce	✓
UVOP-SYS-S10-1	The UAV shall cost less than 75,000 €	✓
UVOP-SYS-S10-2	The operational cost shall be less than <TBD> € per flight hour	TBD
UVOP-SYS-S10-2-MTC.9	The cost of regular maintenance should be less than <TBD> €	TBD
UVOP-STK-11	The system shall be safe to operate	✓
UVOP-SYS-S11-1	The UAV shall have a recovery system	✓
UVOP-SYS-S11-1-STC.11	The recovery subsystem shall be operable after an 20 m/s impact	✓
UVOP-SYS-S11-1-STC.12	The recovery subsystem shall ensure the UAV shall not get significantly damaged upon impact with water or ground	✓
UVOP-SYS-S11-1-COM.19	The recovery subsystem shall communicate its position to the ground station after activation	x

UVOP-SYS-S11-1-REC.2	The recovery subsystem shall be able to operate autonomously	✓
UVOP-SYS-S11-1-REC.3	The recovery subsystem shall have its own power source	N/A
UVOP-SYS-S11-1-REC.4	The UAV shall be equipped with an underwater locator beacon rated up to a depth of <TBD> m	x
UVOP-SYS-S11-3	The UAV shall be capable of slowing descent to 5 m/s with one engine inoperative autonomously	✓
UVOP-SYS-S11-4	The UAV shall be capable of slowing horizontal motion to 0 m/s with one engine inoperative autonomously	✓
UVOP-SYS-S11-5	The UAV shall be able land with one engine inoperative	✓
UVOP-SYS-S11-6	The UAV shall be able land in case of loss of signal autonomously	✓
UVOP-SYS-S11-7	The UAV shall not cause severe injury upon a crash with personnel	TBD
UVOP-SYS-S11-8	The UAV shall be safe to maintain	✓
UVOP-SYS-S11-9	The UAV shall be able to safely land autonomously when the battery is below 20%	✓
UVOP-SYS-S11-10	The UAV system shall have frequent pre and post flight checking procedures in place to verify functioning of critical systems	✓
UVOP-SYS-S11-11	The UAV system shall have pre and post flight checking procedures in place to verify functioning of critical systems	✓
UVOP-SYS-S11-12	The UAV shall have a warning system indicating malfunctioning sensors	✓
UVOP-SYS-S11-13	The UAV shall be limited to an acceleration of 1.55 g	✓
UVOP-SYS-S11-14	The UAV structure shall be designed with a safety of factor of 1.5	✓
UVOP-STK-12	The system shall comply to all regulations stipulating UAS requirements	✓
UVOP-SYS-12-1	The UAV shall be equipped to fly within the airspace around offshore platforms	✓
UVOP-SYS-12-1-COM.20	The UAV shall be equipped a remote id system	✓
UVOP-SYS-12-1-COM.21	The system shall be equipped with a two way radio capable of 8.33khz channel step size	✓
UVOP-SYS-12-1-COM.22	The UAV shall be equipped with a mode S/ELS transponder	✓
UVOP-SYS-12-2	The UAV shall follow SERA 3210 for aircraft avoidance	✓
UVOP-SYS-12-3	The UAV shall be equipped to comply with IFR flight rules	✓
UVOP-SYS-12-3-VFR.1	The UAS shall be equipped with an airspeed indicator	✓
UVOP-SYS-12-3-VFR.2	The UAS shall be equipped with an altimeter adjustable for barometric pressure	✓
UVOP-SYS-12-3-VFR.3	The UAS shall be equipped with magnetic direction indicator	✓
UVOP-SYS-12-3-VFR.4	The UAS shall be equipped with Tachometer for each engine	✓
UVOP-SYS-12-3-VFR.5	The UAS shall be equipped with an Oil pressure gauge for each engine using pressure system.	N/A
UVOP-SYS-12-3-VFR.6	The UAS shall be equipped with an temperature gauge for each liquid-cooled engine.	N/A
UVOP-SYS-12-3-VFR.7	The UAS shall be equipped with an oil temperature gauge for each air-cooled engine.	N/A
UVOP-SYS-12-3-VFR.8	The UAS shall be equipped with a manifold pressure gauge for each altitude engine.	N/A

UVOP-SYS-12-3-VFR.9	The UAS shall be equipped with a fuel gauge indicating the quantity of fuel in each tank.	N/A
UVOP-SYS-12-3-VFR.10	The UAS shall be equipped with a landing gear position indicator, if the aircraft has a retractable landing gear.	N/A
UVOP-SYS-12-3-IFR.1	The UAS shall be equipped with navigation equipment for over water operations	✓
UVOP-SYS-12-3-IFR.2	The UAS shall be equipped with an gyroscopic rate-of-turn indicator	✓
UVOP-SYS-12-3-IFR.3	The UAS shall be equipped with an slip-skid indicator	✓
UVOP-SYS-12-3-IFR.4	The UAS shall be equipped with a generator or alternator of adequate capacity.	✓
UVOP-SYS-12-3-IFR.5	The UAS shall be equipped with an gyroscopic pitch and bank indicator	✓
UVOP-SYS-12-3-IFR.6	The UAS shall be equipped with a gyroscopic direction indicator	✓
UVOP-SYS-12-3-IFR.7	The UAV shall be equipped with an emergency locator transmitter transmitting at 406Mhz	x
UVOP-SYS-12-3-IFR.8	The UAS shall be equipped with a clock that is accurate to the second	✓
UVOP-SYS-12-4	The UAV shall be equipped with anti-collision lighting	✓
UVOP-SYS-12-5	The UAV shall be in line with Operational Safety Objectives derived from Specific Operating Risk Assessment	✓
UVOP-SYS-12-5-COM.23	The UAV shall be equipped with an ADS-B out system	✓
UVOP-SYS-12-5-CTR.13	The collision avoidance system shall avoid all aircraft during flight.	✓
UVOP-SYS-12-5-CTR.14	The flight control system shall automatically keep the UAV within the flight envelope	✓

As can be seen, all stakeholder requirements have been met. Some (sub)system requirements cannot be determined yet, are not applicable to the final design or have not been met. The requirements that cannot be determined yet are a result of the fact that there is simply not enough information available about the current design. The requirements are neither met, nor not met, where more detailed analysis and prototyping in future development is required. The requirements that are no longer applicable (N/A), have been found to be irrelevant to the current design. The three requirements that have not been met, are listed below accompanied with factors as to why:

- **UVOP-SYS-S11-1-COM.19-The recovery subsystem shall communicate its position to the ground station after activation**
This was not considered necessary as the last position before failure is given by navigation system.
- **UVOP-SYS-S11-1-REC.4-The UAV shall be equipped with an underwater locator beacon rated up to a depth of <TBD> m**
Not considered feasible as the drone would no longer be recoverable at this point. Additionally the UAV is designed to float in case of water landing
- **UVOP-SYS-S01-2-HST.4-The hoisting subsystem shall have a redundant independent attachment point for the payload.**
An additional redundant attachment system is not deemed necessary as the time window in which an accidental payload release could cause dangerous is very small (during hoisting and landing operations) the additional weight therefore is not considered worth this marginal increase in safety.
- **UVOP-SYS-12-3-IFR.7-The UAV shall be equipped with an emergency locator transmitter transmitting at 406Mhz.**
Not considered feasible as the drone would no longer be recoverable at this point and the additional signal might alert coastguard which could endanger lives due to too many false alarms.

9. Financial Overview

This section provides a financial projection for the drone’s expected profit in the coming years. To start, all potential costs associated with the production process, and drone operations are analysed to derive an estimated total budget that is needed. Finally, by comparing similar products in the market, informed projections about expected revenue can be made.

9.1. Development Cost

After, the Design Synthesis Exercise, the team is going to continue working on the drone with the aim of the complete development and finally launching it into the market. For this reason, it is decided to create a start-up company. The initial stage is the development phase. During that, the company is established and the vehicle design is completed. This phase is expected to last two months. Its activities are described in the Gantt chart in Section 13.1.

The overview of all the costs is presented in Figure 9.1. The main cost is building prototypes. Two pieces are going to be assembled. That allows for testing and validating the final configuration. Each costs 47,770 EUR as from Section 8.1 and about 2000 EUR is spent on purchasing needed tools. For development, the required effort is estimated to 2000 man-hours: 800 h to senior engineers employed with wage 34 EUR/h [78] and 1200 h to students with a rate of 14 EUR/h [79]. Subsequently, the working space needs to be provided. YESIDELFT provides the office space and laboratories with the estimated cost 2000 EUR/month [80]. Additionally, the team can also use the facilities of Makerspace Delft made for start-ups building prototypes.

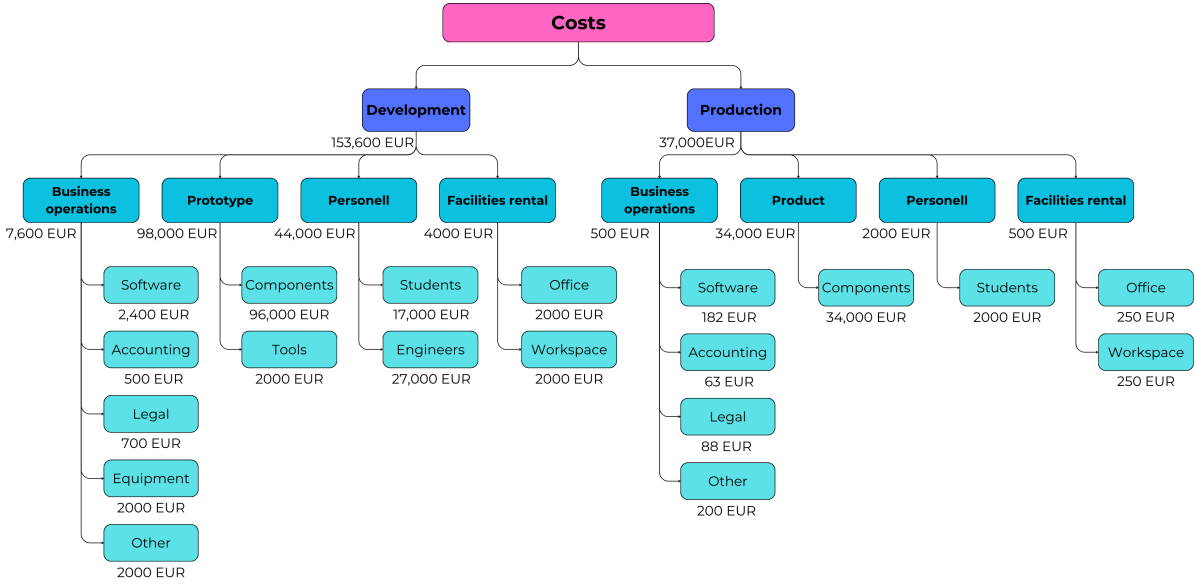


Figure 9.1: Cost Breakdown Structure.

On top of that, there are costs related to the software and business operations. The cost of an Inventor license is 363 EUR/month per user. It is opted to purchase two licences. For Ansys, the chosen finite element analysis software, the license cost is not publicly available, however for start-ups the price ranges between 500 to 3000 EUR yearly. For a start-up with little profit it is safe to assume a 1000 EUR license cost. Finally, the initial office equipment is bought for 2000 EUR. Monthly, 250 EUR is

spend on accounting services, 350 EUR for legal services and 1000 EUR for other expenses such as transportation, marketing etc [81]. The total development costs sum up to 153,000 EUR.

9.2. Production Cost

After the development stage, the production phase begins. The production costs are quantified per drone and it is estimated to produce one weekly. They are visualised in Figure 9.1. These are the costs of purchasing and manufacturing the parts, assembly and company operations. In Section 8.1, all the costs for each subsystems and their components are listed returning the value is 47,770 EUR. It refers, however, to a single piece built. Therefore, with the increased production, parts can be ordered in batches reducing the production costs. As checked with the parts manufacturers and providers, the expected savings are 4,000 EUR on electronics and 10,000 EUR on structures resulting in a price 33,770 EUR per drone. Five students work for five days full time on the production. Their wages and remaining expenses per time interval are specified in Section 9.1. These other expenses related to production are office with workspace rental, Inventor license, accounting, legal services and miscellaneous. The total production cost per drone is 36,000 EUR.

9.3. Return of Investment

The profitability of the drone is subsequently inspected from the perspective of the development team. First, the costs are obtained. The production cost C_P is 36,000 EUR per unit from Section 9.2 and total development costs C_D of 153,000 EUR from Section 9.1.

$$Cost = C_P \cdot N + C_D \quad (9.1)$$

The revenue is calculated based on the price per unit P and the production volume N . The market price was estimated in Section 2.1 to 45,000 EUR per piece.

$$Revenue = P_R \cdot N \quad (9.2)$$

The profit and return of investment are calculated as follows.

$$Profit = Revenue - Cost \quad (9.3)$$

$$ROI = \frac{Profit}{Cost} \quad (9.4)$$

These financial indicators are dependent on product volume. Therefore, they are plotted in Figure 9.3 and Figure 9.2. One can deduce that the break even point is for the amount of 17 drones produced and sold.

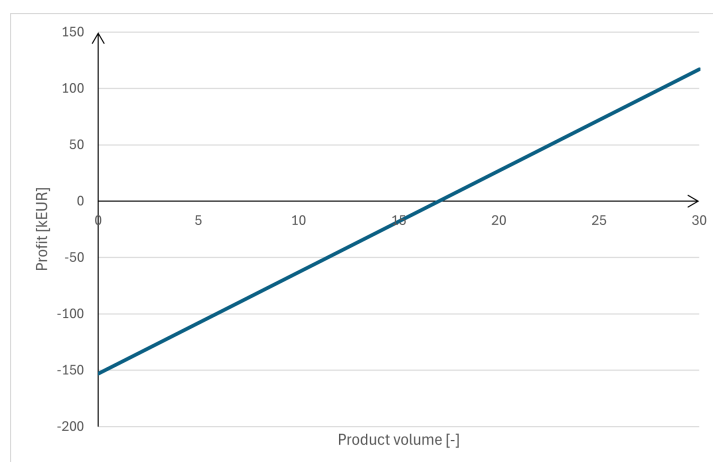


Figure 9.2: Profit versus Product Volume

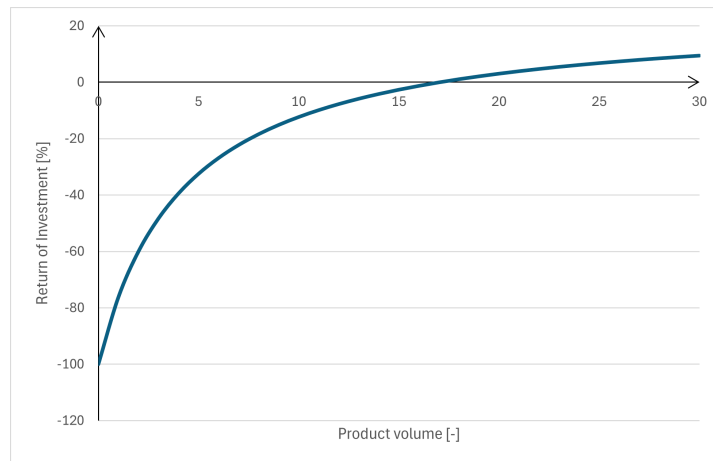


Figure 9.3: Return on Investment versus Product Volume

9.4. Customer Operational Cost

This section aims to give potential customers an overview of the expected costs associated with a standard mission, outlining the financial implications of using this drone for its intended purposes.

Battery Cost

The energy storage capacity for the drone's batteries is 6.6 kWh. With the current consumer electricity rate at €0.40 per kWh for up to 2,900 kWh of usage, the cost to fully recharge this battery would be relatively minimal [82]. Considering that the system operates on a boat, the impact of electricity costs for recharging the drone's battery is even less significant, likely due to the availability of alternative charging methods or energy sources.

Transportation Cost

Given that the drone is intended for offshore operations, it frequently requires transportation by boat. From the team's viewpoint, it is assumed that the boat's use—since the drone primarily serves as a delivery mechanism following turbine inspection—will not factor into the costs associated with operating the delivery drone.

Operator Salary

The average salary for offshore operators in the Netherlands can vary significantly based on specific roles and experience levels. For a company like Van Oord, which specialises in offshore projects, the typical salary for operators is around €50,000 annually [83]. However, for the scope of this project where the operator will handle all drone-related tasks—including piloting, maintenance, and surveillance—the salary has been adjusted to €65,000 per year. This increase is due to the additional responsibilities. The need to attract highly skilled engineers by offering competitive compensations, which is believed to benefit the company in the long term by ensuring high-quality operations and innovation.

Drone Licence

In the EU regulatory framework for drone operations several licenses are required, these add to the operational costs. Operators of drones weighing over 250 grams must obtain the EU Drone License, which comprises two key components, the Root Certificate (A1-A3), this is the basic certificate for drone pilots and the Supplementary Certificate (A2), that is required for drones above 250 grams, it needs additional competencies needed for more complex and heavier drones. The addition of all certificates A1-A3 and A2 adds to a total cost of €199 [84].

This drone falls under EASA's "specific category", needed for higher-risk scenarios. In this context operators must follow more strict regulations. This essentially means obtaining an operational authorisation from the national aviation authority, which involves a Specific Operations Risk Assessment (SORA) to ensure all potential risks are managed in operation.

Once the operator has obtained the A1-A3 and A2 certificates, in order to operate a drone within this specific category, the operator is required to complete both theory and practical training. This is necessary to obtain the pilot certificate, mandatory for EASA Standard Scenario (STS) operations. This certification costs approximately 2,399€ and covers all essential aspects required to operate drones safely in sensitive areas. These include no-fly zones and Extended Visual Line of Sight (E)VLOS operations. It also includes (700€ extra) for the use of Radio Telephony (RT), needed for better communication capabilities, particularly in complex airspace environments. RT includes voice communication and real-time coordinate sharing. The cost of this certificate adds significantly to the overall cost of operations but is crucial to follow compliance and safety regulations [85].

The total cost of the A1-A3 and A2 certificates and the theory and practical training of the specific category, is €2,598. It is to be noted that the theory certificate, is only valid for five years, after five years the operator would have to re-take the theory. This will cost €599 to renew, as this is the price for the theory only [85].

Maintenance Cost

Predicting the maintenance costs for this drone is hard due to factors such as the operational environment and the complexity of its systems. Maintenance often arises from the need to replace components that have reached the end of their useful life or have been damaged. It is crucial for potential customers to consider these aspects, as maintenance is vital for ensuring the safety, efficiency, and longevity of the drone.

Drone Insurance

Given the value and potential risks associated with operating drones, an insurance coverage that guarantees security is essential to protect against possible liabilities and damages. The most common type of drone insurance is a liability insurance, which is crucial as it covers any damage or injuries caused by the drone during operation. This is especially useful as it ensures protection against claims that could arise from accidents involving third parties [86].

In addition to liability insurance, hull insurance is also recommended for this drone. Hull insurance specifically covers any damage to the drone itself, whether from accidents during flight or from other risks such as impact damage while landing. This type of insurance is very important for recovering costs that come with repairing or replacing parts of the drone, if any damage [87].

Looking at available insurance plans, companies like SkyWatch offer packages that combine both liability and hull insurance. For a drone instance, an annual plan from SkyWatch will cost approximately 466 USD, providing coverage and also protection against loss or theft of the drone. This ensures that both the potential liabilities and the investment in the drone itself are well-protected, providing peace of mind and financial stability for not only the team but also the drone operator [88].

Operational Cost Summary

An overview of the accumulated operational costs described previously, can be found in Table 9.1.

Table 9.1: Cost Summary

Category	Expected Cost (€ per year)	One Time Cost
Battery	0	0
Operator	65000	0
Drone Licence	119.8	2598
Insurance	436.36	0
Transportation	0	0
Total Cost	65556.16	2598

10. Operations & Logistics

The operation and logistics of PeliCrane are important parameters to consider for the operator. Firstly, the Reliability Availability, Maintainability and safety characteristics are considered Section 10.1. Next possible mission profiles are considered in Section 10.2. Finally the Technical risk assessment is presented in Section 10.3.

10.1. RAMS

The reliability, availability maintainability and sustainability (RAMS) analysis provides an overview and highlights their significance on the UAV's design and performance.

10.1.1. Reliability

The reliability of the system concerns the likelihood of failure of the entire system or relevant subsystems. In general, the UAV has been designed with a fail-safe design philosophy. Where possible, redundancy has been applied, to ensure part failure does not result in system failure. Furthermore, a safety factor of 1.5 has been applied to the structural design. In Section 10.3, the risks relating to component failure have been classified and relevant mitigation strategies have been applied. The subsystem of the largest concern is the propulsion subsystem, where no redundancy is applied. However in Section 7.6, the UAV response to rotor failure is simulated and discussed.

10.1.2. Availability

Availability relates to the amount of time the UAV is available to perform payload delivery operations. The reliability and maintainability are closely related to the UAV's availability, as failures and maintenance result in significant downtime. The redundancy applied to the design ensures these failures are minimal. Furthermore, an efficient maintenance schedule has to be developed to ensure little downtime.

Operationally the UAV will also have a limit to when it can operate. It is ill-advised to perform nighttime operation and it can only perform within certain weather conditions. This should largely overlap with conditions in which maintenance crews are not performing maintenance work, therefore there would be no downtime. Furthermore, the relatively low frequency of wind turbine maintenance operations would put relatively low time pressure on UAV operations, meaning turnaround time is not of great concern. However other mission profiles, relating to cargo transport and logistics operations, as will be discussed in Section 10.2, have a higher frequency of operations, where turnaround time plays a more crucial role. As a preliminary estimation, the battery charging process, charging at 1 c, the batteries would take approximately 1.5 h to charge, assuming no scheduled maintenance is done. In this time the UAV can also be inspected for damage and necessary maintenance can be performed. A faster turnaround time is theoretically possible with hot-swapping the batteries, however at a higher up-front cost of needing to buy an additional set of batteries. The time required for a specific mission will further be covered in Section 10.2.

10.1.3. Maintainability

Maintenance is an important part of the UAV's operation. Effective preventative maintenance can increase reliability and lifespan, while efficient corrective maintenance after a fault or failure is discovered, reduces the downtime to a minimal amount.

Preventative maintenance has to be carried out regularly and systematically, with some components requiring a higher frequency of maintenance than others, due to their importance to the entire system and likelihood of failure. It has been decided to distinguish three separate levels of maintenance frequency: high, medium, and low. For high frequency, this shows that the maintenance will need to be

repeated in an order of magnitude of days/flights, for medium, this means in the order of magnitude of weeks and for low this entails a frequency in the order of magnitude of months.

This is summarised in Table 10.1

Table 10.1: Preventative Maintenance Activities and Frequency

Subsystem	Maintenance operation	Frequency
Camera	Cleaning lens	High
	Checking gimbal functioning	High
	Cleaning sensor	Medium
	Calibrating	Medium
Propellers	Damage inspection	High
	Tightening bolts	Low
Motors	Lubricating	Medium
	Checking waterproof seals	Medium
	Damage inspection	High
	Benchmark tests	Low
	Corrosion inspection	Medium
Structure	Damage inspection	High
	Corrosion inspection	Medium
	Checking waterproof seals	Medium
Batteries	Recharging	High
	Benchmark tests	Low
Cabling	Check connections	Low
Sensor system	Calibration	Medium
	Benchmark tests	Low
	Damage inspection	High
Winch system	Damage inspection	High
	Winch motor test	High
Flight control system	Calibration	High
	Benchmark tests	Low
Support element	Connection test	High

Most high-frequency maintenance is performed on the exterior the drone, where only visual inspections and simple tasks are performed. This is possible within the aforementioned 1.5 h turnaround time. Most medium and low-frequency maintenance require access to the internals of the drone and are more complex tasks.

For corrective maintenance, self-diagnosis is very important to identify and troubleshoot potential issues, before accessing internal hardware. Ardupilot has integrated diagnosis tools that identify sensor and software issues. If a problem is encountered, the following OR-tree is applicable Figure 10.1.

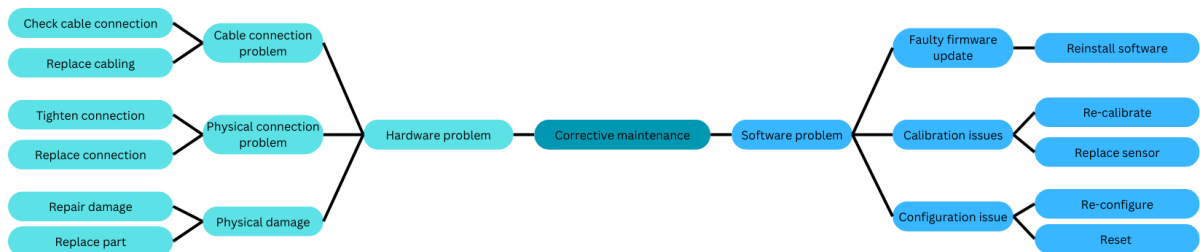


Figure 10.1: Corrective Maintenance Tree

This is a top-level overview of the maintenance that has to be performed in case of (component) failure. One of the largest advantages of this design is the very large amount of OTSC used. This makes replacing and/or repairing parts very simple and straightforward. Components can be disconnected and

dismounted and replacements mounted and connected quickly. An exception to this is certain structural components like the ducts, however it has been made sure that these are manufacturable with relative ease and low cost. Combining corrective and preventative maintenance will ensure minimal down time.

10.1.4. Safety

Due to the close proximity to personnel during operations, safety is of high importance and has been taken into account throughout the entire design process. Inherently, the drone being unmanned means no personnel is needed to physically be on board the UAV, as with helicopters, reducing the risk to life during logistics and delivery operations offshore. Additionally, the following steps have been taken to ensure safe operation

Risk Assessment

In Section 10.3 Figure 10.3, an extensive risk assessment has been performed with mitigation strategies developed and applied to the design process, improving safety as well as reliability.

Parachute and Floatation System

As described in Subsection 5.3.9, a parachute system has been incorporated into the structure to reduce the fall speed of the UAV in case of failure. This parachute system is independent and opens mechanically in case of failure. With the parachute deployed the sink rate is 5 m/s decreasing impact energy significantly.

On top of this PeliCrane has, positive buoyancy due to the structure, especially the ducts. Meaning that upon impact water landing the UAV remains recoverable.

Collision Avoidance

The collision avoidance system integrated within Ardupilot, coupled with the advanced sensor suite as described in Chapter 6 gives the UAV the ability to detect and plot paths around obstacles based on rangefinder sensor inputs, as well as the ADSB system. This ensures a very low likelihood of accidents with both static objects as well as other air-traffic.

Ducts and Propellers

As described in Section 4.4, Ducts have been added to the propellers, to increase the safety of the drone. In case of (low speed) impact with objects the UAV is not significantly damaged. Furthermore, in case of landing, personnel is able to be in closer proximity to the UAV with the propeller blades being protected. Lastly the lower RPM of 4-bladed propellers, compared to 2-bladed propellers, produces less noise and at a lower frequency which gives a safer feeling to nearby personnel.

Redundancies and Scheduled Maintenance

As described above, regular maintenance and built-in component redundancies reduce the likelihood of failure and increase reliability, ensuring that in the unlikely event of component failure the drone remains safe. Furthermore, in case of loss of signal, the UAV is able to return to a pre-set position, which is a built in feature of Ardupilot.

Warning Systems

PeliCrane has incorporated audio and visual warning systems in order to inform nearby personnel of the current state of the drone such as battery status and rotor failure. These are located around the structure of the UAV, and are visible from every angle, ensuring that operations remain safe even in lower-visibility conditions. On top of this, navigation lights are placed on the UAV to comply with regulations. The audio warning system produces a loud buzzing sounds to inform of danger, which audible through hearing protection. Lastly the livery of the UAV has been given safety orange colours, to remain visible.

10.2. Mission Profiles

The UAV has been designed with a flexible mission profile. Based on the performance metrics outlined in Table 8.4 and the drone's ability to land, many options are available. Based on this, some common

mission profiles have been generated. Time and range indications are provided.

Figure 10.2 shows one such profile. In this scenario, the UAV takes off from the service vessel/platform, cruises to its destination, hoists and delivers the payload to the platform, and then returns to the original platform.

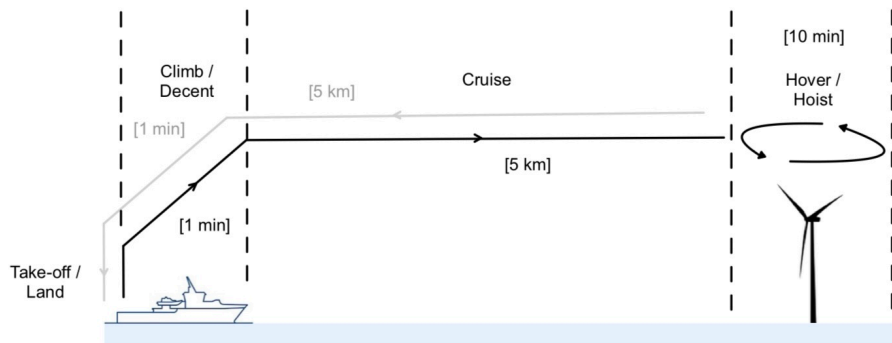


Figure 10.2: Mission Profile One

Figure 10.3 is similar to the previous mission profile, but in this scenario, the payload is delivered by landing. This approach is more suitable for situations where space is not a constraint.

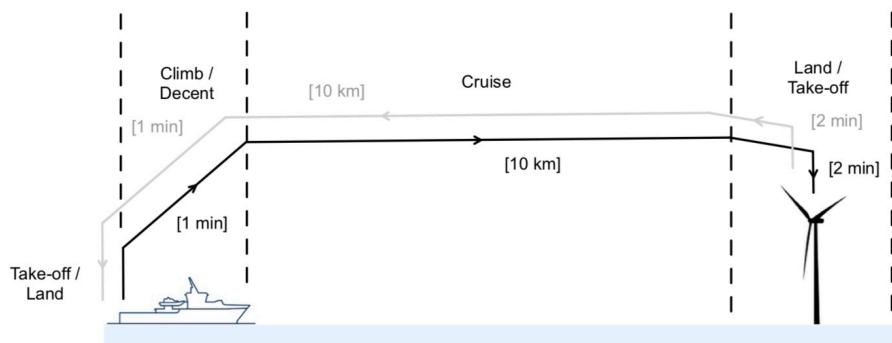


Figure 10.3: Mission Profile Two

Figure 10.4 is likely the least common mission profile. In this scenario, the UAV can be used for moving between platforms.

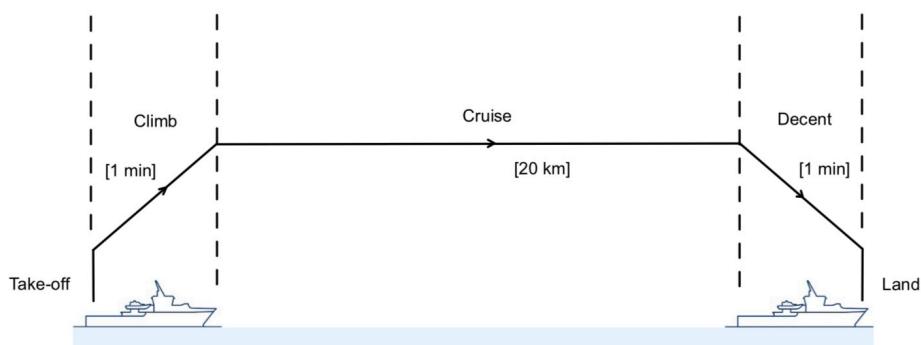


Figure 10.4: Mission Profile Three

These mission profiles demonstrate the flexibility of our UAV. However, as previously mentioned, many

more options could also be feasible.

Another important factor that impacts the mission profile is how fast the payload can be hoisted. The motor that drives the winch system has a rotational speed of 82RPM. This means that the full rope length of 10.5m can be retracted in 49s. However, in practice, the rope will not be fully extended, so the hoisting will take less time.

10.3. Technical Risk Assessment

In this chapter, an assessment of technical risks is conducted. This involves defining the risks, outlining their impact, and assigning responsible members. Subsequently, the risks are displayed on a risk map, which assesses the likelihood and consequences. Mitigation strategies are provided, followed by a post-mitigation risk assessment and updated risk map.

Risk Identification

In order to assess the possible technical and operational risks of the systems, the risks have to be identified first. In Table 10.2 every operational and technical risk to the system is listed together with its consequence and the responsible team member for tracking the risk throughout the design project.

Table 10.2: Technical Risk Definitions

Identifier	Risk Definition	Consequence	Responsible Role
TR-01	The minimum hover time is not met by the design	The desired mission cannot be fulfilled	Lead Eng.
TR-02	The minimum range is not met by the design	The operation might not be fulfilled	Lead Eng.
TR-03	The UAV experiences a Loss of Signal (LoS)	The UAV becomes uncontrollable from the ground station	Control & Operations Eng.
TR-04	The UAV exhausts its battery capacity/catastrophic power system failure	The UAV is lost	Prop & Power Eng.
TR-05	The UAV experiences wind speeds above 6bft	The UAV may become uncontrollable and can be lost	Control & Operations Eng.
TR-06	The UAV experiences heavy rain more than 40mm/hr	The UAV may experience a short circuit/water damage with subsequent damage or failure of (sub)systems	Control & Operations Eng.
TR-07	The crane system malfunctions	The payload cannot be lowered and/or released	Structural Eng.
TR-08	The crane system malfunctions	The payload is released prematurely from the UAV	Structural Eng.
TR-09	The obstacle avoidance system malfunctions	The UAV is at risk of a collision	Control & Operations engineer
TR-10	The maximum payload of 25kg is exceeded	Performance is reduced, regulations are not met	Control & Operations Eng.
TR-11	The recovery system malfunctions	Unable to locate UAV after failure	Control & Operations engineer
TR-12	The recovery system malfunctions	The flotation system malfunctions	Control & Operations engineer

TR-13	The recovery system malfunctions	The UAV receives critical damage upon impact with surface and is lost	Structural Eng.
TR-14	The navigation system malfunctions	The UAV is at risk of deviating from its intended course, with a potential collision risk	Control & Operations Eng.
TR-15	The UAV is involved in a collision with a solid object	Significant damage, potential loss of UAV	Structural Eng.
TR-16	The UAV collides with a human	Injury to personnel and damage to UAV	Chief Designer
TR-17	Loss of multiple propellers	The UAV becomes uncontrollable, potential loss of UAV	Control & Operations engineer
TR-18	Loss of single propeller	The UAV is at risk of becoming uncontrollable, potential loss of UAV	Control & Operations Eng.
TR-19	The UAV exceeds its maximum dimensions	The UAV might not be able to operate in its designated environment	Lead Engineer
TR-20	The UAV experiences unchecked corrosion	The lifetime of the UAV will be lowered, potential (sub)system failure if left unchecked	Control & Operations Eng.
TR-21	The UAV design results in a total cost over €75,000	The UAV might not be competitive enough for the market	Structural Eng.
TR-22	The UAV signal is intercepted and hijacked	The UAV can be controlled by an external party, with possible malicious intent	Control & Operations Eng.
TR-23	The UAV experiences a critical load	The UAV may experience structural failure	Lead Engineer
TR-24	The UAV encounters significantly heavy hail	Damage to UAV (sub)systems, potential loss of UAV	Control & Operations Eng.
TR-25	The UAV encounters icing conditions	(Sub)systems may fail due to freezing, potential loss of UAV	Aerodynamics Eng.
TR-26	The UAV gets hit by lightning	(Sub)systems may fail, potential loss of UAV	Control & Operations Eng.
TR-27	A UAV subsystem overheats	Damage to UAV (sub)systems, potential loss of UAV	Control & Operations Eng.
TR-28	The UAV experiences a failure of a critical system	Potential loss of UAV	Control & Operations engineer
TR-29	The UAV experiences a failure of non-critical system	Operational impact	Structural Eng.
TR-30	Operator incapacitation	The UAV may become uncontrollable during manual flight, potential loss of drone	Control & Operations Eng.
TR-31	Other air traffic interferes with the signal of the UAV	Loss of communication	Control & Operations Eng.
TR-32	Warning light/signal malfunction	Wind turbine personnel unaware of drone condition, potential for collision	Chief Designer

TR-33	Component or material availability	Design has to be reconsidered	Structures Eng.
TR-34	Manufacturability	Design's complexity, material selection, tolerances, or other design attributes do not align with manufacturing	Structures Eng.
TR-35	Propeller collision with duct	Damage to and potential loss of UAV	Control & Operations Eng.
TR-36	PCB interference	Can create intermittent issues or outright failures of the system	Control & Operations Eng.
TR-37	Incorrect sensor positioning	Measurements do not reflect reality	Control & Operations Engineer
TR-38	Inadequate sensor accuracy	Sensor can not provide the required accuracy for operations	Control & Operations Eng.
TR-39	Improper model validation	The reliability of the model's predictions is questionable	Chief designer
TR-40	No stable gains	UAV inoperable	Control & Operations Eng.
TR-41	Non symmetric UAV	Separate pitch and roll tuning required	Control & Operations Eng.
TR-42	High spin rate with one engine inoperable	Parachute deployment failure	Control & Operations Eng.
TR-43	Spring system failure	Parachute deployment failure	Control & Operations Eng.

These risks can then be assessed on the likelihood of the risk occurring, as well as the impact that the risk has on the mission/system. The ranking system used is defined in Table 10.3.

Table 10.3: Risk Assessment System

Number	Likelihood	Impact
1	Very low: Will most probably not happen in the lifetime	Negligible: Inconvenience or non-operational impact
2	Low: Probability of happening once in the lifetime	Significant: Delay in current mission or a reduction in quality of the technical performance
3	High: Will happen once in lifetime	Critical: Current mission has to be immediately terminated/UAV not lost
4	Very high: Will happen multiple times in lifetime	Catastrophic: Immediate mission failure/UAV lost

It is noted that the likelihood is given as a pragmatic measurement of the probability of occurrence, instead of a percentage. This is done to more intuitively assess the likelihood of occurrence. The impact is evaluated with respect to the effect the risk occurring has on the entirety of the mission and the system. The risk is a multiplication of the likelihood and impact and is given for each identified risk in Table 10.4.

Table 10.4: Pre-Mitigation and Contingency Technical Risk Assessment

Identifier	Likelihood	Impact	Risk	Identifier	Likelihood	Impact	Risk
TR-01	1	3	3	TR-23	3	4	12
TR-02	1	3	3	TR-24	2	4	8
TR-03	4	4	12	TR-25	3	4	12
TR-04	4	4	12	TR-26	3	4	12
TR-05	4	4	12	TR-27	3	4	12
TR-06	4	4	12	TR-28	3	4	12
TR-07	3	2	6	TR-29	4	2	8
TR-08	2	3	6	TR-30	4	4	16
TR-09	3	4	12	TR-31	3	4	12
TR-10	4	2	8	TR-32	3	4	12
TR-11	2	4	8	TR-33	2	3	6
TR-12	3	4	12	TR-34	3	3	9
TR-13	2	4	8	TR-35	2	4	8
TR-14	3	4	12	TR-36	3	3	9
TR-15	3	4	12	TR-37	3	3	9
TR-16	2	4	8	TR-38	3	3	9
TR-17	2	4	8	TR-39	2	4	8
TR-18	3	4	12	TR-40	1	4	4
TR-19	1	2	2	TR-41	3	1	3
TR-20	4	4	16	TR-42	2	4	8
TR-21	1	2	2	TR-43	2	4	8
TR-22	2	4	8				

These risks can be visualised in a risk map, as given in Figure 10.5. As can be seen in this figure, many risks are in the red areas, indicating unacceptable risks. The red area indicates unacceptable risks, where mitigation and contingency are necessary. The yellow area indicates warning risks, where mitigation and contingency strategies are not strictly necessary but should be done if possible, these risks should be tracked throughout the project. The green area indicates acceptable risks, where no additional mitigation and contingency is necessary. However for this project, mitigation and contingency strategies have been applied to every risk.

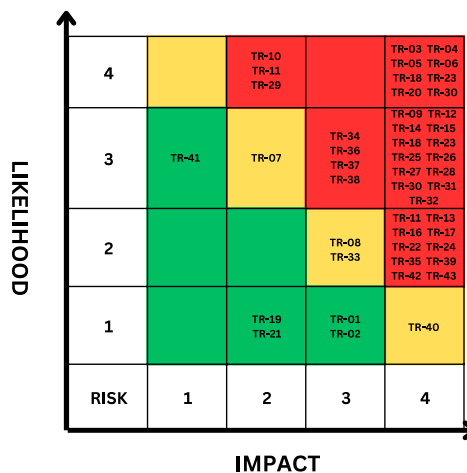


Figure 10.5: Pre-mitigation/contingency Technical Risk Assessment

For each risk, a mitigation and contingency strategy is defined. With the mitigation, the likelihood of the risk occurring can be reduced. If the risk still occurs, contingencies are in place to reduce the impact of the said risk. The mitigation and contingency strategies and their effect on the likelihood, impact and total risk are provided in Table 10.5.

Table 10.5: Post-Mitigation and Contingency Technical Risk Assessment

Identifier	Mitigation	Post-Likelihood	Contingency	Post-Impact	Post-Risk
TR-01	Verify requirements to confirm performance	1	Lower the payload capacity	2	2
TR-02	Verify requirements to confirm performance	1	Lower the payload capacity	2	2
TR-03	Redundancy in communication system	2	Autonomous systems triggering a safe landing	3	6
TR-04	Have a low power warning system in place warning of critical level, autonomous system triggering safe landing on critical battery level	2	Recovery system triggering with own auxiliary power	3	6
TR-05	Operate within weather constraints, include high wind warning	2	Return to safe area, trigger recovery system if applicable	3	6
TR-06	Operate within weather constraints	2	Critical components should have auxiliary waterproofing	3	6
TR-07	Have pre-flight checking procedures in place and regular maintenance	2	Return and safe landing for maintenance	2	4
TR-08	Have pre-flight checking procedures in place and regular maintenance, robust design	1	Redundant Safety system securing payload to UAV	1	1
TR-09	Have a warning message of malfunctioning sensors, pre-flight checking and maintenance	2	Have redundancy within the obstacle avoidance system	2	4
TR-10	Detail and verify the payload weight before starting the mission	1	Continue operation	2	2
TR-11	N/A	2	Search and rescue, flotation system	3	6
TR-12	Have pre-flight checking procedures in place, robust design	2	Emergency locator beacon able to operate underwater	3	6
TR-13	Have pre-flight checking procedures in place, regular maintenance, robust design	1	N/A	4	4
TR-14	Redundancy within the navigation system	2	Collision avoidance system	2	4
TR-15	Collision avoidance system	1	Recovery system	3	3
TR-16	Collision avoidance system, safety precautions	1	Recovery system	3	3
TR-17	Have pre-flight checking procedures in place, regular maintenance, robust design	1	Recovery system	3	3

TR-18	Have pre-flight checking procedures in place, regular maintenance, robust design	2	Design choices, having UAV be controllable after loss of propeller, recovery system	3	6
TR-19	Design according to requirements	1	N/A	2	2
TR-20	Design according to corrosion requirements and have pre-flight procedures in place	1	Regular inspection, anti-corrosion measure applied between missions	1	1
TR-21	Select cheaper components	1	N/A	2	2
TR-22	Have a protected connection to the UAV	1	Collision avoidance system	3	3
TR-23	Control system limits loads to below critical load	1	Design safety factor	1	1
TR-24	Check weather conditions before commencing the mission	1	Material choice, exit from dangerous weather area	3	3
TR-25	Stay within operational temperature requirements	2	De-icing, design within constraints, critical systems resist freezing	2	4
TR-26	Operate within weather constraints,	2	Critical components are protected from lightning	2	4
TR-27	Design safety factors, operate within operational and design requirements, voltage regulation system	1	Warning systems/indicators, recovery system	2	2
TR-28	Design within requirements	2	Recovery system	3	6
TR-29	Design within requirements	3	Continue operation	1	3
TR-30	Operator capability precautions, stringent health and safety requirements	2	Backup operator, Collision avoidance system, stability system	1	2
TR-31	Operate on a frequency band that is less prone to interference	2	Have a collision avoidance and return to base system	2	4
TR-32	Robust design, safety precautions, Pre-flight procedures and maintenance	2	Collision avoidance system, system malfunction error	1	2
TR-33	Use readily available materials, check with supplier	1	Consider other materials with similar performance	2	2
TR-34	Involve manufacturing experts early, prototyping and testing	1	Alternative manufacturing processes, design adjustments	2	2
TR-35	Design with a clearance of at least 5mm	1	Having UAV be controllable after loss of propeller, recovery system	2	2
TR-36	Proper testing, regular maintenance	1	Lower data rate so signal to noise is acceptable, compare multiple sensor data.	2	2
TR-37	Create field of view map to ensure proper positioning	1	Not being reliant on one sensor	2	3
TR-38	Define a minimum sensor accuracy and select appropriately	1	Consider different sensors	1	1

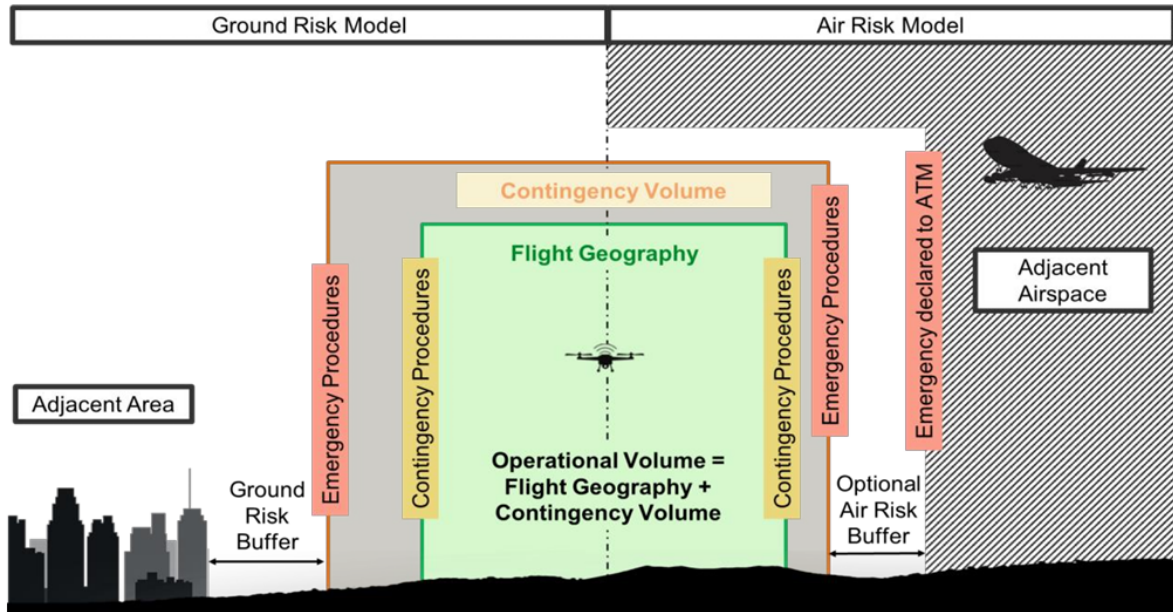


Figure 10.7: SORA Definition of Flight Volume [89]

The SORA definition of flight volume is composed of three elements:

- The Flight Geography which is 30m to each side of the drone.
- Contingency Volume which is 50m to each side of the drone.
- Ground Risk Buffer, Which uses the 1:1 rule meaning that the buffer is the same size as the altitude. which results in 150m.

This results in a flight volume of 230 m to each side of the drone. This is then used to find the intrinsic ground risk class using Table 10.6.

Table 10.6: Intrinsic UAS Ground Risk Class [89]

Intrinsic UAS ground risk class				
Max UAS characteristics dimension	1 m / approx. 3 ft	3 m / approx. 10 ft	8 m / approx. 25 ft	>8 m / approx. 25 ft
Typical kinetic energy expected	< 700 J (approx. 529 ft lb)	< 34 kJ (approx. 25 000 ft lb)	< 1 084 kJ (approx. 800 000 ft lb)	> 1 084 kJ (approx. 800 000 ft lb)
Operational scenarios				
VLOS/BVLOS over a controlled ground area ³	1	2	3	4
VLOS over a sparsely populated area	2	3	4	5
BVLOS over a sparsely populated area	3	4	5	6
VLOS over a populated area	4	5	6	8
BVLOS over a populated area	5	6	8	10
VLOS over an assembly of people	7			
BVLOS over an assembly of people	8			

Given the mission’s offshore nature and the flight volume of 230m, with possible personnel transfers via

a boat within that volume with BVLOS operations. And the UAVs characteristic dimension of 3.3 meters. This would result in a ground risk class of 5. In short this would be BVLOS over sparsely populated area with 8m max UAS characteristic dimension.

The next step will be to determine a mitigation strategy. These strategies can result in a reduction in ground risk. A reduction in ground risk positively influences the Special Assurance Integrity Level (SAIL). This can be seen in Table 10.7.

Table 10.7: Ground Risk Class Mitigation's [89]

Mitigation Sequence	Mitigations for ground risk	Robustness		
		Low/None	Medium	High
1	M1 — Strategic mitigations for ground risk ¹	0: None -1: Low	-2	-4
2	M2 — Effects of ground impact are reduced ²	0	-1	-2
3	M3 — An emergency response plan (ERP) is in place, the UAS operator is validated and effective	1	0	-1

- M1: The operator should make sure that the sea space is closed off from third parties and workers from the operator should be regularly informed of the status and position of the UAV. : -2
- M2: A parachute is included in order to reduce the effects of ground impact: -1
- M3: The UAS operator will be trained and a emergency response plan will has been set up: 0

Applying these mitigation results in a remaining GRC of 2. With the ground risk classified the next step is the air risk class (ARC), EASA provides a flowchart to determine the ARC this is shown in Figure 10.8.

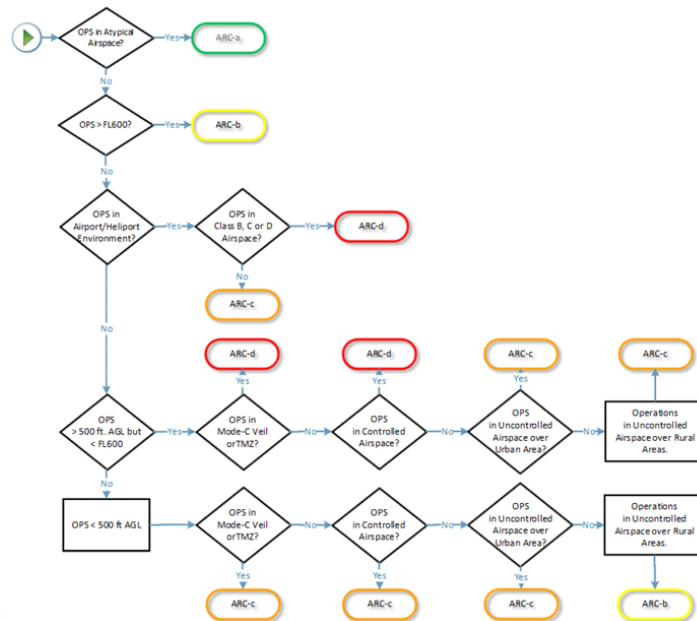


Figure 10.8: Air Risk Class Flow Chart [89]

With the earlier described mission and assumptions this yield the following:

1. OPS in Atypical Airspace: No, since a HPZ and a HTZ are used it can be assumed that there is helicopter traffic in the area.
2. OPS > FL600: No

3. OPS in Airport/Heliport Environment: No
4. OPS > 500 ft. but < FL600: No
5. OPS in Mode-C Veil or TMZ: Yes

The final result is a ARC of class c. This means that there is a risk to other aircraft operating in the area. Using Table 10.8 the required robustness of mitigation measures can be found.

Table 10.8: TPRM [89]

Residual ARC	TMPRs	TMPR level of robustness
ARC-d	High	High
ARC-c	Medium	Medium
ARC-b	Low	Low
ARC-a	No requirement	No requirement

Since the ARC is c, this leads to medium robustness required. To achieve this the UAV is be equipped with an ADS-B out system, this combines with the required mode S transponder to give a robust traffic avoidance system. The combination of the two allows TCAS equipped aircraft to be warned of the drone and it will show up for ADS-B equipped aircraft. The UAVs collision avoidance system also uses this data to avoid other aircraft in its flight path.

With the GRC and the ARC the SAIL can be determined using

Table 10.9: SAIL Classification [89]

SAIL determination				
Final GRC	Residual ARC			
	a	b	c	d
≤2	I	II	IV	VI
3	II	II	IV	VI
4	III	III	IV	VI
5	IV	IV	IV	VI
6	V	V	V	VI
7	VI	VI	VI	VI
>7	Category C operation			

With a GRC of 2 and a ARC of c, this results in a SAIL of 4. This SAIL can then be used to find the required robustness of Operational Safety Objectives (OSO).

EASA has published a table of 24 recommended OSOs [89]. Most of these OSOs govern the operational aspects, however some of them govern the UAV itself or the infrastructure around the UAV operation. One such example would be OSO#05, which is: "UAS is designed considering system safety and reliability" which has to be implemented at medium robustness. Another example is OSO#10, which reads: "Safe recovery from a technical issue". This OSO has to be implemented at a medium robustness for SAIL 4. Both of these have be achieved by redundancy in the communication system, redundancy in the GPS, redundancy in the collision avoidance sensors and the parachute in case of an failure in a critical system. OSO#12 is implemented by Ardupilot's return home feature that is automatically triggered upon signal loss. OSO#18 requires automatic flight envelope protections. OSO#18 is implemented by ardupilot by default if tuned properly. OSO#24 requires the UAV to be designed for adverse weather conditions, given the nature of the expected operating environment this is already covered, this means that this objective is already fully in line with the aims of the design team during the design.

11. Sustainability Strategy

To reduce the footprint of the cargo drone, measures were implemented to minimise environmental impact while maximising societal benefits. During the design phase, sustainable strategies are defined and monitored throughout the project. The objectives were established based on the United Nations' Sustainable Development Goals[2].

11.1. Development Strategy

At the project's outset, the team formulated strategies to ensure that the drone's development would promote environmental sustainability, benefiting both the organisation and the technical process. These strategies were continuously revised, leading to specific goals for the project. The outcomes of these strategies on the design are summarised in Table 11.1.

Table 11.1: Sustainability Strategies of the Design

Materials/Construction		
SS-01	Recyclable	The team selected materials based on criteria such as low environmental impact production and end-of-life for the material trade-off
SS-02	Bought-Off-the-Shelf	In the detailed design, more than 50% of the mass of the parts is made up from existing parts which can be bought online
SS-03	Modular	The team has successfully created a modular design that allows components to easily be replaced, avoiding scrapping of the entire product due to small defects
SS-04	Dimensions / Weight	Dimensions was one of the key criteria in the trade-off, such that a small design was selected over larger sized designs, reducing total material required
Power		
SS-05	Efficient	Efficiencies in hover and cruise were crucial criteria in the configurations trade-off
SS-06	Emissions	The current drone design is fully electric, with no combustion engine
SS-07	Available	The team uses easily available energy sources to allow a wide area of use for the product
SS-08	Renewable	The team aims to make use of existing renewable resources to provide energy to the drone
Health and Safety		
SS-09	Safe Operation	The team has created a design that can be safely operated by minimising human interaction while the drone is operative. In case of interaction, safety has been ensured by implementing ducts and a low RPM
SS-10	Safety Features	The team added safety features to the product to ensure the safety of personnel even during emergency situations, as safety was one of the main criteria
SS-11	Toxicity / Emissions	The team avoids any emission of harmful or toxic products during the entire use of the product
Life Cycle		
SS-12	Length	The team has selected components with an operational lifetime that is as long as possible to reduce the environmental impact and ensure a long operational life for the UAV
SS-13	Modular	The team has created a design that is very modular, so any parts that break can be replaced easily

SS-14	Robust Design	The team has created a design with good corrosion resistance. Any interaction between moving components has been designed to reduce wear due to friction
SS-15	Complexity	The team created a design that is not overly complex and maintenance is possible by operators and promoted by the design through easy access to all critical areas
Pollution of drone design		
SS-16	Toxicity	The team has designed the system to minimise the release of non-toxic materials to reduce environmental impact in the event of a crash
SS-17	Emissions	The team created a design that does not emit any additional toxic or polluting gases/products, on top of those emitted from any propulsion system
SS-18	Crash Resistance	The team has generated a product that does not disintegrate in the event of a crash
SS-19	Recover-Ability	The team created a design that is as recoverable as possible after a crash to avoid unnecessary pollution, by integrating flotation into the design
Economic		
SS-20	Cheap	The team made a design that is affordable to allow a large-scale roll-out of the product, as it uses off-the-shelf parts and is simple to produce
SS-21	Support Cost	The team has reduced support cost by simplifying operations
SS-22	Waste	The team has created a maintainability plan as part of the RAMS characteristics analysis to reduce waste
Efficiency of mission		
SS-23	Mission Efficiency	The mission design of the product minimises the time in the air and reduces ground operations time
SS-24	Payload Planning	The UAV design performs optimally at maximum payload capacity promoting users, whenever possible to, increase payload up to capacity

11.2. Environmental Impact

The status quo is highly polluting. Vessels and helicopters are highly inefficient and worsen the biodiversity of the ocean. Moreover, supporting the wind energy market can help replace the oil and gas sector, which accounts for 5.1 billion tonnes of greenhouse gas emissions [90]. To attach value to the sustainability strategies, the design is compared to certain set goals by the United Nations, out of their 17 Sustainable Development Goals, this project contributes to six of them, these six outlined in Figure 11.1. In addition, the project adheres to other sustainability goals set by communities as the EU, like climate neutrality in 2050 - an economy with net-zero greenhouse gas emissions [91].



Figure 11.1: UN Sustainable Development Goals [2]

Alignment with Sustainable Development Goals

SDG 7: Affordable and Clean Energy

Ensure access to economical, reliable, sustainable, and modern energy for all. This goal focuses on increasing the share of renewable energy in the global energy mix and improving energy efficiency.

- **SS-06 Emissions:** The current drone design is fully electric, which helps in reducing greenhouse gas emissions and contributes to clean energy.
- **SS-07 Available:** The drone uses easily accessible energy sources, promoting the use of affordable and accessible clean energy.
- **SS-08 Renewable:** The drone aims to utilise renewable energy sources, ensuring sustainable energy consumption.

SDG 8: Decent Work and Economic Growth

Promote sustained, inclusive, and sustainable economic growth, full and productive employment, and decent work for all. This goal emphasises the need for higher levels of economic productivity through diversification, technological upgrading, and innovation.

- **SS-02 Bought-Off-the-Shelf:** The use of existing parts supports economic activity by creating demand in the market for these components.
- **SS-20 Cheap:** By making the design affordable, the drone project facilitates widespread economic opportunities and growth.
- **SS-21 Support Cost:** Reducing support costs helps in lowering operational expenses, thus contributing to economic growth.

SDG 9: Industry, Innovation, and Infrastructure

Build resilient infrastructure, promote inclusive and sustainable industrialisation, and foster innovation. This goal aims to develop quality, reliable, sustainable, and resilient infrastructure to support economic development and human well-being.

- **SS-03 Modular:** The modular design enhances innovation in the drone industry by allowing easy replacement and upgrading of components.
- **SS-14 Robust Design:** Ensuring a robust design that can withstand wear and tear promotes the development of resilient infrastructure.
- **SS-15 Complexity:** A design that is easy to maintain fosters innovation and industrial growth by making the product accessible and user-friendly.

SDG 12: Responsible Consumption and Production

Ensure sustainable consumption and production patterns. This goal focuses on improving resource efficiency and reducing waste generation through prevention, reduction, recycling, and reuse.

- **SS-01 Recyclable:** Using recycled materials supports sustainable consumption and reduces environmental impact.
- **SS-22 Waste:** Developing a maintainability plan to reduce waste aligns with responsible production practices.

SDG 13: Climate Action

Take urgent action to combat climate change and its impacts. This goal emphasises the need to integrate climate change measures into national policies, strategies, and planning.

- **SS-16 Toxicity:** Using non-toxic materials minimises environmental damage, supporting climate action goals.

SDG 14: Life Below Water

Conserve and sustainably use the oceans, seas, and marine resources for sustainable development. This goal focuses on preventing and significantly reducing marine pollution of all kinds.

- **SS-19 Recover-Ability:** A design that integrates floating components for recovery after a crash helps reduce pollution in water bodies and protect marine life.

By contributing to the Sustainable Development Goals, the PeliCrane takes crucial steps in advancing the energy transition. As outlined in Chapter 2, this design addresses a market niche, pushing the boundaries of current sustainable solutions for offshore logistics.

12. Production Plan

This section includes a production plan for assembling this drone. It includes detailed descriptions of each structural component and the manufacturing techniques required for each, along with the appropriate materials. Additionally, this guide provides step-by-step instructions on how to assemble the components together. Please note that while the guide aims to be comprehensive, some minor mounts may be missing for inspection purposes and may need to be designed separately. However, all major components are included.

12.1. Components

Table 12.1: Components: Materials and Manufacturing

Component	Materials	Quantity	Manufacturing
Rods	Carbon Fibre	4	Off-the-shelf
Arm Brackets	Polycarbonate	8	SLS 3D Printed
Ducts	Foam + Carbon Fibre Sheet	4	Layered foam sheets + CNC Milling
Inter-duct plates	Polycarbonate	8	SLS 3D Printed
Duct-Central box connector	Polycarbonate	8	SLS 3D Printed
Landing Gear rod	Carbon Fibre	4	Off-the-shelf
Landing Gear feet	Polycarbonate	4	SLS 3D Printed
Landing Gear mount	Polycarbonate	4	SLS 3D Printed
Payload Box	Polycarbonate	1	SLS 3D Printed
Winch System Rope	Polypropylene	1	Off-the-shelf
Winch System Spool	Polycarbonate	1	3D Printed
Central Box top and bottom	AL6061	2	Laser Cut
Central Box Sides	Polycarbonate	4	SLS 3D Printed
Electronics Box	Polycarbonate	1	SLS 3D Printed
4 bladed Propellers	Carbon Fibre	4	Off-the-shelf
Motor Connector	AL6061	4	CNC Milling
Rod in Duct	Carbon Fibre	8	Off-the-shelf
Duct-Rod Connector	Polycarbonate	8	SLS 3D Printed
Parachute Box	Polycarbonate	1	SLS 3D Printing
Camera Stand	Polycarbonate	1	SLS 3D Printing
Short Range Radar Plate	Polycarbonate	3	SLS 3D Printing
Main Radar Plate	Polycarbonate	1	SLS 3D Printing
Radar Clip	Polycarbonate	8	SLS 3D Printing
Lidar Platform	Polycarbonate	1	SLS 3D Printing

Rods

The rods, as specified in [92], are standard off-the-shelf components featuring an outer diameter of 50 mm and an inner diameter of 47 mm. These rods will be cut to a length of 800 mm for the four central arms of the configuration, and 700 mm for the four landing gear legs. This arrangement therefore needs a total of 6 m of carbon fiber rods to accommodate the entire structure, the rods can be ordered in 2m chucks four times. For the Rods, that are located inside the duct, these will also be off the shelf, with an outer diameter of 20 mm and inner diameter of 16 mm [93]. These are sold by 2 m length and will have to be cut to a length of 600 mm, resulting in a final length needed of 4.8 m.

Central Box

The central box, as explained in Subsection 5.3.7 consists of two AL6061 plates and four Polycarbonate sheets that form the sides, as seen in Figure 12.1b, Figure 12.1a and Figure 12.1c respectively. For the aluminium plates, based on a 2D model of these, they can be laser cut. For the Polycarbonate sheets, these can be made using Selective Laser Sintering (SLS) 3D printing - a 3D printing technique that uses a laser to fuse together powdered material.

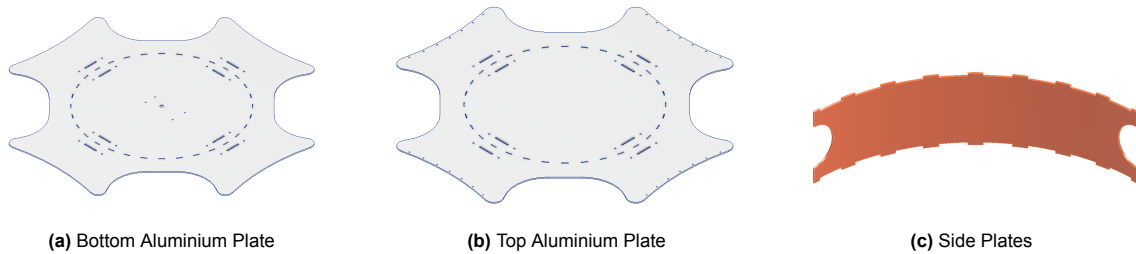


Figure 12.1: Central Box Parts

Electronics Box

As detailed in Subsection 5.3.8, the electronics box is designed as an octagonal configuration. Each side of the octagon is a rectangle measuring 150 cm in length and 10 cm in width. This will be made from Polycarbonate. To achieve this specific shape, SLS 3D printing will be used, ensuring structural integrity. This configuration can be seen in Figure 12.2, with an inside as well as an outside view.

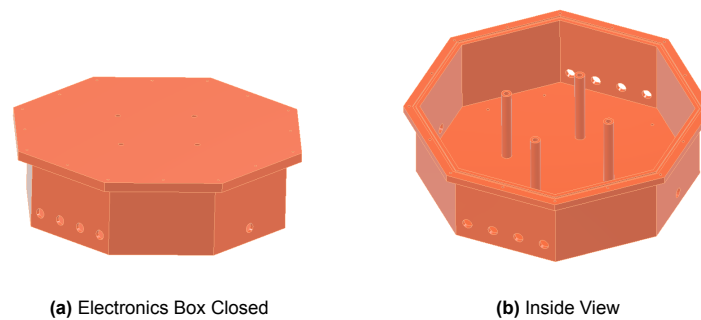


Figure 12.2: Electronics Box

Arm Brackets

The arm brackets will have dimensions of - as can be visualised in Figure 12.3. This will be SLS 3D printed based on the CAD model.



Figure 12.3: Arm Brackets

Inter-Duct Plate

The Inter-Duct Plate were explained in Subsection 5.3.3. The material choice was chosen as polycarbonate, as such it will be SLS 3D printed.



Figure 12.4: Inter-Duct Plate

Landing Gear

For the landing gear, the components depicted in Figure 12.5 include the feet and the mount, both of which are fixed to the landing gear rod, found in Table 12.1. Both of these parts are fabricated using SLS 3D printing. Post-printing, it is crucial to sand the sides of the interfaces where the parts connect with the rod. This process is necessary to achieve a smooth surface and facilitate the assembly to the landing gear.



(a) Landing Gear Feet

(b) Landing Gear Mount

Figure 12.5: Landing Gear 3D Printed Components

Winch System

The winch system consists of two parts: the winch system spool and the winch system rope. For the Spool, it will be SLS 3D Printed, according to the dimensions described in Table 5.12 found in Subsection 5.3.6. For the rope, this will be an off-the-shelf component, a polypropylene floating rescue line such as [37].

Propellers

The propellers selected are four-bladed, as explained in Subsection 4.5.2, it will be an off the shelf selection from the E-PROPS manufacturing firm, the model used is the 4-Q-35-115 found in [34].

Ducts

The ducts will be constructed using Extruded Polystyrene Foam (EPF) as the core material, which is then wrapped with a carbon fiber layer. The interior EPF part is illustrated in Figure 12.6a, providing a view of the foam structure. The external carbon fibre reinforcement is depicted in Figure 12.6b, showing its finish. To construct the duct, the flat sheets of foam can be layered together and sculpted to the desired shape. To glue these flat sheets together a special sprayable Foam Contact Adhesive C8530 can be used [44]. To sculpt these to the adequate shape it can be CNC milled using a 5-axis CNC mill, as it has to be noted that the duct configuration has a hole on each side.

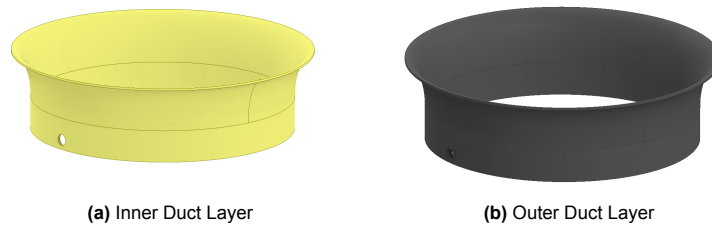


Figure 12.6: Duct Components

Motor Connection

In order to couple the ducts and motors vibrations, the part seen in Figure 12.7 was designed. This part uses AL6061 and will be manufactured using CNC Milling.

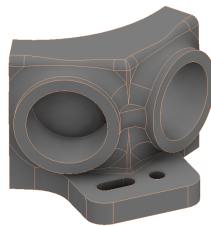


Figure 12.7: Connecting Part to Motor

Parachute Box

The configuration of the parachute box can be seen below, with the box opened in Figure 12.8b and then closed in Figure 12.8a. The box is made of Polycarbonate and will therefore be manufactured using SLS 3D printing.

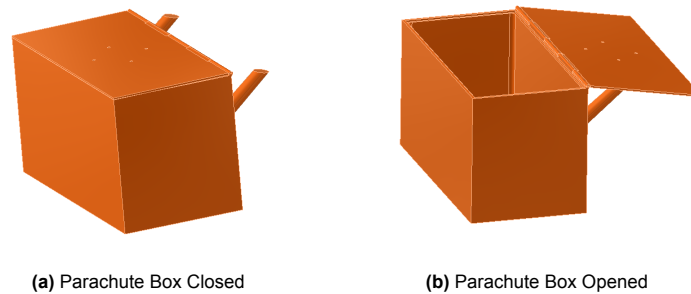


Figure 12.8: Parachute Box

Payload Box

The payload box, as seen in Figure 12.9, consists of two primary components: the frame and 1 mm thick Polycarbonate plates, further explained Subsection 5.3.6. The frame can be produced using SLS 3D printing technique to ensure precision. Meanwhile, the Polycarbonate plates can be fixed to the frame using the C8530, as referenced in Figure 12.1.



Figure 12.9: Payload Box

12.2. Configuration Assembly

The glue used during the assembly is identical to the glue used during the manufacture process of the ducts as this is usable as a general adhesive as well as for foam specifically.

The first step in the assembly process is to mount the motor arm brackets onto the bottom plate using bolts from underneath, the locations are shown in Figure 12.10. The brackets can be installed in any order.

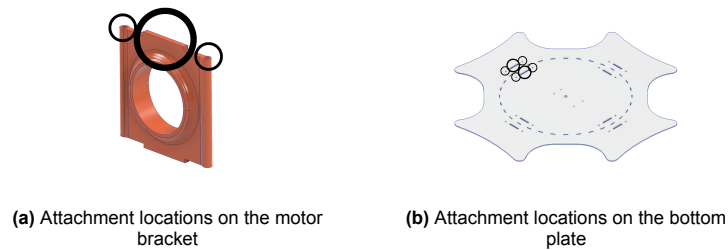


Figure 12.10: Attachment locations of the motor bracket

After the motor arm brackets are installed the side plates of the central box should be installed. These plates should be installed such that the half-circular cutout on each side plate forms a circular hole between a set of motor arm brackets. This circular hole should be in line with the holes in the motor arm brackets.

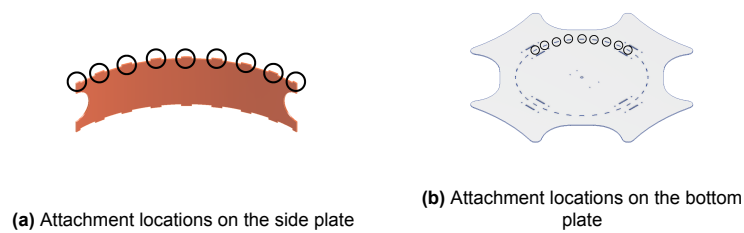


Figure 12.11: Attachment locations of the side plate

After this, the winch can be mounted onto the bottom panel using four bolts on the bottom plate. The locations are shown in Figure 12.12.

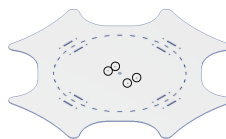


Figure 12.12: Winch attachment points

Once the winch is mounted, the flight computer, the companion computer and the ADS-B transmitter can be mounted to the electronics box. In order to achieve this both computers should be glued bottom of the electronics box using foam tape. The low-voltage battery and PDB should be installed in a similar manner. The holes in the walls of the electronic box should be plugged using the water-tight connectors. The cables should now be routed from the plugged holes. The electronics box can then be closed. The electronics box can be closed using the bolts in the locations indicated in Figure 12.13.

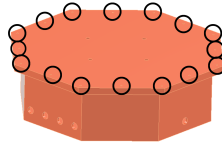


Figure 12.13: Bolt Location of to Close Box

After the cables are mounted the parachute box can be mounted onto of the electronics box using bolts onto the connection points shown in Figure 12.14.

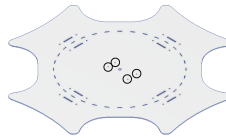


Figure 12.14: Parachute Box Attachment Points

The springs can be glued to the bottom of the parachute box. After this, the using glue the parachute inner box can be loaded on the springs. After this the locking mechanism can be installed to the bracket that still has to be designed. After the locking mechanism, the parachute can be folded and placed in the parachute inner box after which the box can be loaded and locked and the top closed. After this the SF40/C can be mounted on top of the parachute box. Using the LiDAR elevation platform and bolts through holes in the parachute box shown in Figure 12.15.



Figure 12.15: Lidar Attachment Points

After the electronic box and the parachute box are prepared, the engine arms can be inserted through the holes in the engine brackets and the holes in the side plates. Using to be designed clamps the plates and the rods are attached. At this point, the wires to the motors can be routed through the engine arms.

After the engine arms are mounted, the electronic box can be mounted onto the top plate of the central box using bolts. Once the electronic box is mounted the wires to the winch and the data cables from the motor arm can be connected to the electronic box at the appropriate plug.

After this, the duct-central box connectors can be attached to the top and bottom plate of the central box using bolts. The locations are shown in Figure 12.16.

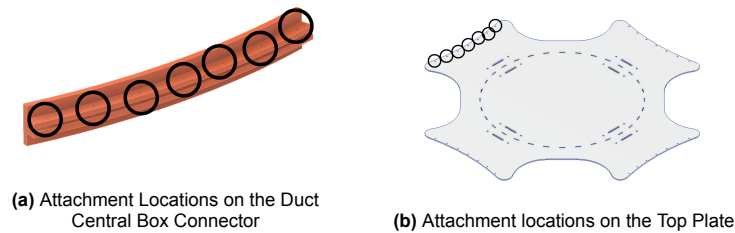


Figure 12.16: Attachment locations of the Duct Central Box Connector

After this, the ducts can be slid onto the motor arms. Care should be taken to ensure that the diffuser points downwards. Before sliding the duct to the end of the motor arm, glue should be applied to the duct-central box connectors and on the motor arm 4 cm to each side of the duct-central box connectors. After the glue application, the duct should be slid to be flush with the connectors and held until the glue hardens. This can be repeated for each duct.

After all ducts are secured the inter-duct connectors can be attached to the inter-duct plates, two per plate, using bolts.

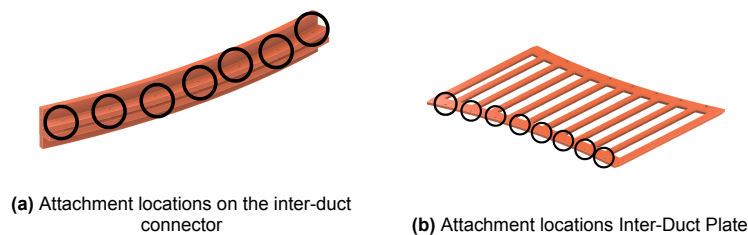


Figure 12.17: Attachment Locations of the Inter-duct Connectors on the Inter-duct Plate

After all eight are assembled, these can be attached to the drone by applying glue on the connectors at the opposite end of the plate. These should be placed between the ducts at the closest points in pairs of two. The bottom of the pair is mounted 1 cm from the bottom of the duct and the top plate is mounted 12 cm from the bottom.

Once the ducts are fully secured to each other, the landing gear mount can be slid onto the motor arm. At 18 cm from the base of the duct, glue should be applied around the motor arm, after the application slide the landing gear mount on top of the glue and wait for it to harden. This should be repeated for each landing gear mount. After the mounts are installed the landing legs can be assembled, these consist of the landing gear rod and landing gear leg, the landing gear leg is glued onto one of the ends of the landing gear rod. Once all landing lags are assembled these can be glued into the landing gear mounts attached to the motor arms. After these harden the drone can be turned upright and be set atop the legs.

After the landing legs, the motors are mounted on the end of the motor arms. During this, the motors are first connected to the wires inside of the motor arms and then the motors are clamped to the motor arm using screws.

After the motors, the Motor Connectors are mounted onto the motors using the excess screw holes left during the installation of the motors. The rods in the duct are attached to the duct rod connectors using glue, these are then glued to both the duct and the motor connectors.

After the motors are installed the batteries are installed and connected to the BMS's on the inter-duct plates. After the batteries, the barometer, GPSs, transmitters, lights, camera, IR-Lock, pitot tube, re-

mote ID module, noise emitter and lights are mounted onto hard points that still have to be designed and wired to the appropriate plug on the electronics box.

The final electronics to be installed are the rangefinders. To mount these the duct radar clips are bolted into the main radar plate and the short-range radar plates. The locations are shown in Figure 12.18.



Figure 12.18: Attachment Locations of the Radar Plates and Clips

Once the main radar plate is assembled, glue is applied to the concave parts of the duct radar clip and then glued to the top of the diffuser of the ducts. This same procedure is applied to both the main radar plate and the short-range radar plate. The main radar is then screwed into the main radar plate. The short-range radars are glued to the short-range radar plate. The attachment of the additional short-range radars to the duct and the radio altimeter to the frame is still to be designed. After the mounting of the rangefinders, they are connected to the appropriate plug in the electronics box.

Finally, the propellers are installed onto the motors.

12.3. Production Flowchart

The production plan discussed above can be summarised in to in Figure 12.19. Additionally, an estimate for the time required per step is added.

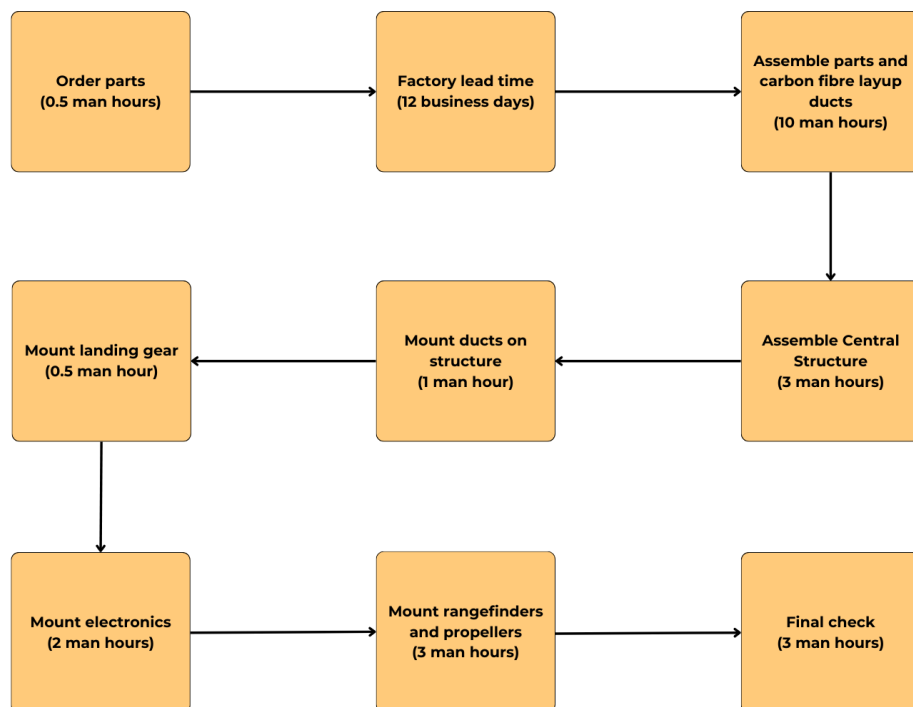


Figure 12.19: Production Overview Flowchart

13. Future Outlook

While a final design is presented in Chapter 8, the product is not yet entirely complete. Most of the design work is done, with only a few brackets remaining, which can be designed quickly and are therefore not included in the post-DSE Gantt chart. In addition to these parts, some software design still needs to be completed, specifically writing a program that matches the pseudo code provided in Subsection 7.3.2. Further CFD and FEM analysis is required due to the complex design of the drone and its ducts.

During this final stage of design refinement, securing funding for the project is essential. Once funding is secured, parts for the initial prototype should be ordered. After receiving these parts, they can be tested and assembled into a prototype, which will then undergo testing to identify and fix any issues.

Following this, an initial production run will begin, and applications for all necessary certifications will be submitted, along with compliance testing. Once the drone is fully certified as required, planning and execution of a marketing campaign can commence, along with filing for patents where applicable.

After this, the production process can be scaled as needed, and further development within the company can proceed.

These steps are further detailed in Figure 13.1.



Figure 13.1: Project Gantt Chart

14. Conclusion

This report aimed to outline the design of all the subsystems of the UAV, and then integration of the into a complete and functional product. The main focus was to create a system that can withstand harsh environmental conditions while ensuring safety, reliability, and performance, while satisfying a 30 min hover and a 5 km range requirement with a 25 kg payload. Through various system engineering and project management processes, the team has successfully achieved this goal.

The first, and probably the most important subsystem that was designed is the propulsion system. In the trade-off it has been decided that a four-bladed ducted quadcopter will be used. Both the four-bladed propeller and the ducted configuration are unconventional, therefore extensive research had to be performed to find out about the characteristics of these designs. For the duct, an elliptical inlet and a small diffuser section configuration was designed, while for the propeller and off-the-shelf four-bladed propeller was selected. This configuration was estimated to be approximately 25% more efficient than a conventional configuration.

The next part of the UAV designed was the structure. The team aimed for maximum weight efficiency, ultimately selecting a configuration with four crossing rods attached to a central box for superior structural resistance. Key materials include Aluminum 6061 for strength and weight balance, Polycarbonate for UV resistance and ease of manufacturing, and Carbon Fiber for its exceptional strength-to-weight ratio. Carbon Fiber was chosen for the rods, Polycarbonate for the arm brackets, and Extruded Polystyrene Foam wrapped in Carbon Fiber for the ducts. The non-retractable landing gear and the payload box were made from Carbon Fiber and Polycarbonate, respectively. The winch system, featuring a 3D printed spool and polypropylene line, was designed for maximum payload efficiency.

The electronics of the UAV were meticulously designed, starting with the selection of key components such as the Cube Orange flight controller and Raspberry Pi for enhanced processing. The low-voltage components were mainly selected based on functionality, compatibility and the mission profile. Due to the large amount of low-voltage component, it has been decided that apart from the high-voltage battery, which provides power to the motors-, a low-voltage battery is also implemented, so that no large step-downs are required. The integration process includes strategic placement of components to reduce interference and optimise performance, with high-voltage AWG8 and low-voltage AWG22/24 wiring ensuring safety and efficiency.

The UAV's control and stability rely on precise RPM control via the ArduPilot flight controller, which uses proportional and PID controllers for attitude control. Stability is managed through CAN signals adjusted by the flight controller, ensuring the drone remains balanced and responsive to inputs. Dynamic simulations in Python and Simulink verify the behaviour of the UAV under various scenarios, including takeoff, axis rotations, and engine failures.

In conclusion, all the main requirements were met, resulting in an efficient and safe product. The PeliCrane can be used for various offshore operation mission profiles, while ensuring reliability and longevity. However, it is not by any means a finished product. Further development must be done in order to have a ready product. As it is an unconventional design, first a CFD analysis must be conducted in order to reveal the aerodynamic characteristics. With that, the whole design must be verified again to get an accurate estimate of performance. After this, funding must be sorted, which is necessary for manufacturing, testing and then later product launch. A more comprehensive overview is provided in Figure 14.1, where all the post project development steps are listed in a logical order. If those are followed, this design has a promising future and could revolutionise the offshore sector.

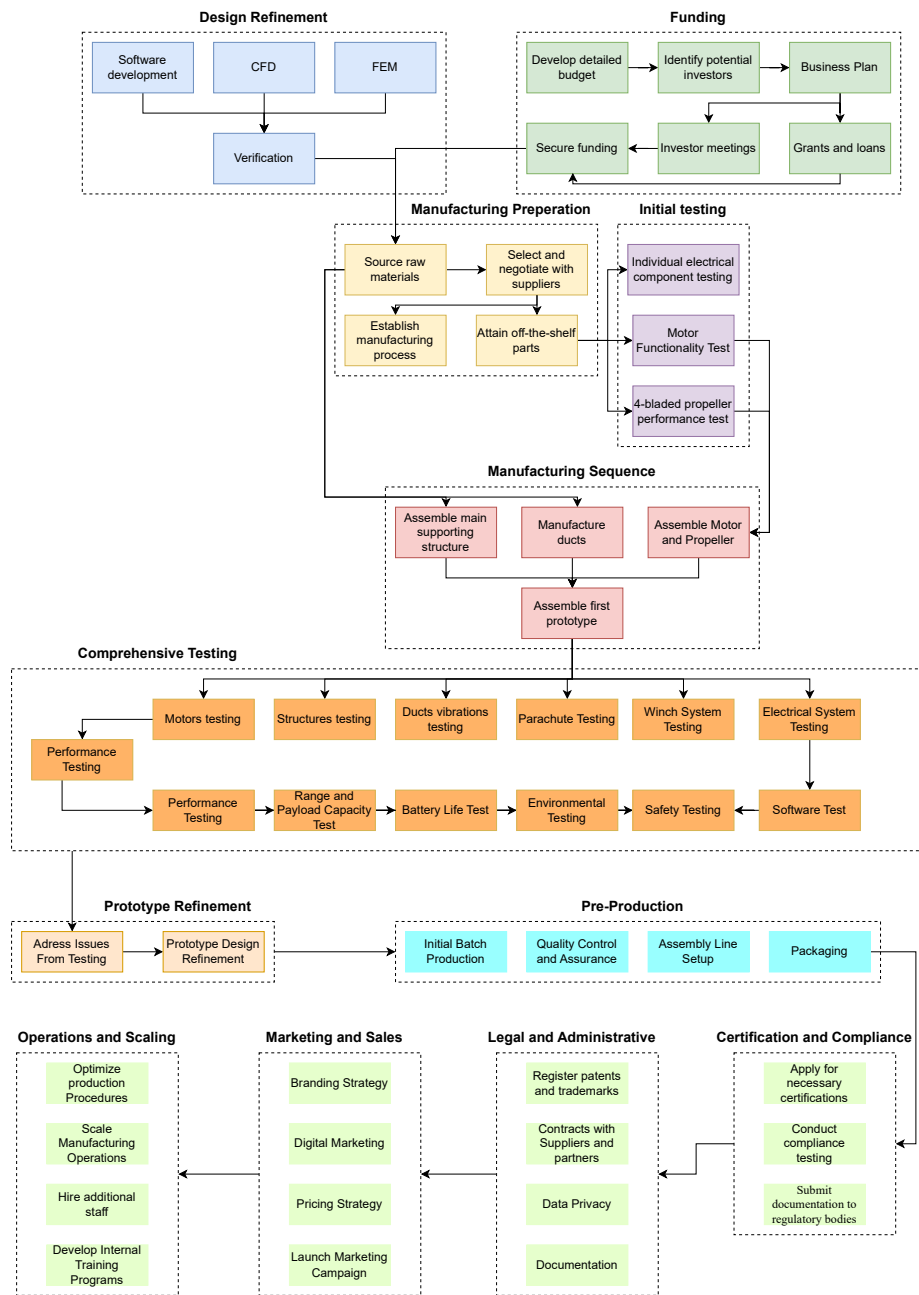


Figure 14.1: Project Design and Development Logic

References

- [1] Statista. *Consumer Drone Market Key Players*. 2024. URL: <https://www.statista.com/outlook/cmo/consumer-electronics/drones/netherlands#price> (visited on 04/25/2024).
- [2] United Nations. *The 17 Sustainable Development Goals*. 2024. URL: <https://sdgs.un.org/goals> (visited on 06/19/2024).
- [3] Global Wind Energy Council. *Global Offshore Wind Report 2023*. 2023. URL: <https://gwec.net/gwecs-global-offshore-wind-report-2023/> (visited on 04/30/2024).
- [4] Grand View Research. *Commercial Drone Market Size, Share & Trends Analysis Report By Product, By Application, By End-use, By Propulsion Type, By Range, By Operating Mode, By Endurance, By Region, And Segment Forecasts, 2023 - 2030*. 2021. URL: <https://www.grandviewresearch.com/industry-analysis/global-commercial-drones-market> (visited on 06/11/2024).
- [5] Statista. *Total Value of the Worldwide cargo drone market in 2023, with a forecast through 2030*. 2024. URL: <https://www.statista.com/statistics/1278381/drone-package-delivery-system-market-size-region/> (visited on 04/26/2024).
- [6] Statista. *Projected Global Drone Delivery Market Revenue in 2023 and 2030, by type (in million U.S. Dollars)*. 2024. URL: <https://www.statista.com/statistics/1238185/global-drone-delivery-market-revenue-type/> (visited on 04/29/2024).
- [7] BBC. *US sanctions drone-maker DJI*. 2021. URL: <https://www.bbc.com/news/technology-59703521> (visited on 06/17/2024).
- [8] M. Morcillo et al. "Salinity in marine atmospheric corrosion: Its dependence on the wind regime existing in the site". In: *Corrosion Science* 42.1 (2000), pp. 91–104. DOI: 10.1016/S0010-938X(99)00048-7.
- [9] Polaris Market Research. *Offshore Wind Energy Market Share, Size, Trends, Industry Analysis Report*. 2020. URL: <https://www.polarismarketresearch.com/industry-analysis/offshore-wind-energy-market> (visited on 04/25/2024).
- [10] McKinsey & Company. *How to succeed in the expanding global offshore wind market*. 2022. URL: <https://www.mckinsey.com/industries/electric-power-and-natural-gas/our-insights/how-to-succeed-in-the-expanding-global-offshore-wind-market> (visited on 04/25/2024).
- [11] Netherlands Enterprise Agency. *New Offshore Wind Farms*. 2024. URL: <https://english.rvo.nl/topics/offshore-wind-energy/new-offshore-wind-farms> (visited on 05/08/2024).
- [12] Ministry of Economic Affairs and Climate Policy. *Offshore wind: The Netherlands well on schedule, tender round to double capacity will start early 2024*. 2024. URL: <https://www.government.nl/latest/news/2023/12/19/offshore-wind-the-netherlands-well-on-schedule-tender-round-to-double-capacity-will-start-early-2024> (visited on 05/08/2024).
- [13] Vattenfall. *Windenergie cruciaal voor de energietransitie*. 2024. URL: <https://www.vattenfall.nl/over-vattenfall/onze-energiebronnen/windenergie/> (visited on 05/08/2024).
- [14] Health and Safety Executive UK. *Manual Handling at Work*. 2023. URL: <https://www.hse.gov.uk/pubns/indg143.pdf> (visited on 04/30/2024).
- [15] SalaryExpert. *Turbine Technician Wind Salary Netherlands*. 2024. URL: <https://www.salaryexpert.com/salary/job/turbine-technician-wind/netherlands> (visited on 06/19/2020).
- [16] M. Morcillo et al. "Salinity in marine atmospheric corrosion: its dependence on the wind regime existing in the site". In: *Corrosion Science* 42.1 (2000), pp. 91–104. DOI: 10.1016/S0010-938X(99)00048-7.

- [17] S.J. Price and R.B. Figueira. "Corrosion Protection Systems and Fatigue Corrosion in Offshore Wind Structures: Current Status and Future Perspectives". In: *Coatings* 7.2 (2017). DOI: doi.org/10.3390/coatings7020025.
- [18] J.P. Coelingh, A.J.M. van Wijk, and A.A.M. Holtslag. "Analysis of wind speed observations on the North Sea coast". In: *Journal of Wind Engineering and Industrial Aerodynamics* 73.2 (1998), pp. 125–144. DOI: 10.1016/S0167-6105(97)00285-7.
- [19] Y.B. Lee and J.S. Park. "Hover performance analyses of coaxial co-rotating rotors for Evtol Aircraft". In: *Aerospace Science and Technology* 9.3 (2022), p. 152. DOI: 10.3390/aerospace9030152.
- [20] Y. Hong et al. "Exploration of stacked rotor designs for aerodynamics in hover". In: *Aerospace Science and Technology* 141 (2023), p. 108557. DOI: 10.1016/j.ast.2023.108557.
- [21] Q. Quan. *Introduction to Multicopter Design and Control*. 1st ed. Singapore: Springer Singapore, 2017.
- [22] MAD Components. *MAD Drone Components*. 2024. URL: <https://mad-motor.com/> (visited on 12/24/2020).
- [23] J.D. Anderson. *Fundamentals of Aerodynamics*. 6th ed. New York: McGraw-Hill, 2016.
- [24] T-Motor. *Drone Propulsion Systems*. 2023. URL: <https://uav-en.tmotor.com/> (visited on 06/10/2024).
- [25] HobbyWing. *HobbyWing Components*. 2024. URL: <https://www.hobbywingdirect.com/> (visited on 06/10/2024).
- [26] R. Goudswaard. "Aerodynamic Performance of a Small-Scale Ducted Rotor in Hover: An Experimental Study on the Effect of the Tip Gap". In: *Delft University of Technology* (2021). URL: <https://repository.tudelft.nl/islandora/object/uuid%3A727fd73b-ddb1-40d9-b7fd-2617f769136d>.
- [27] Y. Li, K. Yonezawa, and H. Liu. "Effect of Ducted Multi-Propeller Configuration on Aerodynamic Performance in Quadrotor Drone". In: *Journal of Aerospace Engineering* 5.3 (2021), p. 101. DOI: 10.3390/drones5030101.
- [28] S. Yilmaz, D. Erdem, and M.S. Kavsaoglu. "Performance of a ducted propeller designed for UAV applications at zero angle of attack flight: An experimental study". In: *Aerospace Science and Technology* 45 (2015), pp. 376–386. DOI: 10.1016/j.ast.2015.06.005.
- [29] J.L. Pereira and I. Chopra. "Hover and Wind-Tunnel Testing of Shrouded Rotors for Improved Micro Air Vehicle Design". In: *Department of Aerospace Engineering* (2008), p. 351. URL: <https://apps.dtic.mil/sti/tr/pdf/ADA595716.pdf>.
- [30] A.H. Sacks and J.A. Burnell. "Ducted propellers—a critical review of the state of the art". In: *Progress in Aerospace Sciences* 3 (1962), pp. 85–135. DOI: 10.1016/0376-0421(62)90017-9.
- [31] Mad Motor. *M40C30 Specifications*. 2023. URL: <https://mad-motor.com/products/mad-components-m40c30-ipe-paramotor?VariantsId=10793> (visited on 06/04/2024).
- [32] Hobbywing. *XRotor X11 MAX*. 2015. URL: <https://www.hobbywing.com/en/products/xrotor-x11-max271.html> (visited on 06/04/2024).
- [33] T-MOTOR. *U15L Specifications*. 2023. URL: https://uav-en.tmotor.com/html/2019/Manned_Aircraft_0703/274.html#&gid=1&pid=4 (visited on 06/04/2024).
- [34] E-Props. *4 Bladed Propeller*. 2022. URL: <https://vtol.e-props.fr/index.php?language=en> (visited on 06/05/2024).
- [35] Hobbywing.com. *XROTOR X13-13825 specification sheet*. 2015. URL: <https://www.hobbywing.com/en/products/xrotorx13.html> (visited on 06/11/2024).
- [36] MAD Components. *M50C35 PRO EEE Manned Drone motor*. 2024. URL: <https://mad-motor.com/products/mad-components-m50c35-pro-eee?VariantsId=10547> (visited on 06/19/2024).
- [37] premiumropes. *FLOATING RESCUE LINE*. 2023. URL: <https://www.premiumropes.com/rescue-line> (visited on 06/10/2024).

- [38] Independence Paragliding. *Ultra Cross LIGHTEST HIGHT-PERFORMANCE RESERVE*. 2024. URL: <https://www.independence.aero/en/reserves/ultra-cross/> (visited on 06/11/2024).
- [39] Fruity Chutes. *IRIS ULTRA 168" COMPACT PARACHUTE - 156LB AT 20FPS; 87LB AT 15FPS*. 2024. URL: <https://shop.fruitychutes.com/collections/iris-ultra-compact-chutes/products/iris-ultra-168-compact-chute-156lbs-20fps-87lbs-15fps> (visited on 06/11/2024).
- [40] Hermans Verenfabriek. *HV-32252 Default compression spring*. 2024. URL: <https://hermans-veren.com/eng/shop-hv-32252> (visited on 06/11/2024).
- [41] NASA. *NASA TECHNICAL STANDARD*. 2014. URL: <https://standards.nasa.gov/sites/default/files/standards/NASA/B-w/CHANGE-3/3/2022-10-24-NASA-STD-5001B-w-Change-3-Approved.pdf> (visited on 06/05/2024).
- [42] Ansys. *Ansys Mechanical*. 2024. URL: <https://www.ansys.com/products/structures/ansys-mechanical> (visited on 06/24/2024).
- [43] xometry. *Where Big Ideas Are Built | Production Parts and Prototypes | Xometry*. 2024. URL: <https://www.xometry.com/> (visited on 06/19/2024).
- [44] Bondrite Adhesives. *Sprayable Foam Contact Adhesive C8530 – 5 Litre*. 2024. URL: <https://bondrite.co.uk/product/sprayable-foam-contact-adhesive-c8530-5-litre/> (visited on 06/17/2024).
- [45] ArduPilot. *The Cube Orange/+ With ADSB-In Overview*. 2014. URL: <https://www.jkbms.com/product/jk-b1a24s/> (visited on 06/19/2024).
- [46] SIYI. *SIYI A8 mini 4K 8MP Ultra HD 6X Digital Zoom Gimbal Camera*. 2023. URL: <https://shop.siyi.biz/products/siyi-a8-mini> (visited on 06/19/2024).
- [47] SIYI Technology. *SIYI - A2 mini Gimbal Camera*. 2024. URL: <https://www.3dxr.co.uk/camera-fpv-c57/cameras-c309/siyi-technology-siyi-a2-mini-gimbal-camera-p5531> (visited on 06/06/2024).
- [48] lightware. *SF40/C (100 m)*. 2023. URL: <https://lightwarelidar.com/shop/sf40-c-100-m/> (visited on 06/19/2024).
- [49] Ainstein. *US-D1: All-Weather Radar Altimeter*. 2023. URL: <https://ainstein.ai/us-d1-all-weather-radar-altimeter/> (visited on 06/19/2024).
- [50] Mouser Electronics. *Jorjin MM5D91-00 60GHz mmWave Radar Module*. 2022. URL: <https://nl.mouser.com/new/jorjin/jorjin-mm5d91-00-sensor-module/> (visited on 06/19/2024).
- [51] Nanoradar. *77GHZ Collision Avoidance Radar MR72*. 2019. URL: <http://en.nanoradar.cn/Article/detail/id/488.html> (visited on 06/19/2024).
- [52] RS. *RS PRO Red Panel Mount Indicator, 12V, 14mm Mounting Hole Size, IP67*. 2024. URL: <https://nl.rs-online.com/web/p/panel-mount-indicators/0208273?gb=s> (visited on 06/19/2024).
- [53] FireHouseTechnology. *Firehouse Technology Navigation Light*. 2022. URL: <https://nl.rs-online.com/web/p/panel-mount-indicators/0208273?gb=s> (visited on 06/19/2024).
- [54] 3DXR. *Cubepilot Buzzer*. 2023. URL: <https://www.3dxr.co.uk/autopilots-c2/the-cube-aka-pixhawk-2-1-c9/cube-cables-accessories-sensors-c15/cubepilot-usb-extension-and-buzzer-p3830> (visited on 06/19/2024).
- [55] NBLEISON. *120W Dc Gear Motor*. 2023. URL: <https://www.nbleisonmotor.com/120W-Dc-Gear-Motor-pd6775924.html> (visited on 06/19/2024).
- [56] J.J. Eckert et al. "Electric Vehicle Drivetrain Optimization". In: *IET Electrical Systems in Transportation 7.1* (2017), pp. 32–40. DOI: 10.1049/iet-est.2016.0022.
- [57] A. Fuhs. *Hybrid vehicles: And the future of Personal Transportation*. CRC Press, 2017.
- [58] S.F. Hoerner. *Fluid-Dynamic drag*. 1st ed. p3-17. Brick Town, N.J: Hoerner Fluid Dynamics, 1965.
- [59] MAD Components. *6S 25Ah Drone Battery*. 2023. URL: <https://store.mad-motor.com/products/6s-25ah-high-power-density-light-weight-drone-solid-state-lithium-battery> (visited on 06/19/2024).

- [60] JKBMS. *JK-B1A24S*. 2019. URL: <https://www.jkbms.com/product/jk-b1a24s/> (visited on 06/19/2024).
- [61] Matek Systems. *Power Module PM20S-2*. 2024. URL: <https://www.mateksys.com/?portfolio=pm20s-2> (visited on 06/12/2024).
- [62] Belden. *Belden Master Catalog*. Richmond, IN: Cooper Industries, Belden Division, 2006.
- [63] N. Li et al. "Study on the environmental adaptability of lithium-ion battery powered UAV under extreme temperature conditions". In: *Energy* 219 (2021), p. 119481. DOI: 10.1016/j.energy.2020.119481.
- [64] ArduPilot. *Connect ESCs and Motors — Copter documentation*. 2024. URL: <https://ardupilot.org/copter/docs/connect-escs-and-motors.html> (visited on 06/12/2024).
- [65] C. de Visser. *Tuning in the Frequency Domain - Slides - AE2235-I Aerospace Systems & Control Theory (2022/23 Q4)*. 2023. URL: <https://brightspace.tudelft.nl/d21/le/content/512927/viewContent/2900383/View> (visited on 06/12/2024).
- [66] ArduPilot. *Manual tuning of Roll and Pitch — Copter documentation*. 2024. URL: https://ardupilot.org/copter/docs/ac_rollpitchtuning.html (visited on 06/12/2024).
- [67] ArduPilot. *Copter Attitude Control — Dev documentation*. 2024. URL: <https://ardupilot.org/dev/docs/apmcopter-programming-attitude-control-2.html> (visited on 06/12/2024).
- [68] Ardupilot. *ArduPilot*. 2024. URL: https://github.com/ArduPilot/ardupilot/blob/master/libraries/AP_Scripting/applets/VTOL-quicktune.lua (visited on 06/12/2024).
- [69] ArduPilot. *QuikTune — Copter documentation*. 2024. URL: <https://ardupilot.org/copter/docs/quiktune.html> (visited on 06/12/2024).
- [70] ArduPilot. *AutoTune — Copter documentation*. 2024. URL: <https://ardupilot.org/copter/docs/autotune.html> (visited on 06/12/2024).
- [71] MadBotix. *I2CXL-MaxSonar-EZ Datasheet – MaxBotix*. 2024. URL: <https://maxbotix.com/pages/i2cxl-maxsonar-ez-datasheet> (visited on 06/12/2024).
- [72] S. Campbell. *Basics of the I2C Communication Protocol*. 2023. URL: <https://www.circuitbasics.com/basics-of-the-i2c-communication-protocol/> (visited on 06/12/2024).
- [73] S. Campbell. *Basics of UART Communication*. 2023. URL: <https://www.circuitbasics.com/basics-uart-communication/> (visited on 06/12/2024).
- [74] S. Corrigan. *Introduction to the Controller Area Network (CAN)*. 2024. URL: <https://www.ti.com/lit/an/sloa101b/sloa101b.pdf> (visited on 06/12/2024).
- [75] E. Mooij and M. Naeije. *AE3212-I – Aerospace Flight Dynamics and Simulation*. 2024. URL: <https://brightspace.tudelft.nl/d21/le/content/615481/viewContent/3627078/View> (visited on 06/12/2024).
- [76] ArduPilot. *SITL Simulator (Software in the Loop) — Dev documentation*. 2024. URL: <https://ardupilot.org/dev/docs/sitl-simulator-software-in-the-loop.html> (visited on 06/13/2024).
- [77] Autodesk. *Autodesk Inventor Overview*. 2024. URL: <https://www.autodesk.com/eu/products/inventor/overview?term=1-YEAR&tab=subscription> (visited on 06/24/2024).
- [78] salary.com. *Hourly wage of engineer*. 2024. URL: [Hourly%20Wage%20for%20Engineer%20%7C%20Salary%20in%20the%20United%20States](https://www.salary.com/research/salary/hourly-wage-of-engineer/) (visited on 06/19/2024).
- [79] Government of the Netherlands. *Minimum wage amounts*. 2024. URL: <https://www.government.nl/topics/minimum-wage/minimum-wage-amounts-as-of-2024> (visited on 06/21/2020).
- [80] TDVG BV. *Rent offer*. 2024. URL: <https://tdvg.nl/en/contact-2/now-for-rent/> (visited on 06/21/2020).
- [81] 42workspace. *Costs of setting up a company in the Netherlands: An Overview*. 2024. URL: <https://www.42workspace.com/guide/setting-up-a-company/> (visited on 06/21/2020).
- [82] Government of The Netherlands. *Price cap for gas, electricity and district heating*. 2023. URL: <https://www.government.nl/topics/energy-crisis/cabinet-plans-price-cap-for-gas-and-electricity> (visited on 06/13/2024).

- [83] Van Oord. *Van Oord Salaries*. 2024. URL: <https://www.glassdoor.nl/Salarissen/Van-Oord-Salarissen-E142320.htm> (visited on 06/13/2024).
- [84] Drone Class. *EU Drone Proof*. 2024. URL: <https://www.eudronebewijs.nl/products/eu-dronebewijs> (visited on 06/13/2024).
- [85] Drone Class. *Theory + Practice VLOS*. 2024. URL: https://www.eudronebewijs.nl/products/basisopleiding-specifieke-categorie-vlos-praktijk?_pos=1&_fid=a11b2d088&_ss=c&variant=40083611254889 (visited on 06/13/2024).
- [86] J. Kagan. *Liability Insurance: What It Is, How It Works, Major Types*. 2022. URL: https://www.investopedia.com/terms/l/liability_insurance.asp (visited on 06/13/2024).
- [87] New Age. *Marine Hull Insurance: What It Covers, What It Excludes, and How to Claim*. 2019. URL: <https://www.newageib.com/what-is-marine-hull-insurance/> (visited on 06/13/2024).
- [88] SkyWatch. *Drone Insurance*. 2024. URL: <https://www.skywatch.ai/us/home> (visited on 06/13/2024).
- [89] EASA. *Easy Access Rules for Unmanned Aircraft Systems*. 2024. URL: <https://www.easa.europa.eu/en/document-library/easy-access-rules/easy-access-rules-unmanned-aircraft-systems-regulations-eu> (visited on 05/01/2024).
- [90] IEA. *Emissions from Oil and Gas Operations in Net Zero Transitions*. 2024. URL: <https://www.iea.org/reports/emissions-from-oil-and-gas-operations-in-net-zero-transitions> (visited on 06/19/2024).
- [91] European Commission. *2050 long-term strategy*. 2024. URL: https://climate.ec.europa.eu/eu-action/climate-strategies-targets/2050-long-term-strategy_en (visited on 06/19/2024).
- [92] EasyComposites. *50mm (47mm) Woven Finish Roll Wrapped Carbon Fibre Tube*. 2024. URL: <https://www.easycomposites.co.uk/50mm-woven-finish-carbon-fibre-tube> (visited on 06/17/2024).
- [93] Faserverbundwerkstoffe. *CARBON fibre tubes pultruded*. 2024. URL: <https://www.r-g.de/en/art/730302> (visited on 06/17/2024).

A. Consulted Resources

This appendix lists the experts and companies consulted during the DSE project. It includes their positions, means of contact, and the weeks in which they were contacted.

Table A.1: Consulted Resources

Expert / company	Position	Means of contact	Date
Dr. Donatella Zappalá	Assistant Professor at TUDelft	Email + Interview	Week 2
Evangelos Ntouros	PhD Control & Simulation at TU Delft	In person meeting	Week 1
Jarno de Jong	Student Computer science at UvA/VU	Personal correspondence	Week 8
Dr. Calvin Rans	Associate Professor at TUDelft	Email	Week 8
Jaxon Keller	Mid-Market Account Executive at Xometry	Email	Week 9
Dr. Danielle Ragni	Full professor	In person meeting	Week 1
Mezijlik propellers	Marketing	Sales	Week 6
E-props	Sales	Email	Week 6
Brian Püroja	Drone Designer at TU Delft	In person meeting	Week 1
Dr. Jianning Dong	PHD DC System and Energy Conversion and Storage at TU Delft	Email	Week 6
Frank Schilder	Design Engineer at DEMO, TUDelft	Email	Week 8
Ventolines: Bart Ummels	Wind Farm Developer & TU Delft offshore wind lecturer	Visited offshore wind farm with him	Week 3